THE LIFTING OF A DEEP SEA MINING COLLECTOR FROM A SOFT COHESIVE SOIL

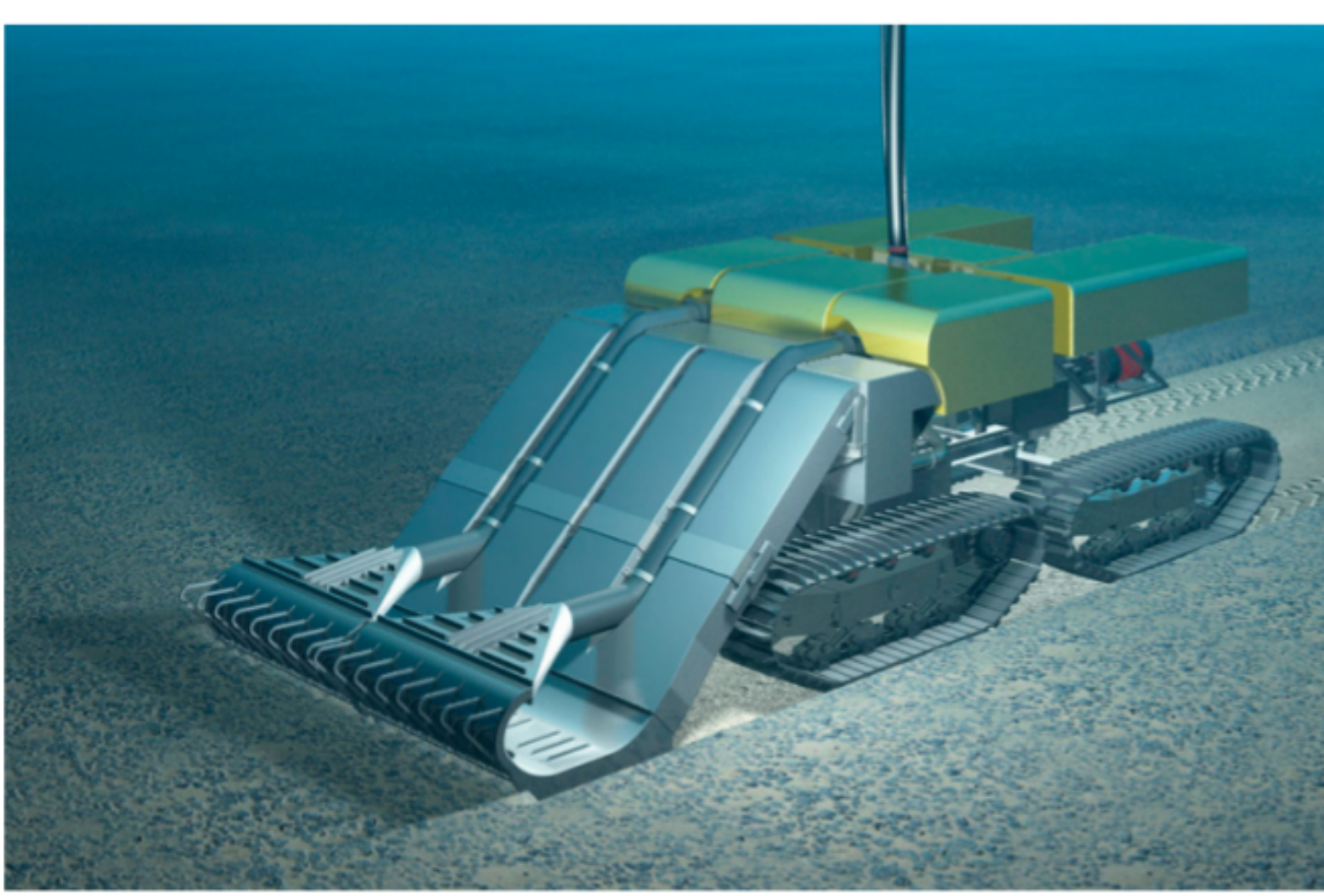

M. Broeren

Offshore and Dredging Engineering

University of Technology Delft

TU Delft

THE LIFTING OF A DEEP SEA MINING COLLECTOR FROM A SOFT COHESIVE SOIL

by

Margo Broeren

to obtain the degree of Master of Science
at the Delft University of Technology,
to be defended on 25 March 2021

Student number:	4351142	
Thesis committee:	Dr. ir. S. Miedema,	TU Delft, chairman
	Dr. ir. R. Helmons,	TU Delft, supervisor
	Ir. M. Souliotis,	Allseas, mentor
	Dr. ir. N. Mallon,	Allseas, mentor
	Ir. B. Yenigul,	Allseas, mentor
	Dr. ir. W. Broere,	TU Delft, third committee member

Abstract

Deep sea mining is an upcoming industry that comes with many unknowns. One of these uncertainties is the interaction between the deep sea mining collector and the seabed. Allseas collaborates with DeepGreen Metals to collect nodules in the Clarion Clipperton Zone (CCZ) in the Pacific Ocean. The CCZ seabed consists of a very soft cohesive soil. During a blackout, the collector sinks considerably into the soil. It must be retrieved as losing such an expensive asset is not desired. The umbilical is intended to lift the collector from the seabed. However, the umbilical has its limits due to its lifting capacity. Therefore, research is done to estimate the breakout force of the collector and to find possible load reduction options to stay within the umbilical's boundaries.

The breakout process is time-dependent and contains multiple soil resistance forces. These soil resistance factors are the suction, adhesion, side resistance and added soil mass. The soil suction is the dominant force, adding resisting during a breakout. Different load reduction options (e.g. eccentric lifting, perforations) are discussed, to reduce the breakout force of the object. However, in previous research the extracted objects are rigid, while the tracks of the collector are flexible to some extent. Experiments are conducted to investigate the effect of flexibility on the breakout force compared to rigid objects.

Four experiments are executed in the laboratory, to test four different effects on the breakout, namely: the flexibility, grousers, eccentric lift and in situ time experiments. A test setup is designed to execute these experiments and five different test samples are selected, varying in size and material properties. During the experiments, the samples are extracted from an artificial CCZ soil. The experimental results are used to calibrate and validate the model.

The model is developed to simulate the breakout process and to make an estimation of the required force to lift the collector from the seabed. The model consists of three main components: the lifting mechanism, soil and the object that should be lifted.

A combination of the literature survey, experiments and the model provides sufficient information to estimate the lifting force of the collector. Load reduction options can be applied to reduce the breakout force during a quick lift. During a slow lift the collector can be retrieved from the seabed without additional load reduction options.

Preface

On the 19th of February, which is my birthday, I started my graduate internship at Allseas. When I arrived at Allseas the birthday garlands were hung for me, so I immediately felt welcome. At that moment I did not know that a month later Corona took over and I had to continue my graduation adventure from home. Due to Corona it was sometimes difficult to communicate and to update everybody on my work. Also ordering parts for my experiment didn't always go as easy. I experienced some setbacks, but always kept looking forward.

I want to thank all my supervisors from Allseas, Niels, Marinos and Buket, for supporting me, even though we were not able to see each other at the office. You helped me during several online meetings with useful tips and questions, that triggered me to get the best out of myself. Also a big thank you to my supervisors from the TU Delft, Sape Miedema and Rudy Helmons. Almost weekly meetings with Rudy helped me a lot to stay on track in these difficult times. We had some nice discussions about different topics and you gave me helpful feedback on my work.

Unfortunately, I lost my grandpa and grandma during my graduation period. These were difficult times for me, but I managed to get through them. Especially my grandfather really wanted to be there when I graduate. He always said: 'I want to be on the first row, when you give your presentation.' Sadly that won't happen anymore, so I want to dedicate my graduation work to my grandpa. I am sure he would love it.

I am curious what the future will bring me. After six and a half beautiful years as a student, I am ready for the next step. Hopefully this will be a challenging career as an offshore engineer!

Margo Broeren
Delft, March 2021

Contents

1

Introduction

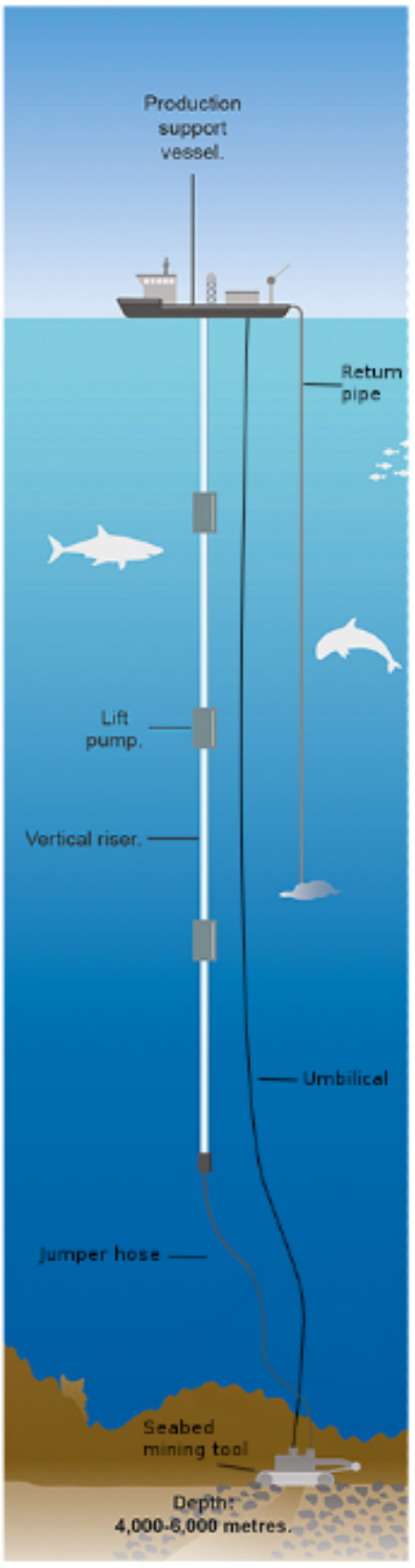

Figure 1.1: Deep sea mining setup. Source: Miller et al. [36].

Allseas collaborated with the Canadian company DeepGreen Metals to carry out a deep sea mining project [27]. The deep sea mining industry is an upcoming business with many unknowns. The concept is to retrieve minerals and metals from the deep ocean seabed. These materials are valuable and are used in high technology applications and in the renewable energy industries. Deep sea mining can be categorised in three types, according to the deposits at the seafloor, namely: Cobalt Rich Crusts (CRC), polymetallic nodules and Seafloor Massive Sulphides (SMS). This deep sea mining project focuses on the collection of polymetallic nodules, which are rock-like deposits containing nickel, copper, zinc, manganese, cobalt and other minerals. The nodules lie on the seabed surface or within a few centimeters depth.

Many of the deep sea mining regions are recognized as vulnerable marine ecosystems (VMEs) and human activities are not allowed. This changed when the International Seabed Authority (ISA) was established in 1994 and started issuing contracts for mineral exploration. DeepGreen Metals got a license, for the pilot project, to gather the nodules from the seafloor of the Clarion Clipperton Zone (CCZ) in the Pacific Ocean at a water depth of 4 to 6 kilometers. The seabed in the CCZ consists of very soft cohesive soil, which presents several challenges for the project such as; getting stuck in the soft soil or sinking away in case a blackout occurs.

All mining operations are based on a similar concept involving a seabed mining tool (SMT), vertical transport system (VTS) and production support vessel (PSV). A tracked collector is considered as SMT in this project. From the support vessel it is released into the ocean and after descending several kilometers it reaches the seabed. Now the actual mining can begin; the collector moves across the seabed and collects the potato-sized nodules by the use of a nozzle which is located in the front of the collector. The nodules are pumped out of the collector through the jumper hose and finally end up in the vertical riser, which brings the nodules to the support vessel (figure 1.1). At

the PSV the nodules are separated from the unwanted sediment; this excess sediment will be returned to the ocean.

Since the collector is remotely operated it is necessary that information from and to the collector can be transported. The umbilical is a cable connecting the support vessel to the collector to provide control, communication and power. Another function of the umbilical is that it can be applied as a lifting asset, it will therefore be used for the deployment and retrieval of the collector.

1.1. Problem statement

The seabed in the operation zone consists of a very soft cohesive soil. Because of this the collector will probably sink considerably into the seabed, especially when at rest during a blackout. To retrieve the collector in case of a blackout when it gets stuck in the seabed, the umbilical is intended to be used to lift it out of the soil. If the load limit of the umbilical is exceeded the collector cannot be retrieved. Hence, there will be a high risk that the collector will end permanently on the bottom of the ocean and should be considered as a lost asset.

1.2. Objective

The main objective of this study is to determine the required lifting force to retrieve the collector when it gets stuck in the soft cohesive soil during a blackout. If this force exceeds the limits of the umbilical, an additional tool or lifting configuration might be needed to reduce the loads allowing the collector to be retrieved. To achieve this objective the following two research questions along with sub-questions have been formulated:

- What will be the required lifting force when the tracked collector gets stuck during a blackout in the soft cohesive soil?
  - What is a realistic initial condition for the sunken collector when it has to be retrieved?
  - What is the effect of the soil resistance acting on the collector when it has to be lifted?
  - What is the effect of the design of the tracks on the required lifting force?
  - What is the effect of the flexibility of the tracks on the breakout?
- How to reduce the loads such that the collector can be retrieved using the umbilical and/or an additional tool?
  - Which phenomena have the most significant impact on the required lifting force?
  - What are load reduction options that need no significant power supply?
  - To what extend can eccentric lifting help in reducing the required lifting force?

1.3. Relevance

The retrieval of the collector is of great importance for Allseas. Since loosing such an expensive collector and its umbilical will be a huge setback. Future projects must be postponed till a new collector is built, which will take a significant amount of time, if financially possible. Also, the ongoing project will be on hold while the collector is stuck on the bottom of the ocean. This will lead to unwanted adverse effect on Allseas reputation as well as the future business of the company. Furthermore, when the collector is left on the seabed it might have a negative impact on the environment and affect the marine life.

Moreover this study will be of help for similar kind of projects involving an embedded object in the seabed waiting for retrieval, for example a deep sea trencher. The principle of a stuck object on the seabed, an uplift force and soil resistance is in all cases more or less similar, so the results of this thesis are applicable for multiple situations.

1.4. Approach

First, a literature study is performed to define the current knowledge about this topic and get a better understanding of the problem. Next, it is decided to perform an experimental program instead of making an extensive theoretical model based on existing experiments. A test setup is designed to measure the lifting force of an embedded object in a soft cohesive soil. Besides doing experiments a computational model is

developed to make an estimation of the required lifting force. The model is calibrated and validated with the experimental results. If the limits of the umbilical are exceeded, an additional tool or different lifting configuration must be introduced to reduce the loads.

1.5. Outline of thesis

The structure of the thesis is as follows: Chapter 2 presents the current knowledge about different topics found in the literature. The main topics are: tracked subsea vehicle, interaction between soil and collector, hydrodynamic loads, breakout force, load reduction options and simulation model. Chapter 3 deals with the different stages of the computational model. The theoretical model and relevant parameters are discussed. The next chapter, chapter 4, includes the processes of the experiment. First the test setup design, experiment type and samples are discussed. Then, the actual execution of the experiments and the test parameters are described. Closing this chapter with the results and the validation of the model. Chapter 5 contains the analysis and discussion of this thesis. The results of the experiments and model are discussed and reflected on the research questions. Closing the report with chapter 6, which presents the conclusion and recommendations.

2

Literature survey

During a deep sea mining operation many elements affect the behaviour of the collector. Think of the weight, buoyancy, environment and soil. When the collector gets stuck in the soft seabed some loads, e.g. added mass, adhesion and suction, will increase. The suction load can increase up to twice the submerged weight [55]. This makes it difficult to lift the collector by simply using the umbilical. An additional tool or lifting configuration can support the umbilical to lift the collector when it is stuck in the seabed. To identify the state of the art concerning these loads and the breakout process of an embedded object in a soft cohesive soil a literature survey is performed.
In the first section, the relevant components of the tracked SMT and the loads acting on it, are discussed. In the following section 2.2, the interaction between the soil and the vehicle is analyzed. Besides the soil, the hydrodynamic loads of the environment also play a role. This will be discussed in section 2.3. After the introduction of all loads that will have a significant influence on the collector, the actual breakout force will be further analyzed in section 2.4. In the next section 2.6 the existing load reduction options will be discussed. The load reduction concepts may be implemented when the umbilical reaches its load limits. To determine the required breakout force a computational model will be made, different simulation models have been investigated in section 2.5. Closing the chapter with a conclusion to discuss the missing knowledge, which will be further investigated in this thesis.

2.1. Tracked subsea vehicle

In this project, a tracked subsea vehicle is used as a collector for polymetallic nodules, similar vehicles are also used in trenching projects. The tracks will act as the propulsion system of the collector. Through the use of a Coanda nozzle, the nodules are collected. The nodules end up in the main body of the collector and continuing their way through the jumper hose and vertical riser to finally being stored at the support vessel. The collector has the following dimensions: m long, m wide and m high. The main components, the blackout scenario and the loads due to buoyancy and weight will be explained in the subsections below.

2.1.1. Components of collector

The collector consists of many components. The most relevant parts for this research are; the nodule pickup unit, the tracks and the umbilical, these will be discussed next and these are shown in figure 2.1.

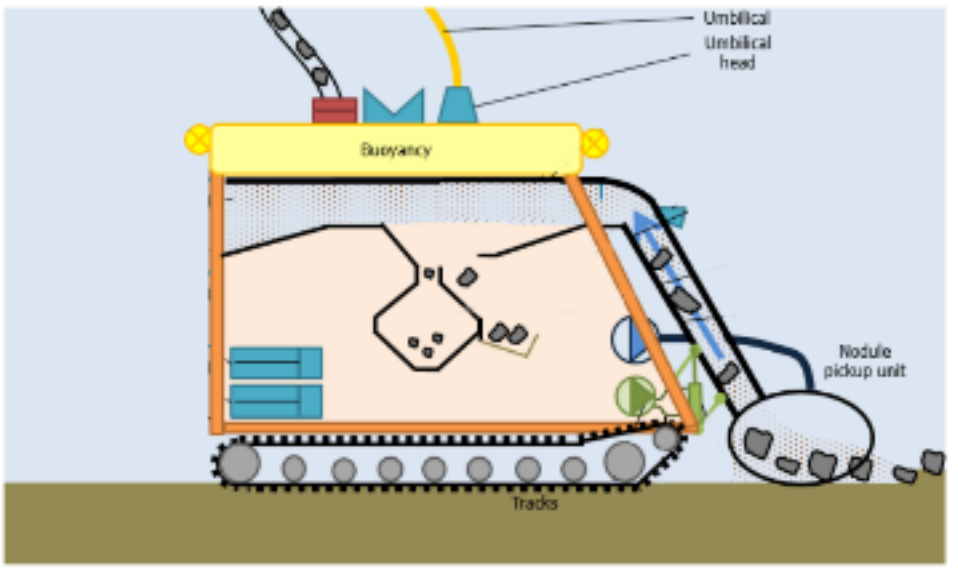

Figure 2.1: Overview of the important components of the tracked collector. Source: Allseas.

Nodule pickup unit

To collect the nodules from the seabed a Coanda nozzle is used. The waterjets from the Coanda nozzle will create a negative relative pressure which sucks up the nodules and sediment, just like a vacuum cleaner. The nozzle is installed at the entrance of the collector, indicated in figure 2.1 as nodule pickup unit. Henri Coanda, the inventor of the nozzle, described the Coanda effect as: 'the tendency of a jet of fluid emerging from an orifice to follow an adjacent flat or curved surface and to entrain fluid from the surroundings so that a region of lower pressure develops.' This concept is ideal for this project, since the flow adheres to the surface of the access pipe of the collector. When the nodules are pumped into the nodule pickup unit they will follow the shape of the access pipe, instead of being left behind at the seabed. The nodule pickup unit floats a few centimeters above the seabed. There will be actuators that allow the pickup unit to adjust the height such that it remains at the height with the optimal efficiency. It is assumed that the nodule pickup unit will remain above the soil, in case the collector sinks into the soil during a blackout.

Tracks

Movement in the very soft cohesive seabed is a challenging task, as slip, low traction and sinkage will occur. To manage this, the collector will be driven by two tracks. Tracks are often used to reduce soil pressure and increases the traction on soft soil, these conditions are very useful for this project and that is why Allseas decided to use this propulsion concept.

Traction is the force that generates the motion of the vehicle. It is the horizontal shear force that will be developed at the track-soil interface. It is proven that rubber tracks have a poor traction on soils with a high moisture content [28], this is why Allseas decided to use pistenbully tracks. A pistenbully track consists of rubber bands with aluminum grousers, see figure 2.2. Increasing the height of the grousers shows an increase in the traction force. However, it also causes a larger slip sinkage, meaning the tracks will sink due to the tracks slipping in the soil. An optimal trade-off of the shape and height of the grouser will result in a high traction force [25]. The tracks used in this project consist of , centimeter wide, rubber belts, which have a spacing of centimeter in between each other and one central gap of centimeter, see figure 2.3. On top of the rubber belts triangular aluminum grousers are assembled with a height of centimeter and a centimeter base. The grousers are spaced centimeter from each other. Figure 2.3 gives an overview of all the dimensions. A second set of short 'summer' grousers is placed between the main grousers for practical reasons. It is assumed that their effect on traction is insignificant. The total width of one track is meter and its length is approximately meter.

Figure 2.2: Pistenbully tracks.

The design of the tracks has an influence on the settlement and retrieval of the collector. The total contact area between the two tracks and the soil is approximately m^2. According to D.J. White [53], open spacing between the tracks results in a lower bearing capacity. However, this has to be weighted against the beneficial fact that the spacing reduces the soil resistance when lifting the collector from the seabed. A more detailed explanation about the bearing capacity can be found in section 2.2.3.
In addition to the pistenbully design, a steel plate is placed between the tracks, figure 2.3. This plate protects the equipment of the collector from wave loads in the splash zone, but it also increases the contact area (m^2) and thus reduces further sinkage in the seabed.

Figure 2.3: Overview of the dimensions of the track with grousers and . Left: top view of track. Right: side view of track.

The tracks will have a Young's modulus of approximately GPa. The estimated tension per track is about kN total. So kN at the top half and kN at the bottom half. The stiffness of the tracks will have an effect on the settlement depth and uplift force, this is further discussed in section 2.2.2.

Umbilical

An umbilical is the connection cable between the subsea equipment and the support vessel or platform at the surface. It provides control, communication, power and chemical services to the subsea equipment. The internal parts are composed of pipes, conductors/wires and a filler material to keep everything in place. Steel wires or high strength synthetic fiber materials are used to protect the outer parts [18].
Nowadays the limits of the umbilicals are challenged by using them in deeper and harsher environments. Flexibility, resistance to environment, high pressure and fatigue need to be considered when going into deeper water. In this project, the umbilical is also intended to be used as a lifting tether, which complicates its design even more.

Umbilical boundary conditions

During an operation, the umbilical experiences several internal and external loads. The umbilical is affected by ocean currents, the water depth and the motion of the ship and collector. When the collector and the attached umbilical are released in the water, buoyancy will act on it. It will sink under its own submerged weight (W_{umb}) of kg per kilometer to the seabed. The umbilical has a length of km and operates in 4.5 km deep water, thus the submerged weight of the umbilical will be kN. The hydrostatic pressure will have an impact on the umbilical going into deeper water. Every 10 meters the pressure increases by 1 bar. Higher pressure can lead to the deformation of the umbilical if it is not well protected.
The ocean current will add a drag force to the umbilical. The sheared current causes the umbilical to take different configurations. According to Vaz [49], it is of great importance to consider these configurations, since there is a large uncertainty in the prediction of them. The umbilical will likely take a catenary shape during the operation.
The design guides of the umbilical give a minimum breaking load value, this value is determined with a high safety factor. Exceeding this value will lead to the failure of the umbilical. The umbilical used in this project has an estimated breaking strength of kN, according to Allseas.
Another failure that could be catastrophic for the project is the deformation of the copper wires. If the copper wires deform or break, the umbilical will not function anymore. Allseas estimated that the copper wires will have a maximum strain of % before they fail, this results in a maximum working load of approximately kN.

Umbilical lifting tool

Besides the just mentioned functions of the umbilical it will also be used as a lifting tool to deploy and retrieve the collector. In a worst case scenario, i.e. in case of a blackout, the collector can only be retrieved by using the umbilical. The support vessel will haul in the umbilical, generating an uplift force acting on the collector. How large the uplift force must be to retrieve the stuck collector will be investigated in this thesis.
The breaking limit of the umbilical is kN, as mentioned in the section above. However, the strain limitations of the copper wires within the umbilical dictates that the allowable force must be below kN. The umbilical does not only carry the collector but also has to support its own weight. This means that the critical section of the umbilical lies near the surface. To determine the actual allowable lifting force a dynamic amplification factor (DAF) must be added. The DAF is a factor that considers that the dynamic loading is more severe than the static loading of the same overall value. Taking all this into consideration, the allowable lifting force is determined using equation 2.1. Allseas uses a DAF of , which lies in the range of DAF used for offshore lifting [15]. With the maximum static load at the surface of kN and the submerged weight of the umbilical, this will result in an allowable lifting load of kN. If the required load to lift the collector of the seabed exceeds the allowable lifting load of kN, an additional tool or lifting configuration must support the umbilical to succeed the retrieval. The determined limit is problem specific and will be different for other umbilical types.

$$F_{allow} = \frac{F_{max}}{DAF} - W_{umb} \tag{2.1}$$

Where:

F_{allow} = Allowable lifting load [kN]
F_{max} = Maximum load at surface [kN]
DAF = Dynamic amplification factor [-]
W_{umb} = Submerged weight of umbilical [kN]

2.1.2. Blackout effect

One of the worst case scenarios is the collector experiencing a blackout. It is important to consider these cases and to be prepared for it. During a blackout the collector has no power supply and there is no communication, which means it is stuck on the seabed. The tracks cannot be actuated which means that the collector cannot move and the tracks cannot be used to disturb the soil to reduce the uplift force. Further operation is no longer possible until the collector is retrieved by the umbilical or another tool that does not need any significant power supply. Since such a blackout has a large impact on the project, it will be considered in this thesis.

2.1.3. Weight and Buoyancy

The weight and buoyancy of the collector have a big impact on the behavior of the collector on the soft cohesive soil. If the collector is too heavy, it will exceed the bearing capacity of the soil and quickly sink into the seabed. Buoyancy elements can add an extra upward force to minimize this sinkage. A more detailed description is given in the next sections.

Weight

The collector has a variable weight when operating on the seabed, this variation is due to the nodules and residuals being inserted. It is estimated that the collector has an in-air mass of tonnes. The submerged mass after it is released in the ocean will be approximately tonnes. Adding the variable weight (i.e. nodules and residuals) gives the collector a maximum submerged mass of tonnes.
The bearing capacity of the soil and the collector's weight have a huge impact on how far the collector sinks into the soft seabed, this will be further discussed in section 2.2.3. The total pressure the collector will apply on the seabed can be determined using equation 2.2. Using the maximum submerged mass of tonnes and a contact area of m^2 for the tracks results in a total pressure of kPa.

$$P = \frac{W}{A_{tracks}} \tag{2.2}$$

Where:

P = Pressure [kPa]
W = Submerged weight collector [kN]
A_{tracks} = Contact area tracks [m^2]

When the collector gets stuck in the seabed an extra added mass will be the soil on the tracks, this has to be considered when determining the required uplift force. The added soil mass (W_S) can be expressed using the effective submerged soil unit weight (γ') and volume of the mass. To determine the submerged unit weight of the soil, the unit weight of seawater should be subtracted from the saturated unit weight of the soil. Allseas investigated the soil and estimated a submerged unit weight between kN/m^3 for the CCZ soil [57]. The volume will depend on the settlement depth and the area of the tracks that will be covered by the soil. If the tracks are shallow embedded, only the soil immediately above the tracks will be considered as the added soil mass according to Vesic [51]. He stated that; an object is shallow embedded when the ratio between settlement depth and object width, $\frac{D_f}{B}$, is 2.0 or lower for soft clay. The added soil weight (W_s) for both tracks can be determined using equation 2.3

$$W_s = 2nBLD_f\gamma'. \tag{2.3}$$

Where:

W_s = Added soil weight [kN]
n = Number of rubber belts per track [-]
B = Width track belt [m]
L = Length tracks [m]
D_f = Settlement depth [m]
γ' = Submerged soil unit weight [kN/m^3]

Buoyancy
When an object is submerged in water a buoyancy force will act on it. The buoyancy force is equal to the weight of the liquid displaced by the object, according to Archimedes' principle, see equation 2.4.

$$F_b = \rho_f V_{disp} g \tag{2.4}$$

Where:

F_b = Buoyancy force [kN]
ρ_f = Density of fluid [kg/m^3]
V_{disp} = Volume of displaced body of fluid [m^3]
g = Gravity [m/s^2]

The buoyancy force acts as an upward force on the collector. Adding extra buoyancy elements will increase this force and reduces the submerged weight. This helps to stay within the bearing capacity limits and reduces the sinkage of the collector in the seabed. The buoyancy elements consist of syntactic foam. Combining hollow glass microspheres and rigid, high strength resin system results in an ultra low density buoyancy element. The syntactic foams can be added to the collector and shaped to conform the hull contours. The density of the foams can reach up to 600 kg/m^3, which means an additional buoyancy force of approximately 4500 N per cubic meter, assuming a sea water density of 1050 kg/m^3 at a depth of 4.5 kilometers [24].
The submerged weight of the collector can be determined using equation 2.5. Here it can be clearly noticed that if the buoyancy force increases the submerged weight will decrease.

$$W_{sub} = W_{dry} - F_b = mg - \rho_f V_{disp} g \tag{2.5}$$

Where:

W_{sub} = Submerged weight [kN]
W_{dry} = Weight of collector outside the water [kN]
F_b = Buoyancy force [kN]

2.2. Interaction between soil and collector

The CCZ consists of a very soft cohesive soil, which makes it a harsh environment to work in. In the following subsections, the impact of the soil resistance on the collector is discussed. The soil characteristics, settlement, bearing capacity and soil failure are treated, followed by the adhesion and suction force of the soil. The soil resistance will have a large influence on the required lifting force to retrieve the collector.
Important to mention is that during a blackout the collector is at rest and not moving.

2.2.1. Soil characteristics

Understanding in what type of soil the project is conducted in is very important, since it can have a big impact on the settlement and breakout process. A very soft cohesive soil, means a sticky soil which can be termed as clay or silty clay. Clay behaviour can be categorised as undrained for the time intervals of interest, since the rate of loading is greater than the rate at which pore water is able to move in or out the soil voids. The behaviour of a saturated undrained clay is often described as elasto-plastic (Muga [37]) or even perfectly plastic (Finn and Byrne [19]), but experimental evidence shows that it behaves like an elastic visco-plastic material [44]. This means that the soil deformation depends on the rate at which loads are applied and if a load level is reached, it undergoes unrecoverable deformation.

Most seabed clays show an increasing undrained shear strength with depth. At the surface of the seabed this value is approximately 2 kPa and increases up to 10 kPa in deeper depths. The strength usually increases linearly with a gradient (k) of 1-2 kPa/m [40]. Allseas also analysed the seabed characteristics by taking several soil samples from the CCZ [57]. According to miniature vane (MV) tests the undistributed undrained shear strength at the seabed will be about kPa. It increases with depth to about kPa at 0.4 meter below the seabed. The remoulded undrained shear strength varies between kPa at the surface to kPa at 0.4 m below surface. This confirms that the undrained shear strength increases with depth as shown in the literature.

The internal friction angle, ϕ, is the angle on the graph of shear stress and normal effective stresses, Mohr's Circle, at which shear failure occurs. Clays with a very low permeability are described by the undrained shear strength and the internal friction angle is considered equal to zero. This is concluded from triaxial shear tests that show that the effective soil stress remains unchanged when changing the confining pressure (σ_3) without allowing further consolidation. Meaning that the shear stress and thus the radius of Mohr will not increase, resulting in a failure envelope with no slope according to the Tresca criterion (figure 2.4).

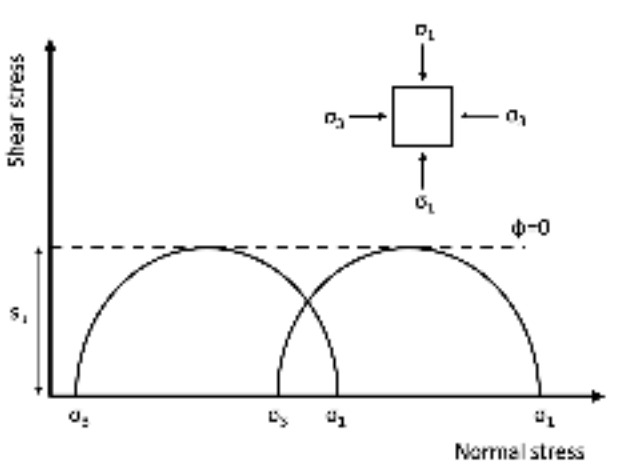

Figure 2.4: Mohr's circle showing an internal friction angle of zero.

During the project the tracks will remould the soil surrounding the collector, causing the soil to become less viscous. Over time the soil regains its form and strength, this phenomenon is called thixotropy. Thixotropy is an isothermal, reversible, time-dependent process, which influences the amount of lifting force needed to retrieve the collector. Rheology is a study that deals with this deformation and flow of materials, also accounting for the time-dependent behaviour.

2.2.2. Settlement

The settlement of an object can be divided into three parts: the elastic settlement (S_e), the primary consolidation settlement (S_c) and the secondary consolidation settlement (S_s). The total settlement (S_t) can be determined by summing up those components as shown in equation 2.6 [12]

$$S_t = S_e + S_c + S_s. \tag{2.6}$$

The elastic settlement is caused by the deformation of the seabed without a change in moisture content. Primary and secondary consolidation settlement depends on the consolidation as stated in their name. Consolidation refers to pore pressure diffusion. The soil slowly changes in volume when reacting to a change in pressure, this change in pressure is caused by the collector being placed on the seabed. The load squeezes the water out of the soil, so the soil particles will tightly pack together. The primary consolidation settlement is time-dependent and occurs when the volume change happens. After the primary consolidation the secondary process follows as a result of plastic adjustment of soil fabrics, also referred to as creep. For foundations in clay the primary consolidation settlement is more dominant than the secondary one.

The flexibility of an object settling into the soil has also an impact on the settlement. Breeveld [7] investigated the interaction between soil and object based on the relationship of their stiffness. In figure 2.5 the comparison of settlement, contact stress and bending moment under a uniform load for a flexible and stiff plate is shown. From this figure can be seen that the flexible plate has the largest settlement in the middle,

the contact stress is equally distributed and it has small moments. The stiff plate settles across its length, has large contact stresses at the edges and undergoes larger moments.

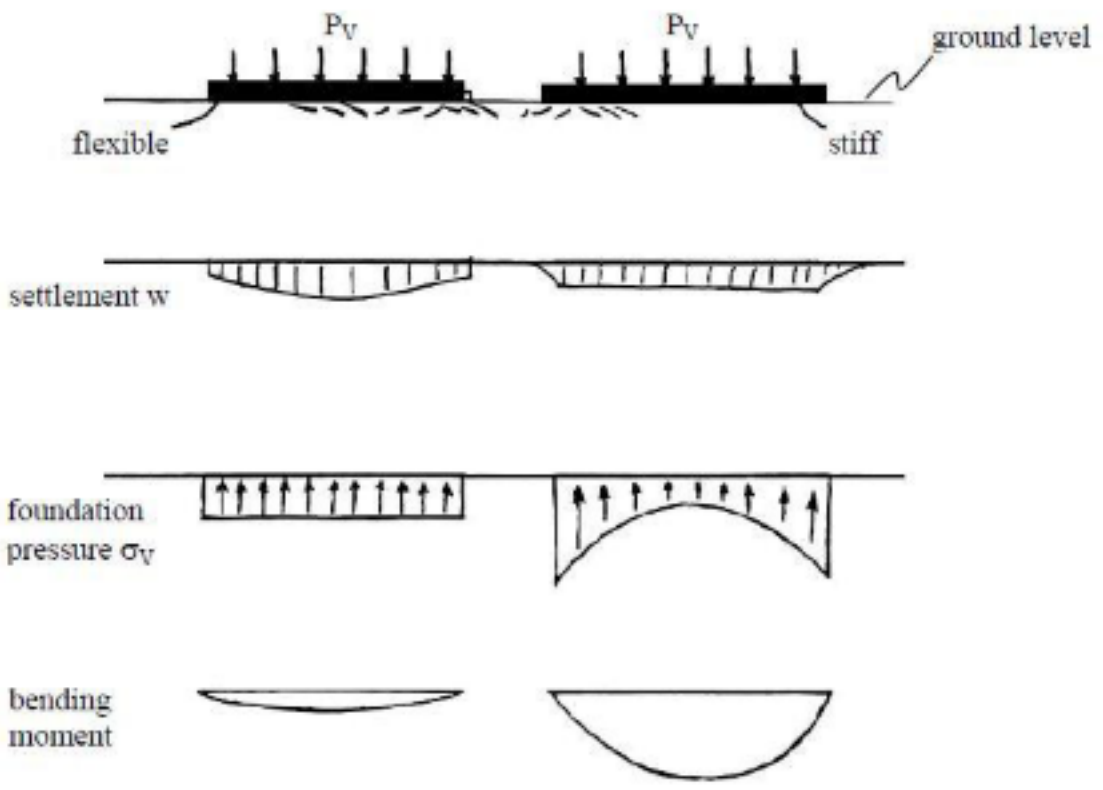

Figure 2.5: The comparison of the interaction between the soil and a flexible or stiff plate. Source: Breeveld [7].

2.2.3. Bearing capacity

The bearing capacity of a soil is defined as the capacity of the soil to support the loads coming from the foundation. In this project, the tracks are considered as the foundation with the load of the collector acting on it. First the grousers penetrate the soil, in this case there is a smaller contact area and thus a bigger ground pressure. After the grousers fully penetrate the soil the contact area increases to the surface of the rubber belts and later on to the area of the protective plate.

For a shallow foundation under vertical load the ultimate bearing capacity, q_u, can be expressed by equation 2.7 according to Meyerhof [34], who refined the Terzaghi [48] equation. Meyerhof introduced shape (s_c,s_q,s_γ) and depth (d_c,d_q,d_γ) factors to the equation to make it applicable for multiple types of foundations. Based on the internal friction angle the factors can be determined. Hansen [22] did further research on the work of Meyerhof and slightly adjusted these factors to get a more accurate result. Figure 2.6 shows the shape and depth factors, assuming an internal friction angle of $\phi = 0$ for clay, of both Meyerhof and Hansen. For this project the improved shape and depth factors of Hansen will be used. The bearing capacity factors N_c, N_q and N_γ for clay turn out to be 5.14, 1.0 and 0.0 respectively.

$$q_u = cN_c s_c d_c + \gamma D_f N_q s_q d_q + 0.5\gamma B' N_\gamma s_\gamma d_\gamma \tag{2.7}$$

Where:

q_u	= Bearing capacity of soil [kPa]	s_q	= Shape factor [-]
c	= Cohesion of soil [kPa]	N_q	= Bearing capacity factor [-]
N_c	= Bearing capacity factor [-]	d_q	= Depth factor [-]
s_c	= Shape factor [-]	B'	= Effective foundation width [m]
d_c	= Depth factor [-]	N_γ	= Bearing capacity factor [-]
γ	= Unit weight of soil [kN/m^3]	s_γ	= Shape factor [-]
D_f	= Settlement depth of foundation [m]	d_γ	= Depth factor [-]

Factor	Meyerhof 1963	Hansen 1970
s_c	$1 + 0.2\ K_p^* (B'/L')$	$1 + (N_q/N_c)\ (B'/L')$
s_q	1	$1 + (B'/L') \tan(\varphi)$
s_γ	1	$1 - 0.4\ (B'/L')$
d_c	$1 + 0.2 \sqrt{K_p^*}\ (D_f/B')$	$1 + 0.4\ (D_f/B')$
d_q	1	$1 + 2 \tan(\varphi)\ (1-\sin(\varphi))^2\ (D_f/B')$
d_γ	1	1
$^*K_p = \tan^2(45° + \varphi/2)$		

Figure 2.6: The shape and depth factors according to Meyerhof [34] and Hansen [22]. B' is the effective width, L' the effective length, Df the foundation depth and ϕ the internal friction angle, which is zero for clay.

The tracks that will be used by Allseas are considered as a strip foundation with an effective width of 1.5 meter for each track. Looking into the vertical loading of a strip foundation in clay, under undrained conditions, the soil can be modelled as a material with c = s_u, with s_u the undrained shear strength, and as earlier mentioned $\phi = 0$. For a strip foundation on the surface of the seabed equation 2.7 can be turned into equation 2.8. Since, the bearing capacity factor N_q is one and N_γ is zero as earlier mentioned. The shape and depth factors s_q and d_q of a strip foundation will be 1.0 according to Hansen [22] (figure 2.6). Adjusting these things in the general equation for the bearing capacity (equation 2.7) will lead to the simplified equation 2.8.

$$q_u = N_c s_u s_c d_c + \gamma D_f \tag{2.8}$$

Using the plasticity theory, multiple studies have considered the impact of soil strength heterogeneity on the bearing capacity factor Nc ([13], [47]). To implement this heterogeneity the cohesion parameter is adjusted to equation 2.9. Figure 2.7 shows the linear increase of the undrained shear strength with depth.

$$c = c_0 + k_c z_{soil} \tag{2.9}$$

Where:

c_0 = Undrained shear strength at surface [kPa]
k_c = Rate of increase in c [-]
z_{soil} = Soil depth [m]

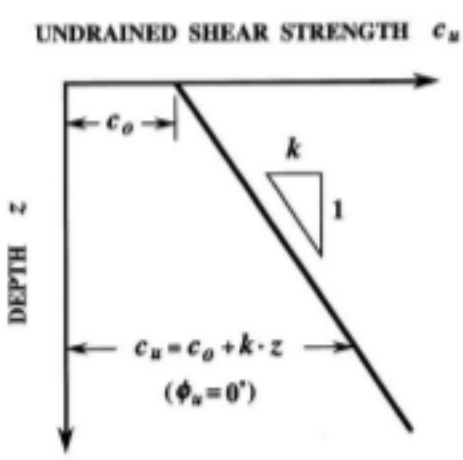

Figure 2.7: Linear increase in undrained shear strength with depth. Source: Tani and Craig [47].

For large foundations, such as the tracks of the collector, the variation of c with depth has a significant effect on the bearing capacity. Results show that an increase in undrained shear strength with depth below the foundation, increases the foundation capacity and the bearing capacity factor. In general the linear increase in strength with depth is indicated as a dimensionless vertical strength gradient $kB'/c0$. Davis and Brooker [13] came up with a modified version of the bearing capacity equation of Hansen [22], considering undrained conditions and the linearly increasing shear strength with depth, shown in equation 2.10 [21]. The correction factor (F_{cor}) for smooth and rough footings can be found in figure 2.8. The shape factor s_c' and depth factor d_c' are also adjusted to the linear increasing soil shear strength and can be found by equation 2.11 and 2.12.

$$q_u = F_{cor}(5.14 c_0 + \frac{kB'}{4})(1 + s_c' + d_c') + \gamma D_f \tag{2.10}$$

$$s_c' = s_{cv} \frac{B'}{L'} \tag{2.11}$$

Where:

s_{cv} = Shape factor vertical loaded circular foundation [-], see table 2.1

$$d'_c = 0.3\frac{c_{01}}{c_{02}} arctan(\frac{D_f}{B'}) \tag{2.12}$$

Where:

c_{01} = Average undrained shear strength above foundation base level [kPa]
c_{02} = Equivalent undrained strength below foundation base level [kPa] = $F_{cor}(5.14c_0 + \frac{kB'}{4})/5.14$

Table 2.1: Shape factor of vertical loaded circular foundation. Source: Salençon and Matar [43].

$\frac{kB'}{c_0}$	s_{cv}
0	0.2
2	0.0
4	-0.05
6	-0.07
8	-0.09
10	-0.10

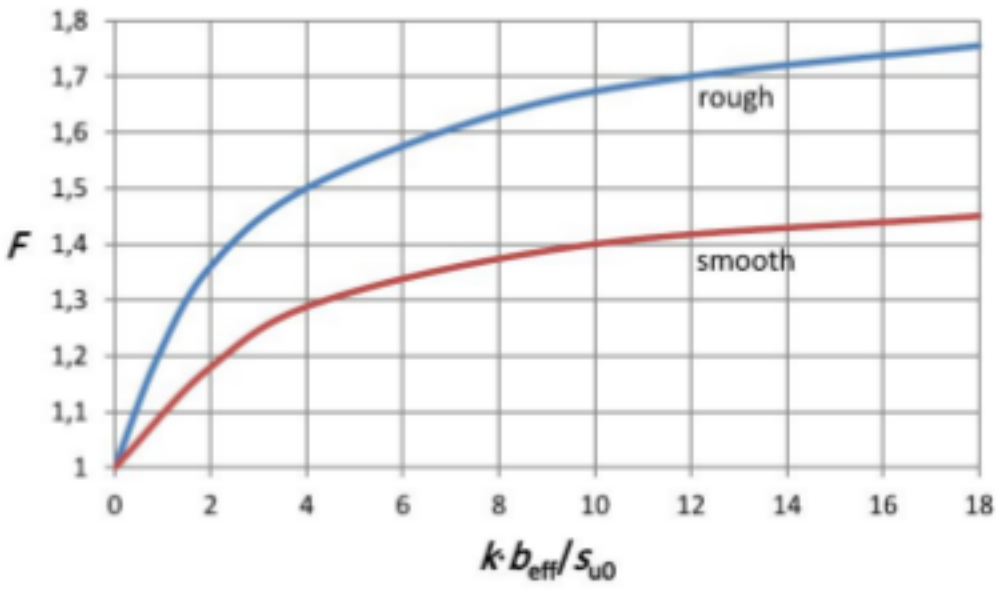

Figure 2.8: Correction factor F_{cor} for smooth and rough footings. Source: DNVGL-RP-C212 [21].

The grousers of the pistenbully tracks will act like skirts. Tani and Craig [47] demonstrated that vertical skirts improve the foundation capacity by trapping soil between the skirts, so the applied load is transferred to the soil at the level of the skirt tips. Yun and Bransby [58] showed that skirted foundation capacity under vertical load may be considered normal as if the foundation is rigid with an embedment depth equal to the skirt depth. However, if this is applied, the weight of the soil within the skirt has to be added up to the self-weight of the foundation.
The effect of the grousers will be neglected in the determination of the bearing capacity for this project, because the grousers are relatively short in comparison to the dimensions of the tracks. So their contribution to the bearing capacity is small and can be neglected.

The spacing between the tracks also has an impact on the bearing capacity. Martin and Hazell [32] and White et al. [53] investigated the bearing capacity of perforated foundations on non-homogeneous clay. The studies show that an increase in perforations results in a decrease of bearing capacity. This is mainly caused by the reduction of contact area over which bearing resistance could be mobilised. However, the perforations will also reduce the peak pull-out resistance, this reduction is more dependent on the effective width between the holes than the perforation ratio (i.e. the perforated area divided by the total area). The effective width of the rubber belt is the dominant factor because the lower the effective width the easier the soil can flow through the open spaces.

2.2.4. Soil failure

If the vertical load on the tracks is too large the bearing capacity will be exceeded, causing soil failure. The three most common soil failure mechanisms are: general shear failure, local shear failure and punching shear failure, see figure 2.9. General shear failure totally ruptures the soil underneath the object. As indicated in the graph with a dot, there is a specific load at which the soil fails, this is the ultimate bearing capacity. The soil is pushed up on both sides of the object, in practice it is often pushed up to only one side making the object being tilted. Local shear failure ruptures the soil immediately below the object and pushes some soil to the sides of the object but significantly less than in the general shear failure. The local shear failure can be seen as a transitional phase between general and punching shear failure. The point in the graph where the settlement starts increasing rapidly can be seen as the bearing capacity. Punching shear failure does not or barely affect the soil outside the loaded area. There is also minimal soil pushed to the sides of the object. The soil directly below the object will be compressed. In the graph no extreme break can be seen, but the first non-linearity indicated the bearing capacity. Punching shear failure occurs in soils that are in a loose or soft state.

For a surface footing the soil failure mechanism is a general shear failure, this transforms into a local shear failure for a buried footing. Depending on how deep the tracks will settle, the CCZ soil will likely experience a general or local shear failure.

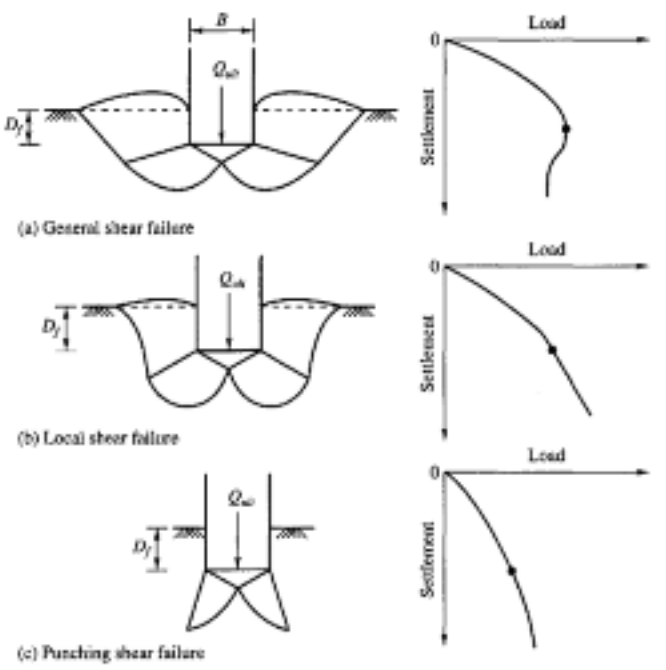

Figure 2.9: Three types of soil failure. Source: Vesic [50].

The foundation roughness has also an impact on the failure mechanism within the soil. For smooth foundations the Hill type mechanism is mostly used and for rough foundations the Prandtl type mechanism, see figure 2.10. In the Hill type the soil underneath the foundation displaces both in vertical and horizontal direction, for the Prandtl type the soil only has vertical displacement. Since the tracks are considered to be a rough foundation, the Prandtl type mechanism is expected to occur.

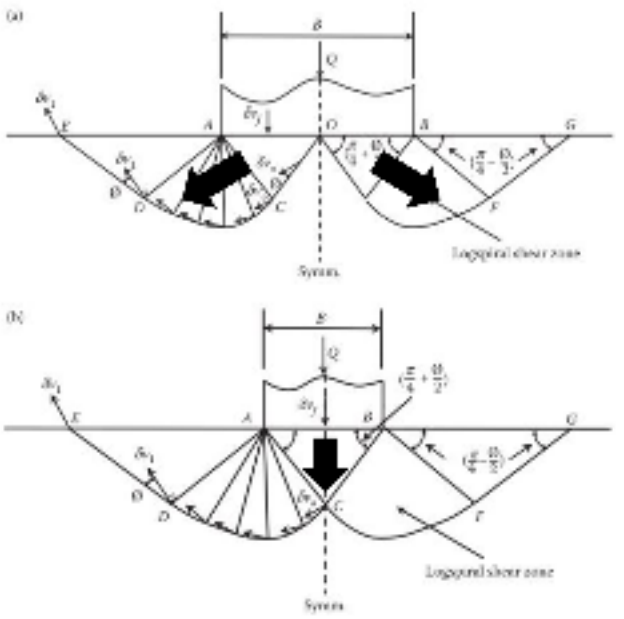

Figure 2.10: a) Hill type failure mechanism b) Prandtl type failure mechanism. Source: Huang and Yu [26].

2.2.5. Adhesion

According to Myers [5], adhesion can be defined as 'the state in which two bodies are held together by intimate interfacial contact in such a way that mechanical force or work can be applied across the interface without causing the bodies to separate. So adhesion is the tendency of dissimilar molecules/surfaces to stick to each other. Important is the difference between adhesion and cohesion, where cohesion is the tendency of similar molecules/surfaces to stick to each other. In this project the adhesion between the CCZ soil and

collector is considered, since the soil adhesion can have negative effects on the breakout. Adhesion loads will act on the tracks, nozzle and frame of the collector.

Zimnik et al. [60] split the adhesion (a_{ad}) in two components; tensile adhesion and shear adhesion. The stress needed to pull off the clay in the direction perpendicular to the contact surface is defined as the tensile adhesion (a_t, figure 2.11-A) and the stress needed to initiate sliding parallel to the contact surface (without normal stress) is the shear adhesion (a_s, figure 2.11-B). For the vertical lifting of the collector from the soil the tensile adhesion has the biggest impact. The adhesive tensile strength can be determined using equation 2.13.

$$a_t = \frac{F_{ad}}{A_s} \tag{2.13}$$

Where:

a_t = Adhesive tensile strength [kPa]
F_{ad} = Pulling force adhesion [kN]
A_s = Effective soil-body contact area [m^2]

An important property of clay is the adhesion factor. According to Chen et al. [10] there are two types. The first type is the ratio between the overall external shear resistance and the undrained shear strength. The second type is the ratio between the actual adhesive resistance versus the undrained shear strength. For this project the second type of adhesion factor is applied. It can be rephrased as the ratio between adhesion and cohesion of the soil. According to Miedema [35] the ratio can be found using equation 2.15. The ratio generally ranges from zero up till two. In case the ratio is zero this means there is no adhesion.

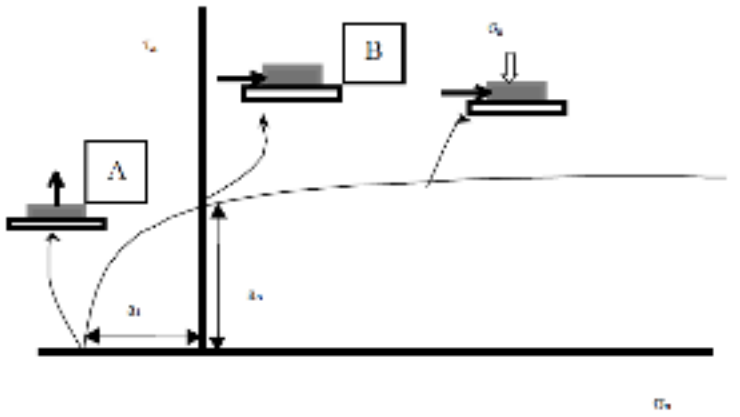

Figure 2.11: Adhesive tensile stength, a_t (Normal direction) and adhesive shear strength, a_s (tangential direction). Source: Zimnik et al. [60].

$$\alpha = \frac{a_{ad}}{c} \tag{2.14}$$

When the collector is lifted from the seabed the soil will either fail at the horizontal plane at the bottom of the grousers, figure 2.12 left, or it will fail around the full profile of the grousers, figure 2.12 right. For the failure of the soil at the bottom of the grousers, the adhesion force can be determined using equation 2.13. When it fails around the grousers, the following equation can be used:

$$F_{ad} = \alpha c_0 (A_s + 2 n_g H_g B') \tag{2.15}$$

Where:

F_{ad} = Pulling force adhesion [kN]
A_s = Effective soil-body contact area [m^2]
α = Adhesion factor [-]
c_0 = Undrained shear strength [kPa]
B' = Effective width tracks [m]
H_g = Grouser height [m]
n_g = Number of grousers [-]

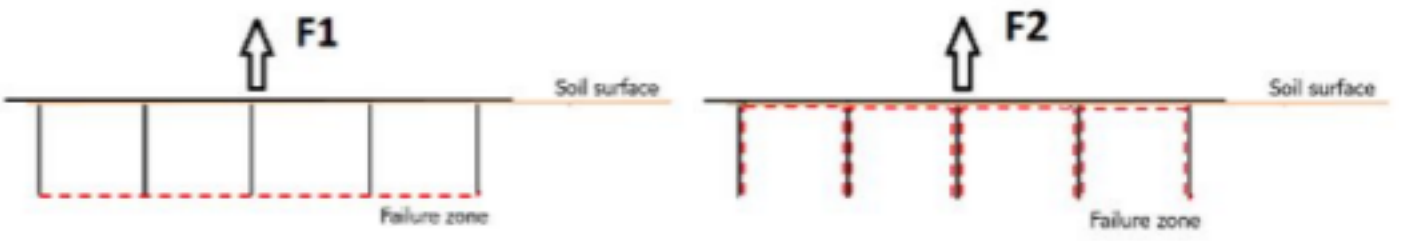

Figure 2.12: Left: Soil failure at bottom of grousers. Right: Soil failure around grouser profile. Source: Allseas [57].

2.2.6. Suction development in soil

The stresses in the soil can be divided into effective stresses (σ') and pore pressures (p), equation 2.16. The steady state solution of the pore pressure at the end of the consolidation process is defined as p_{steady}. If a load, like the collector, is placed on top of the soil excess pore pressure (p_{excess}) is generated.

$$\sigma = \sigma' + (p_{steady} + p_{excess}) \tag{2.16}$$

When the load of the collector is removed the seabed will rebound, regaining some of the pore volume which it had lost due to the pressure of the load. Water flows back into the pores under the collector which gives a certain resistance, this is also called negative pore pressure or suction. Darcy's law describes the relation between the specific flow q and the pressure difference Δp as shown in equation 2.17

$$q = \frac{k\Delta p}{\rho_w g \Delta s}. \tag{2.17}$$

Where:

q = Specific flow [m^3/s]
k = Permeability [m^2]
Δp = Pressure difference [kPa]
ρ_w = Density water [kg/m^3]
g = Gravity constant [m/s^2]
Δs = Flow length [m]

It is generally considered that the suction force can sustain a reverse bearing failure mechanism under certain conditions, namely when fully undrained conditions occur due to rapid loading [9] [33]. This is the same as the failure mechanism in compression as described in section 2.2.4 but in opposite direction, for shallow foundations.

The suction force has a dominant role in the uplift resistance, it can get up to twice the submerged weight of an object according to the results of Bouwmeester et al. [6], who tested in soft cohesive soils (undrained shear strength < 20 kPa) like the CCZ seabed. The embedment depth and uplift velocity influence the suction force. An increase in depth and/or uplift velocity results in an increase in suction force. Adding skirts to a foundation causes the suction to sustain for an even longer time according to Chen et al. [9]. Studies have also shown that perforations and/or eccentric lifting can reduce the suction force [9] [51] [55]. Also the flow of water beneath the bottom of the embedded object will provide suction reduction. These methods to reduce the suction force are further discussed in section 2.6.

2.3. Hydrodynamic load

Hydrodynamic loads arise from water particles velocity and acceleration. The hydrodynamic load can fluctuate in the case of waves or is constant for steady currents. At the surface waves and currents act on the support vessel and umbilical, while at the seabed only the impact of currents remains. The currents vary in velocity from a few centimeter per second to a few meter per second.
The hydrodynamic load consists out of drag and inertia forces, and will act on the umbilical and collector. There are two cases to consider: the umbilical and collector are at rest, and the collector is lifted from the seabed.
In the first case only the seawater has a velocity and acceleration, to determine the hydrodynamic loads the Morison equation 2.18 can be used.

$$F_f(t) = \frac{1}{2}\rho_{sea} C_d A_d v^2 + \rho_{sea} C_m V_{obj} \dot{v} \tag{2.18}$$

Where:

$F_f(t)$ = External fluid force [kN]
ρ_{sea} = Density of seawater [kg/m^3]
v = Velocity seawater [m/s]
C_d = Drag coefficient [-]
A_d = Drag area [m^2]
C_m = Inertia coefficient [-]
$\dot{v}$ = Acceleration seawater [m/s^2]
V_{obj} = Volume [m^3]

In the second case the umbilical and collector will be moving. The Morison equation can also be used, but must be adjusted to equation 2.19. Where the relative vertical velocity between the collector and seawater flow is considered.

$$F_f(t) = \frac{1}{2}\rho_{sea} C_d A_d (v-u)^2 + \rho_{sea} C_m V_{obj} \dot{v} - \rho_{sea} C_a V_{sea} \dot{u} \tag{2.19}$$

Where:

u = Velocity object [m/s]
V_{obj} = Volume of object [m^3]
C_a = Added mass coefficient [-]
V_{sea} = Volume of seawater directly above object [m^3]

Drag can be referred to as fluid resistance or friction, it is the force acting opposite to an object with respect to a surrounding fluid (first part of equation 2.18). If the velocity of the object increases the drag force increases quadratically. The inertia force is the resistance of an object to a change in velocity, and is determined by summing up the Froude-Krylov force and hydrodynamic mass force shown in the second part of equation 2.18.

The drag coefficient (C_d) is related to the Reynolds number and the roughness of the object. Song et al. [45] investigated the drag force along a flexible riser, which is comparable to the umbilical. Their results showed a mean drag coefficient between 1.3 and 2.0. The drag coefficient decreases when the Reynolds number increases. Via experiments the drag force and coefficient of more specific objects, such as the collector, can be determined.

The inertia coefficient (C_m) is given as $1 + C_a$, with C_a the added mass coefficient. Newman [38] provides added mass coefficients for 2D and 3D submerged bodies. For a circular cylindrical object, like the umbilical, the added mass coefficient in longitudinal/lateral direction can be found via $\pi\rho a^2$ with a the radius of the cylinder. The umbilical has a radius of 8.4 centimeter, thus the added mass coefficient will be about 5.8. Xiaozhou and Shaojun [56] investigated the added mass coefficient for a comparable tracked mining tool. Their collector had a dry mass of 30 tonnes and a submerged mass of 12 tonnes. They used two methods, the Hess-Smith method and Fluent method. The results of the Hess-Smith method show an added mass of 56 tonnes, which is almost twice the dry mass of the collector. Both methods have a similar outcome of about 2.8 for the added mass coefficient C_a in vertical direction of the collector. Since the collector used in this experiments is similar to the collector used by Allseas, it is assumed that the added mass coefficient will be in the same range.

2.4. Breakout force

One of the most important aspects of this thesis is to find the breakout force of the stuck collector. In the following subsections the breakout phenomenon and existing experimental studies considering the breakout force will be discussed.

2.4.1. Breakout phenomenon

The breakout phenomenon is defined as the lifting force overcoming the opposing loads resulting in the release of the collector from the seabed. The opposing loads that should be overcome are already mentioned in the previous sections, these are: suction (P_w), adhesive force (F_a), soil resistance (R_v), submerged weight of collector (W) and added soil mass (W_s). Vesic [51] investigated the breakout of embedded objects in the ocean bottom and illustrated the forces acting on the embedded object in figure 2.13.
Various other studies are done on the breakout force, all giving their interpretation of the breakout force [11] [14] [30]. One thing they all agree on is that the suction force in soft cohesive soils is the primary resisting force when lifting an embedded object. Another important factor is the time dependency of the breakout problem. This time dependency is due to the plastic property of the soil. Liu [31], Muga [37] and Rodderick and Lubbad [42] formulated an empirical equation, based on their experimental tests, considering the breakout time.

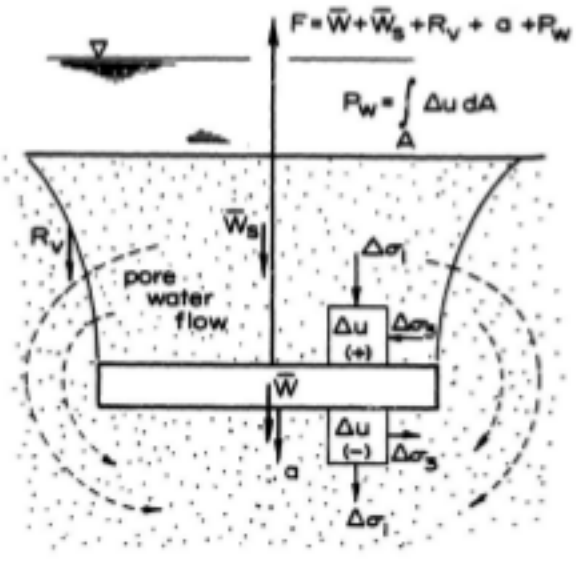

Figure 2.13: Forces acting on embedded object when lifted from seabed. Source: Vesic [51].

There are two types of breakout; the immediate breakout and the long-term breakout. During the immediate breakout the loading is so rapid that no significant amount of water can flow into the sediment below the object. In the case of the long-term breakout, the force will be lower than the immediate breakout force, but will accomplish the same over a longer period of time. The difference between these breakout types depend on the soil the object is resting on. Van Kesteren [29] made a distinction between the slow, transient and fast processes based on the effective soil stress. Drained soils are typical for slow processes and undrained soils are typical for fast processes. The distinction between drained and undrained is determined by the use of the pore-Peclet number (equation 2.20) and is illustrated in figure 2.14. For the immediate breakout an undrained soil can be expected with a pore-peclet number larger than 10. For the long-term breakout, it tends more to an intermediate to drained soil with a pore-peclet number between 1 and 10.

$$\xi_{Pe} = \frac{V D_f}{D} \tag{2.20}$$

Where:

ϵ_{Pe} = Pore-Peclet number [-]
V = Velocity [m/s]
D_f = Settlement depth of foundation [m]
D = Pore pressure diffusion coefficient [m^2/s]

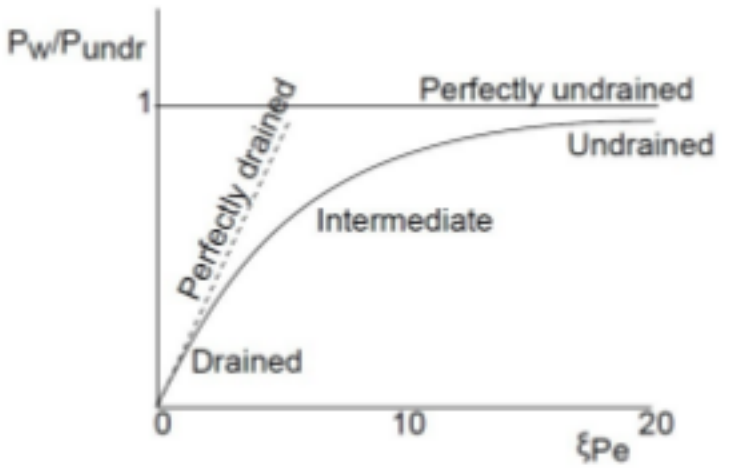

Figure 2.14: Drained and undrained conditions based on the pore-Peclet number. Source: van Kesteren [29].

A quick upward force increases the suction force as earlier mentioned in section 2.2.6. Decreasing the lifting force will reduce the suction making it easier to lift the object over a longer period of time [9] [51]. Lee [30] states that it is often more economical to use the long-term breakout, since a smaller force is needed so less equipment is required and the waiting time is only several hours or a few days. However, over a long period it is difficult to maintain a constant force, the weather could deteriorate and a longer period means more costs, thus leaving the collector at the seabed for a few days is not preferred.

The in situ rest time of an object has an impact on the breakout force needed. When the collector is sunken into the seabed, the surrounding soil is remoulded. This means that the soil strength decreases and the contact between the collector and soil is loose. When time passes by the soil regains a part or all of its strength due to a thixotropic process. Thixotropic regain is a time dependent shear thinning property, where the soil will become less viscous under stress and when time passes it returns back to a more viscous state as mentioned in subsection 2.2.1. After a while, the loose soil will flow back around the collector due to static pressure. Together with afore mentioned strength regain of the soil, it will be more difficult to extract the collector from the seabed after a long in situ rest time. Roderick and Lubbad [42] investigated the effect of a longer in situ time for an embedded sphere and cylinder in a soft cohesive sediment. The results show that the breakout force ratio, which is the breakout force divided by the submerged weight of the object, can increase by 59%

for an in situ time of 32 hours versus an in situ time of 2 hours. Experiments will be conducted to investigate the effect of a longer in situ time on the breakout force of the collector.

If the collector is lifted from the seabed, it relieves the soil bearing pressure underneath the tracks. The collector will not move until the bearing pressure and side friction are counterbalanced. When it is balanced, the lifting force will cause the collector to move in upward direction. When moving upward, the collector will experience resistance from the shear force of the surrounding soil and soil tension resistance (i.e. suction and adhesion) under the collector. Eventually plastic deformations in the soil will occur, leading to changes in the pore pressure and stress system of the sediment. If this continues, a few things can happen according to Liu [31], namely; soil shear stress failure, adhesion force failure or soil tension failure. The soil shear stress failure occurs when the interior shear stress exceeds the yield strength and fractures develop leading to failure. Adhesion failure is when the adhesion between soil and object fails, as discussed in section 2.2.5. The last failure, tension failure, happens when fluid saturation diminishes the cohesive strength of the soil. This happens during a long term breakout, when the water flows to the pores.

Finn and Byrne [19] also divided the breakout mechanism in two parts; general shear failure and local shear failure, these are earlier discussed in subsection 2.2.4. The general shear failure is much larger than the local shear failure according to their experimental tests. General shear failure can occur at high suction forces, if these high suctions cannot be developed due to anomalies in the drainage conditions then the local shear failure will occur and the needed breakout force will be less.

What can be concluded from these studies is that the breakout force can be determined using either the bearing capacity theory under fully undrained conditions or an empirical equation based on experimental tests with partially drained conditions. Lee [30], Liu [31] and Muga [37] introduced different empirical equations based on their experimental results, including the time dependency during a breakout. These equations have the advantage of being simplistic and directly include the time effect. However, they are only applicable for a specific type of soil and under specific placement and pull out conditions. In this deep sea mining project the conditions will be different, so these equations and/or parameters must be adjusted to be applicable. For example, the empirical equation of Muga [37], which is shown in equation 2.21, can be used to determine the breakout force for this deep sea mining project. However, the constants Q, R and t_0 must be derived from in situ field test data, which are not available for this specific project.

$$F = Q A_{max} q_d e^{-R(t-t_0)} \tag{2.21}$$

Where:

F	= Breakout force [N]	R	= Slope of failure line [-]
Q	= constant [-]	t	= Breakout time [min]
A_{max}	= Maximum contact area [m^2]	t_0	= Reference time [min]
q_d	= Bearing capacity [N/m^2]		

The other way to determine the breakout force is to use the bearing capacity theory [11] [19] [51]. This method is a proven approach, but does not directly involve the time dependency. It does indirectly include the time effect via the strength and deformation parameters of the soil. Vesic [51] mentioned the rheological approach which should be added to the bearing capacity based breakout force.

2.4.2. Experimental studies

Many experimental studies investigated the breakout force and time of an embedded object in a soft cohesive soil. Different object are used in these experiments varying from rigid solid shapes (e.g. spheres, cubes, cylinders) to scale model mudmats. Most experiments are done in laboratory, but some of them are tested in the actual field. Lee [30] and Liu [31] analysed experimental tests of different solid objects being extracted from fields in the Gulf of Mexico, these test are executed by the Naval Civil Engineering Laboratory (NCEL). The objects were allowed to settle to equilibrium under their own weight.

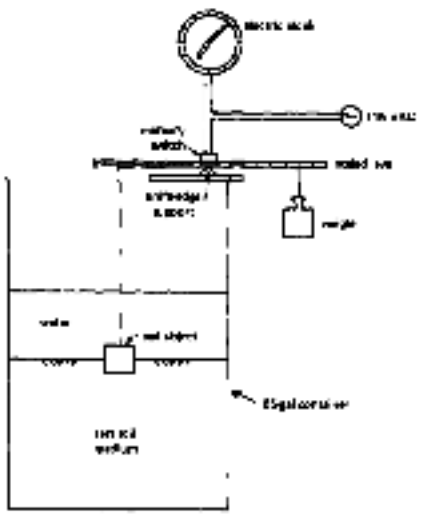

Figure 2.15: Test setup for laboratory breakout tests.
Source: Liu [31].

To extract the object from the seabed two pontoons were connected in series to a cable, when inflated they create an uplift force. The applied force is measured using a dynamometer and the movement with a displacement indicator. The valid field test data are too limited to interpret and correlate them, so additional data is obtained in the laboratory doing small scale model tests. A lever, container with soil and a clock are used for the laboratory test setup. Weights are attached to the lever to create an upward force to extract the scale model. The breakout time is determined using an electric clock with a mercury switch. The test setup is shown in figure 2.15.

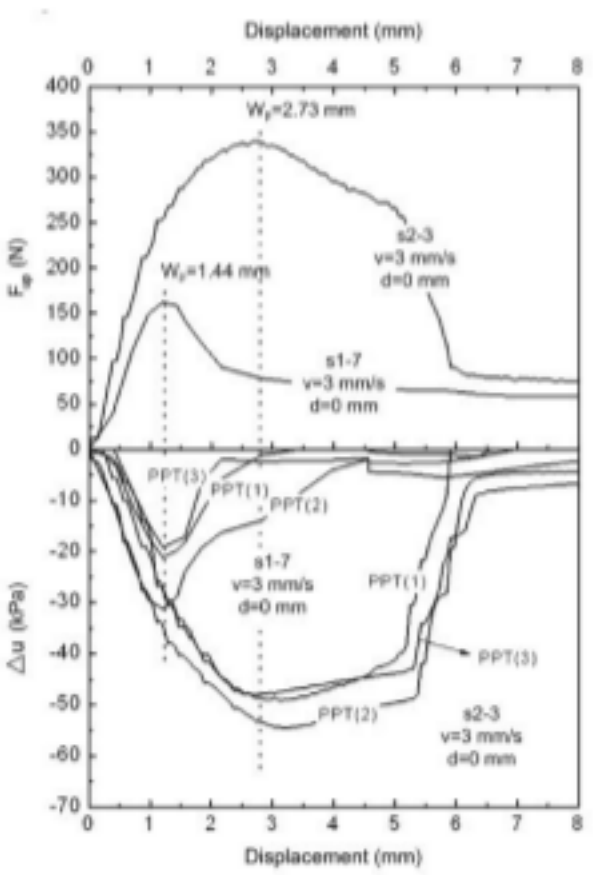

Figure 2.16: Uplift force and difference of pore pressure against the vertical displacement of two separately tested mudmat models. Source: Chen et al. [9].

Other laboratory tests use approximately the same test setup containing; an extracting device, container with soil, object to extract, weights to create a lifting force and measurement equipment. Das [11] and Roderick and Lubbad [42] considered the effect of the in situ rest time and the breakout time of the object in their laboratory experiments. Multiple in situ rest times were chosen, at the end of a chosen in situ time the embedment depth was determined and a lifting force was applied. The force was kept constant until breakout was attained then the timer was switched off to determine the breakout time.

Chen et al. [9] and Den Hertog [23] investigated the breakout of mudmats. The main focus of their experiments lies with finding the amount of suction, since this is supposed to be the biggest resisting force. Chen et al. did the experiments in a drum centrifuge with the advantage of testing multiple times on a consistent soil sample. Den Hertog did his tests in a reservoir with the advantages of simplicity, good visibility and low costs. With pore pressure transducers (PPT) and differential pressure (DP) sensors they determined the suction force acting on the mudmats. Besides investigating the suction underneath the mudmats, Chen et al. also investigated the effect of skirts added to the mudmats. They concluded that an increase in skirt length results in an increase in breakout force and suction. Figure 2.16 shows the uplift force and the suction force against the displacement of the mudmat. All mudmats are 100 mm long, 50 mm wide and 2.5 mm thick. Sample S1-7 had no skirts and sample S2-3 had 10mm skirts, both were lifted from the centre with an uplift velocity of 3 mm/s. It can clearly be seen that the sample with skirts requires a larger breakout force.

2.5. Simulation model

A simplistic simulation model should represent the extraction of the collector from the seabed. The main parts of this model will consist of the umbilical, the soil and the object itself. In the literature different approaches to construct such a model can be found. The subsections below will treat all parts of the model separately.

2.5.1. Umbilical

The dynamic behavior of the umbilical is a complicated subject. To simplify the umbilical, it can be assumed to be a large, single spring with a certain damping. The stiffness of the umbilical when lifting the collector can be determined by equation 4.1, which is discussed in section 3.4. Since the umbilical has a complex design, the Young's modulus (E) of steel does not apply over the whole cross sectional area and length of the umbilical. Instead a reduction factor should be applied or the data from the manufacturer should be used.

Considering the umbilical as a single spring does not capture the full behavior of the umbilical. By using multiple spring and damper elements, the behavior can be simulated in a more realistic way. Over many years, a lot of research has been done trying to realistically simulate the behavior of underwater cables.

The three main methods that are used are: finite difference method, lumped mass method and the finite element method. All models solve the partial differential equations (PDEs) that describe the cable, so the behaviour can be predicted. Ablow and Schlechter [1] used the finite difference method to model an underwater towed cable. The flaw in their model is that the algorithm becomes singular when there is no tension in the cable. Buckham [8] considered the bending and tension force on a towed cable using the lumped mass method and validated the model experimentally. Later on, the finite element method was used by Fang et al. [17] to make an accurate prediction of the deformation in the cable of a towed system. Eidsvik and Schjolberg [16] also used the finite element method to solve the Euler-Bernoulli beam equations for the umbilical of a remotely operated vehicle (ROV).

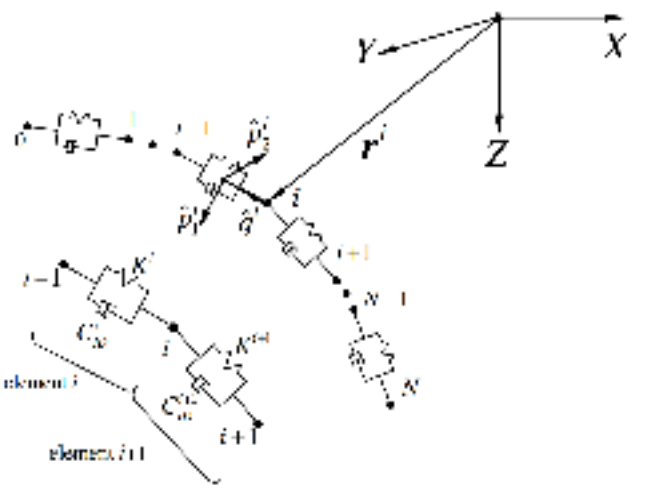

Figure 2.17: N visco-elastic elements in a lumped mass model using the Voigt model for the mechanical properties of the individual cable elements. Source: Buckham [8].

Important properties of the umbilical are the flexibility and elasticity, which have a significant effect on the lifting of the collector and thus should be implemented into the simulation model. Buckham [8] considered the elasticity of a cable in his method. He idealises the visco-elastic elements of the umbilical as a parallel combination of an ideal spring and viscous damper, referring to the Voigt model. The combination of the lumped mass method and Voigt model is illustrated in figure 2.17. Multiple spring and damper elements are attached to each other and together construct the umbilical. How the umbilical is implemented in the simulation model for this project will be explained in chapter 2.5.

2.5.2. Soil

The modelling of the soil is a difficult matter, since a lot of factors play a role. Two commonly used soil modeling approaches are the Winkler model [54] and the continuum based approach. The Winkler model idealizes the soil as a series of independent springs and is described according to the linear stress-strain behaviour, figure 2.18. The advantage of this model is that it uses only one parameter to describe the soil (i.e. 'k_r', the modulus of sub-grade reaction parameter). Hook's law can be used to represent the elastic load-deformation relationship as shown in equation 2.22.

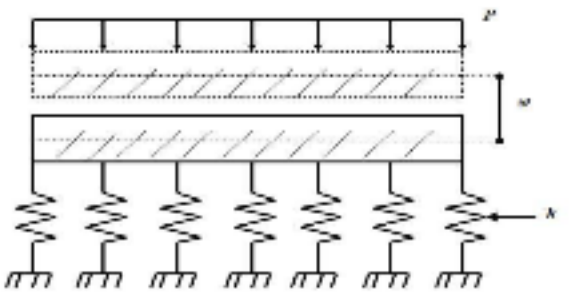

Figure 2.18: Winkler model to construct the soil. Source: Breeveld [7].

In the continuum based approach the soil is modeled as a semi-finite and isotropic material. A big advantage of this model is its simplicity, since it only uses the soil elastic modulus (E) and the Poisson's ratio (ν) as input parameters. However, it also has it limitations as it might be inaccurate at the edges of the resting foundation and with the determination of the surface displacement [46].

$$p = k_r w \tag{2.22}$$

where:

p = Pressure $[kN/m^2]$
k_r = Modulus of sub-grade reaction $[kN/m^2/m]$
w = Settlement [m]

The two classic soil models discussed above consider the behavior of the soil to be linear. However, the seabed soil has a stress-strain relationship that behaves non-linear. To simulate the soil in a more realistic manner this non-linearity should be added to the model. Aubeny et al. [3] investigated the non-linear soil stiffness.

They presented a power law expression shown in equation 2.23 to determine the soil resistance. The fitting coefficients a and b are given in table 2.2. For this project the fitting coefficients are $a = 6.73$ and $b = 0.29$, since the tracks are considered to be a rough footing and will be shallow embedded.

$$P_{soil} = a(\frac{D_f}{B})^b c_0 B \tag{2.23}$$

Where:

P_{soil} = Soil resistance [kN/m] B = Width of object [m]
a = Fitting coefficient [-] b = Fitting coefficient [-]
D_f = Embedment depth [m] c_0 = Undrained shear strength [kPa]

Table 2.2: Power law fitting coefficients. Source: Aubeny et al. [3].

Interface condition	Smooth	Rough
D_f/B≤0.5	a=4.97 b=0.23	a=6.73 b=0.29
D_f/B>0.5	a=4.88 b=0.21	a=6.15 b=0.15

To include the time dependency of the soil, the overstress theory created by Perzyna [39] can be used. The total deformation of a soil element is divided into an instant and a delayed component in this theory. The instant strain component is elastic, reversible and time independent, while the delayed strain component is irreversible and time dependent. Equation 2.24 shows the total strain rate (ϵ_{ij}) which is decomposed into the elastic (ϵ_{ij}^{el}) and the visco-plastic (ϵ_{ij}^{vp}) component [20]. The elastic visco-plastic behavior of the soil can be introduced into the simulation model with a Hookean spring element in conjunction with a Coulomb element. Those springs and dashpots can be connected in series or parallel [52].

$$\dot{\epsilon}_{ij} = \dot{\epsilon}_{ij}^{el} + \dot{\epsilon}_{ij}^{vp} \tag{2.24}$$

2.5.3. Object

To simulate the collector on the seabed, it can initially be assumed to be a rectangular object. The design of the object can have a significant impact on the outcome of the simulation model. Some important properties of the object are the submerged weight and contact area.
The submerged weight has a dominant role to what depth the object will penetrate the soil, and thus the required breakout force. Increasing the submerged weight in the model will cause the breakout force to be higher. Another important property is the contact area. Reducing the contact area will result in a higher pressure on the seabed, but also reduces the breakout force since there will be less suction and adhesion, as mentioned in section 2.6. The tracks of the collector have an open design with gaps in between the rubber belts, but when the collector sinks significantly the soil will hit the protection plate (see section 2.1.1), which increases the contact area. This variation in contact area over settlement has to be implemented into the simulation model.
Later on in this thesis, load reduction options will be investigated. Not all options can be implemented in the simulation model, but some of them can. For example the just mentioned contact area or submerged weight of the object could be modelled.

2.5.4. Object seabed interaction

Al-Shamrani and Sture [2] came up with a time dependent model for anisotropic cohesive soils, similar to the time dependent, non-linear models discussed in section 2.5.2. Followed by Al-Shamrani [44] who used the finite element method (FEM) to analyse the breakout problem using this earlier developed model. In his model he describes the elastic visco-plastic, path-dependent, rheological and non-linear stress-strain-strength properties of cohesive soils under general loading conditions. Al-Shamrani concluded that using the finite element model is satisfactory and in good agreement with other studies and empirical equations (see section 2.4). Using FEM gives the opportunity to implement various factors that impact the breakout force such as the soil strength and deformation characteristics, object geometry and weight, embedment and pullout conditions.

Randolph and Quiggin [41] made a non-linear hysteretic soil model that simulates the penetration of the seabed. Figure 2.19 illustrates the four penetration modes they use, namely: not in contact, initial penetration, uplift and repenetration. For our model the blue line ((1) initial penetration) and green line ((2) uplift) are the most relevant.

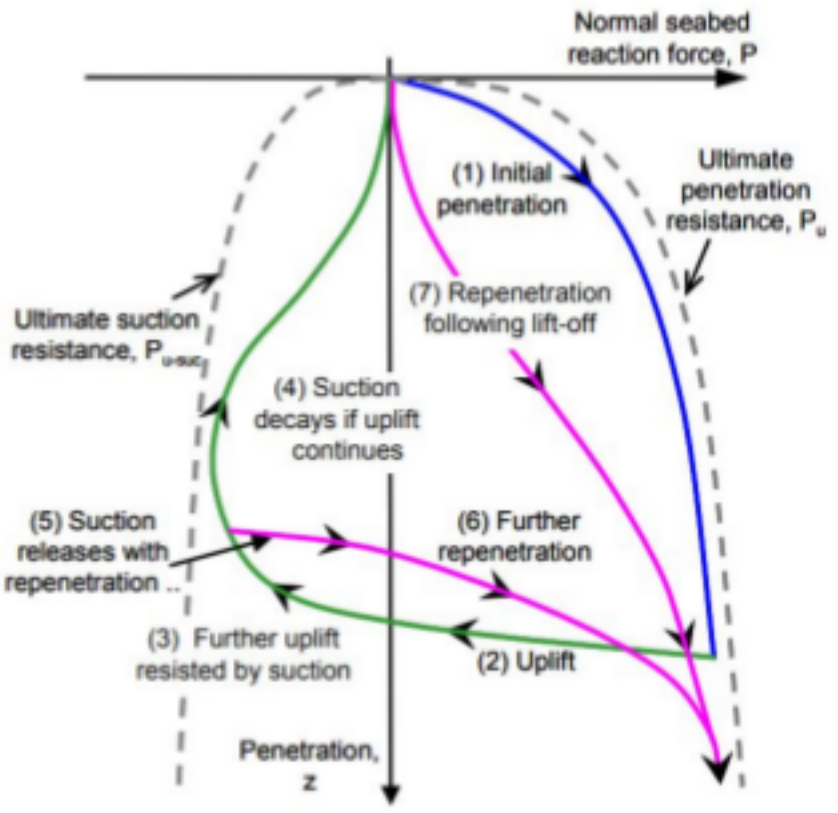

Figure 2.19: Seabed modes during penetration, repenetration and uplift. Source:Randolph and Quiggin [41].

When the collector is deployed at the seabed of the CCZ it will penetrate the soil, this is the initial penetration. The resistance of the soil is arranged in such a way that if the penetration increases the resistance asymptotically approaches the ultimate penetration resistance (P_u). If the collector is lifted from the seabed the penetration depth will decrease and the resistance will approach the ultimate suction resistance (P_{u-suc}), as can be seen in figure 2.19. The ultimate penetration resistance can be determined using the earlier mentioned non-linear soil resistance, equation 2.23. For the suction resistance equation 2.25 can be used. The suction resistance ratio (f_{suc}) lies between 0 and 0.7 according to Randolph and Quiggin [41].

$$P_{u-suc}(D_f) = -f_{suc} P_u(D_f) \tag{2.25}$$

Where:

$P_{u-suc}(D_f)$ = Ultimate suction resistance [N/m]
f_{suc} = Suction resistance ratio [-]
$P_u(D_f)$ = Ultimate penetration resistance [N/m]

2.6. Load reduction options

If the retrieval of the collector requires a breakout force exceeding the amount the umbilical can handle, the load must be reduced or an additional tool is needed to accomplish retrieving the collector. Looking at the load reduction several factors can be adjusted, for example the suction or adhesion. On the other hand, an additional tool providing extra lifting capacity could also be considered. Multiple methods are possible, but eventually the option with a beneficial effect and which is economically advantageous will be chosen. In the subsection below the existing load reduction options are discussed.

2.6.1. Existing concepts

Several studies have investigated options to reduce the uplift force required to break free an embedded object from a soft cohesive soil. The dominant resisting force resulting in a higher uplift force is the suction. To reduce this suction force perforations can be added to the object or the object can be lifted eccentric. Xiaojun [55] investigated both the effect of perforations and the eccentric lifting by doing multiple experiments.

He used the same experimental setup as Chen et al. [9], as discussed in section 2.4.2. Chen et al. already stated that eccentric lifting reduces the uplift force, because of the balancing suction force. A portion of the mudmat's weight is still supported by the sediment when lifting eccentric, so at the side of the lift negative pore pressure (i.e. suction) occurs while on the opposite side positive pore pressure is created. Vesic [51] also investigated the eccentric lifting of an embedded object and showed these balancing suction forces (P_w) in figure 2.20. Xiaojun confirmed that eccentric lifting will reduce the peak uplift resistance by 66 to 79% when lifting a non-perforated mudmat. He also did experiments with two different perforated plates. The first plate had large perforations and the second plate had small perforations, but the perforation ratio of both plates were the same (19%). For the smaller perforated plate, the peak uplift resistance was reduced by 74% compared to a central lift of a non-perforated plate, while for the bigger perforation this reduction was only 45%. This reduction due to perforations is because of the acceleration of dissipation of the negative pore pressure. Xiaojun stated that the average length of drainage paths between perforations is the relevant parameter when determining the effect of perforations. Reducing the length of the drainage path will increase the dissipation of negative pore pressure. Another way to reduce the suction force is reducing the uplift velocity to achieve partially drained conditions [9]. However, this method has limited applications for the offshore industry due to the long duration of extracting the object. The uplift force will be affected by the motion of the support vessel, so applying a constant force over a longer time period will be difficult.
Liu [31] mentioned pivoting under the object, jetting, oscillating force and propulsion as possible ideas to reduce the load. Pivoting or jetting under the object will cause a flow of water underneath the object, which makes the breakout easier. An oscillating force applied to the object or propulsion of the object itself are other ways to reduce the load. Liu did not further investigated these load reduction options.

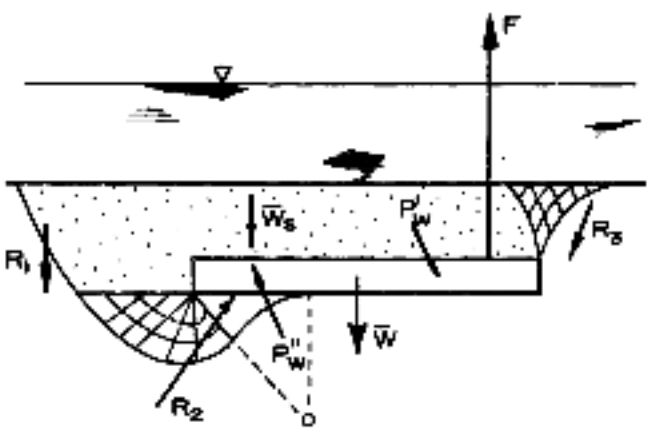

Figure 2.20: Eccentric lift of embedded object. Source: Vesic [51].

Another factor that affects the breakout is the adhesion. If less soil sticks to the collector and the side friction is lower, than the force needed to extract the collector will decrease. Bitar [5] investigated multiple adhesion reduction options, these are summarised in figure 2.21. The methods are divided in the design of the soil-engaging component, mechanical and electro-chemical/magnetic.

In the current project the design of the tracks is already established, so the only changes that can be made are coating or additions to the tracks. Studies have proven that the surface material of the soil-engaging component has a significant effect on the amount of soil sticking to the component. Low surface energy materials, such as polymeric materials, are hydrophobic which will resist the sticking. However, this material wears out quickly which is certainly not convenient in a deep sea mining project. The solution is to apply a coating to the surface of the soil-engaging component. Bitar suggests using a polymer composite coating, which reduces both normal adhesion and sliding resistance.
Using the mechanical method is better applicable to this project, by using vibration, jetting, scraping or heating the soil adhesion can be reduced. Applying vibrations perpendicular to the soil-track interface will reduce the soil contact, resulting in less soil sticking to the surface of the tracks. However, it is questionable if this method is useful in the deep sea environment, since the water will damp the vibrations and it might cause damage to the equipment. Another good option is jetting, which is already often used in offshore trenching. Jetting is the spraying of water under high pressure to cut the soil. In shallow waters divers can operate the jetting tool, but in deep waters the tool must be remotely operated. Bienen et al. [4] investigated the reduc-

tion of the extraction resistance of a spudcan with the use of water jetting. They concluded that jetting gives a positive contribution to the reduction of suction, but will not totally release the spudcan from it. Adhered soil to the tracks can also be removed using the water jetting tool. The pressure of the jetting tool can get up to multiple mega pascals (MPa), which easily cuts the soil loose from the surface.

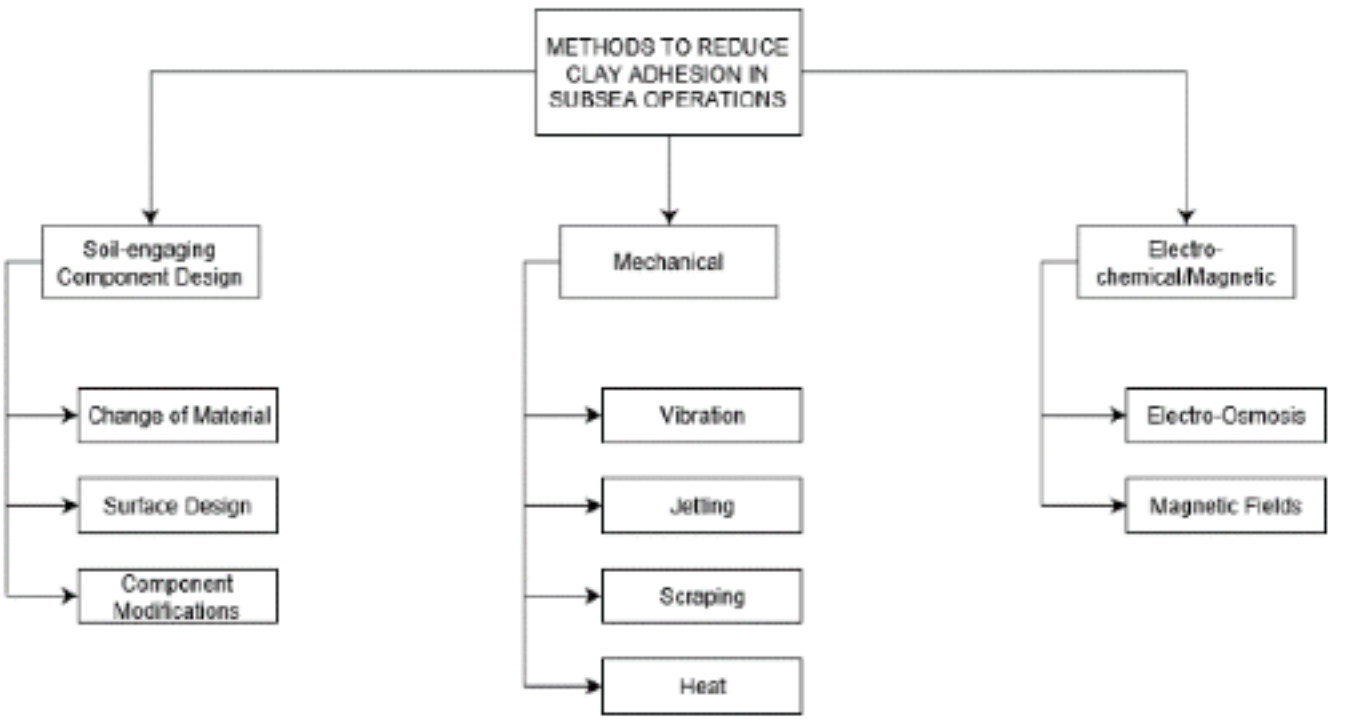

Figure 2.21: Adhesion reduction options for subsea operations. Source: Bitar [5].

Scraping is another method to remove the adhered soil from the tracks, and is performed with hand tools used by divers. However, the water depth of this project is far too high for divers to descend to, so this option is cancelled. The final method is heating, heating minimizes the surface tension by a decrease of viscosity of the water film at the soil-tool interface. This method is difficult to realize in the deep water conditions and requires much energy resulting in high costs.

So it seems that perforations, eccentric lifting, coating and jetting are methods to reduce the breakout force of the collector by decreasing the adhesion and suction forces. However, the blackout should be taken into account, which means there is no power supply during the retrieval of the collector. Thus, the remaining load reduction options are perforations, eccentric lifting and coating.

2.7. Conclusion

Many studies have been done considering the breakout of an embedded object in a soft cohesive soil. For this thesis accurately determining the breakout force of the deep sea mining collector is important. The breakout of an embedded object occurs when the lifting force overcomes the resisting loads. These opposing loads are suction, adhesion, soil resistance, weight of collector and added mass. The suction will be the dominant soil resistance force.

There are two ways to find the breakout force; by creating an empirical equation from experiments or by using the bearing capacity theory. Multiple empirical equations are formulated with the advantage of simplicity and including the time dependency, but with the downside of being very problem specific. The bearing capacity theory is a proven approach, but does not directly include time dependent behaviour and partially drained conditions. For the partly embedded tracks the bearing capacity can be determined using the comparable strip footing approach. However, a strip footing does not have the open spacing, grousers and flexible material the tracks have. The design of the tracks will affect the breakout force. According to the literature the open spacing in the tracks will reduce the required breakout force, but also reduces the bearing capacity. On the other hand, the grousers will act like skirts and improve the bearing capacity by trapping soil between them.

In the existing breakout experiments all tested objects are rigid bodies and have little or no flexibility. Here a lack of knowledge can be found, which can be quite useful in our problem since the tracks consist of rubber belts that are flexible to some extent. As shown in the literature, the flexibility of an object does have an im-

pact on the settlement, contact stress and bending moment and thus on the breakout force. To investigate the effect of the flexibility of an object during breakout experimental tests will be done.
A computational model, based on the information found in the literature, will determine the required breakout force. The model consists of three elements: the umbilical, object and soil. The experimental results will be used to validate the model. If the breakout force turns out to exceed the limits of the umbilical, than the discussed load reduction options should be further investigated. One of the most efficient methods is an eccentric lift, it can reduce the breakout force up to 74% for perforated objects. Other load reduction options, that need no significant power supply, are perforations and coatings. More load reduction options will be investigated and designed later on this thesis.

3

Model

The process of lowering an object onto a soil, the settlement of the object and the retrieval, can be simulated in a numerical model. In this graduation project, the software Simulink and Matlab are used. The model has three main parts: the lifting mechanism, the soil and the object. When correctly built, the model will give an estimation of the required lifting force. The event that the collector needs to be retrieved, when stuck in the seabed during a blackout, can be simulated in the model. The results will show if the required lifting force exceeds the load limit of the umbilical. In this chapter, the design of the model and the results are discussed. An overview of the model parameters can be found at the end of this thesis.

3.1. Introduction model

The goal of the model is to simulate the breakout of an embedded object from a soft cohesive soil and to estimate the required lifting force. To model this, the software Simulink is used. Simulink is a block diagram environment for multidomain simulation and model-based design. In combination with the software Matlab, which is used for the storage of parameters and making graphs, the model is built.
As mentioned above, there are three main parts. First, the lifting mechanism to mimic the deployment and retrieval of the collector/sample with the umbilical or steel cable. Second, the soil, which represents the (artificial) CCZ soil along with the soil resistance forces. And finally, the object which acts as the collector (tracks) or experimental sample. The results of the experiments are used to calibrate and validate the model.

3.2. Lifting mechanism model

To simulate the cable that lowers and lifts the object onto and from the soil, a mass spring damper system is designed (figure 3.1). The mass is the load from the object, so in this case the submerged mass of the object (m_{sub}). The damping of the system (c) is the cable damping and the axial drag of the water. To determine the drag, the relative velocity is used. The spring mimics the effect of elongation of the cable, thus the axial stiffness (k_{cable}). Equation 3.1 is applied to determine the stiffness of the cable when the length increases or decreases. The Young's modulus, E, for the steel cable of the experiments is 183.9 GPa and for the umbilical a reduction factor of is assumed since the umbilical consists of multiple materials.

$$k_{cable} = \frac{EA(z + L_0 + x)}{L_0 + x} \tag{3.1}$$

Where:

k_{cable}	= Axial stiffness [kN/m]	z	= Position of object [m]
E	= Young's Modulus [GPa]	L_0	= Initial length cable [m]
A	= Cross sectional area [m^2]	x	= Payout length [m]

The payout velocity of the cable is integrated to find the payout length. If the velocity is negative the cable length increases, when the velocity is positive the cable is hauled in so the length decreases. The object is lowered onto the soil, then it settles for a given amount of time and after the settlement it is extracted.

Considering the experimental case, the attachment point (z_a) above the container is about 3 meter high and the initial length of the cable ($L0$), when the sample is submerged, is 2.5 meters. This results in a start position of 0.5 meters above the soil. The soil start at $z = 0$, so a negative value for z means the object stands in the soil. The payout and hauling in velocity of the cable is based on the rotational speed of the winch. The payout/hauling in velocity during the experiments is estimated at 0.008 m/s, for a short term breakout.

The simulation of lowering and lifting the collector is similar to the lifting mechanism discussed above. Allseas has a passive heave compensation (PHC) system, which reduces the impact of waves on the lifting operation. Since this system is available, the vessel position at z_a is assumed to remain constant. The initial length of the umbilical is much larger, since the water depth is approximately 4.5 kilometers. For simplification it is assumed that the umbilical is not affected by currents or other environmental impacts. The payout and hauling in velocity of the umbilical is taken as m/s for a short term breakout and m/s for a long term breakout.

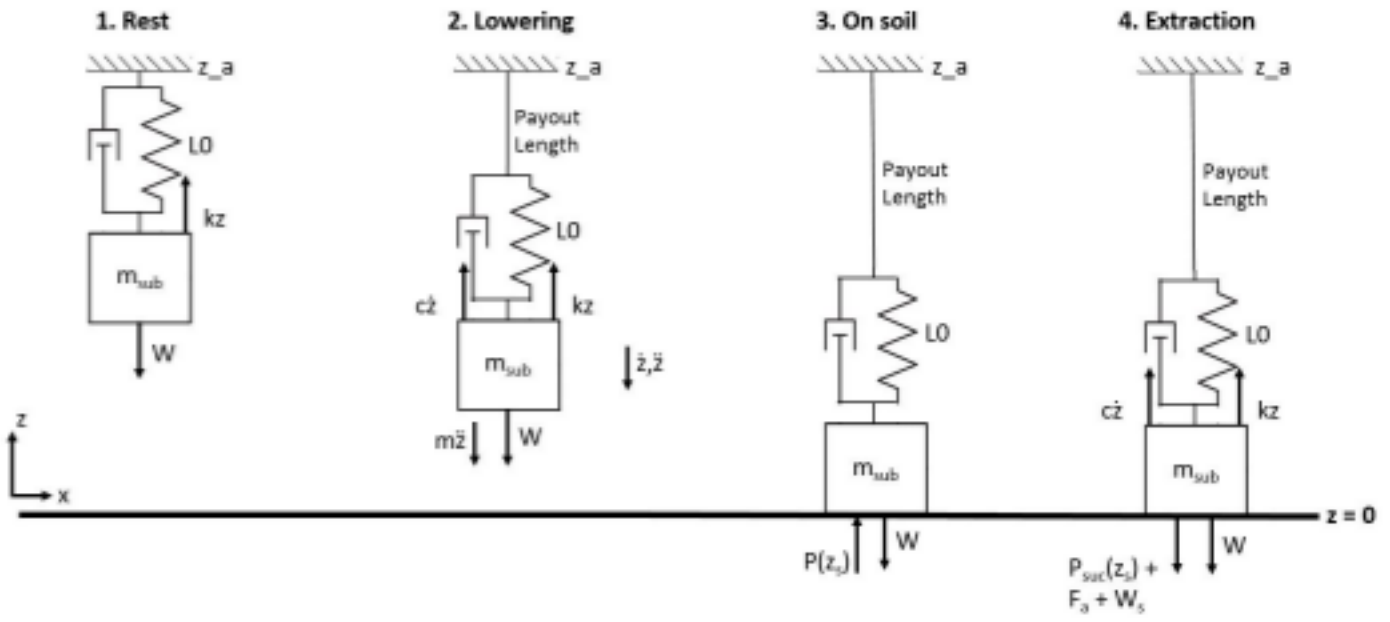

Figure 3.1: Lowering and retrieval of an object, modelled as a mass spring damper system. Four modes: object at rest, lowering, on soil and extraction.

A schematic overview of the forces acting on an object are shown in figure 3.1. When the object is at rest (1.), it hangs above the soil and there is no movement. The cable is simulated by the spring and supports the submerged weight of the object. When the cable length increases, the mass accelerates and moves towards the soil (2.). The cable stiffness varies as the cable becomes longer and shorter. As the object rests on the soil (3.), the force in the cable is zero and the soil resistance starts acting on the object. The soil resistance is based on the bearing capacity, this determines how far the object settles. The settlement depth also depends on the submerged weight of the object, which applies a pressure to the soil. How the soil resistance force is modelled is discussed in section 3.3. When the object is extracted from the soil (4.) the suction force acts on the sample, just like the added soil weight and adhesive force. These resistance forces will also be discussed in section 3.3. A general equation (equation 3.2) is made to describe the behaviour of the object and the forces acting on it. The general equation can be rewritten for the four different modes, as described in equation 3.3.

$$m\ddot{z} = k_{cable}z + c\dot{z} - W + P(z_s) - P_{suc}(z_s) - F_a - W_s \tag{3.2}$$

$$\begin{aligned}
&1.) \quad k_c z = W \\
&2.) \quad m\ddot{z} = kz + c\dot{z} - W \\
&3.) \quad W = P(z_s) \\
&4.) \quad -m\ddot{z} = kz + c\dot{z} - W + P(z_s) - P_{suc}(z_s) - F_a - W_s
\end{aligned} \tag{3.3}$$

The validation of the lifting mechanism, when using the experimental parameters, is shown in figures A.1, A.2, A.3, A.4, A.5 and A.6 in Appendix A. Figure A.1 and A.2 show the payout length and total cable length, that determine the position of the experimental sample. The cable stiffness is shown in figure A.3, which depends on the cable length. When the sample touches the soil, the cable force becomes zero, as shown in figure A.4. Figure A.5 shows the displacement and velocity of the sample and figure A.6 shows the corresponding damping effect and natural period. In these figures only the soil penetration resistance is added, other soil resistance forces (i.e. suction, adhesive force, added soil weight) are not present.

3.3. Non-linear soil model

The soil and object characteristics determine how deep the object settles and how much resistance the object experiences when it is retrieved. To model the soil-object interaction, the non-linear soil model of Quiggin and Randolph [41] is implemented in the Simulink model. It is a mathematical model that presents the reaction normal force to the soil. Quiggin and Randolph focused on the interaction between a pipeline and the seabed. Since the tracks will have a similar interaction with the soil, this model is used with certain modifications, which are discussed in this section.

The model of Quiggin and Randolph consists of four penetrations modes, as discussed in section 2.5.4. However, for the Simulink model the focus is on three of these modes, namely the not-in-contact mode, initial penetration mode and uplift mode. In not-in-contact mode, the object floats above the soil. When the object is lowered and touches the soil, the initial penetration mode starts. The object settles in the soil for a certain amount of time and is then retrieved. The retrieval of the object is the uplift mode and lasts until the penetration becomes zero. For each mode there is an analytic equation, with all equations containing a hyperbolic factor. This hyperbolic factor causes the resistance ($P(z_s)$) to asymptotically approach the ultimate soil penetration resistance as the settlement depth increases. In uplift mode the suction resistance will asymptotically approach the ultimate suction resistance as the settlement depth decreases. Figure 2.19 in section 2.5.4 shows these modes and the corresponding soil resistance.

3.3.1. Ultimate soil penetration and suction resistance

The primary parameters for this model are the geometry of the object, the soil shear strength profile with depth and the soil density. Equations 3.4 and 3.5 determine the ultimate penetration and ultimate suction resistance. Instead of using the diameter of the pipeline, the object's width (B) is used in these equations. The suction resistance ratio (f_{suc}) controls the ultimate suction limit. A higher value results in a greater uplift resistance. The constant factor is a simplification that represents the elements that influence the suction, namely the local soil strength and the uplift velocity. For a long term breakout this value should be lower and for the short term breakout higher, generally it has a value between 0.5 and 1.0 for single lifts. Based on the experimental results, a suction resistance ratio of 0.35 for the long term breakout and 1.0 for the short term breakout is assumed. This is further explained in section 4.7.

$$P_u(z_s) = N_c(z_s/B)\, s_u(z_s) B \tag{3.4}$$

$$P_{u-suc}(z_s) = -f_{suc} P_u(z_s) \tag{3.5}$$

Where:

$P_u(z_s)$ = Ultimate penetration resistance [N/m]
$N_c(z_s/B)$ = Bearing capacity factor. If $(z_s/B) \geq 0.1$, $N_c(z_s/B) = a(z_s/B)^b$
= Bearing capacity factor. If $(z_s/B) < 0.1$, $N_c(z_s/B) = N_c(0.1)\sqrt{10(z_s/B)}[-]$
$s_u(z_s)$ = Undrained soil shear strength [Pa]
B = Width of object [m]
$P_{u-suc}(z_s)$ = Ultimate suction resistance [N/m]
f_{suc} = Suction resistance ratio [-]

3.3.2. Soil penetration resistance

Now the limits for the penetration and suction resistance are determined, the actual penetration and suction resistance will be presented. In not-in-contact mode the resistance $P(z_s)$ is zero, when it touches the soil for the first time (initial penetration mode) the penetration resistance is given by equation 3.6. The hyperbolic factor $H_{IP}(\zeta)$ depends on the non-dimensionalized penetration ζ, which is the penetration depth (z_s) divided by the objects width (B) over the normalized maximum stiffness (K_{max}). The normalized maximum stiffness parameter controls the stiffness during the penetration and determines how fast the resistance force approaches the ultimate

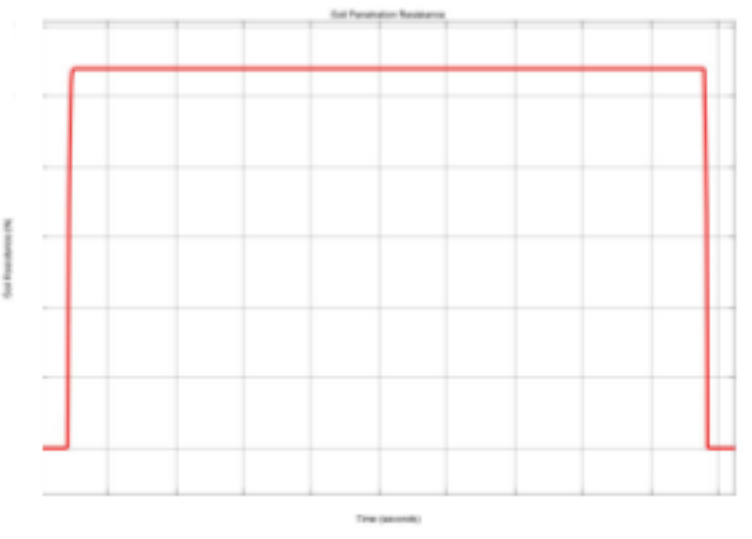

Figure 3.2: Soil penetration resistance for the experimental sample 1.

penetration or suction resistance ($K_{max} = \frac{B}{P_u} \frac{dP}{dz_s}$). Since the CCZ soil is very soft, the K_{max} value is quite low with a range of 150 to 250. In the model a K_{max} value of 200 is implemented. The hyperbolic factor is zero at the start of penetration, equals 0.5 when $\zeta = 1.0$ ($z_s = B/K_{max}$) and asymptotically approaches 1.0 as the penetration gets large compared to B/K_{max}.
To check if the soil penetration resistance is correctly added to the Simulink model, the same mathematics are executed with an Excel file. In figure A.7 in Appendix A the results of the Excel file are shown compared to the Simulink model. The values match, so the penetration resistance in the Simulink model is correctly implemented. Figure 3.2 shows the penetration resistance for sample 1 (stainless steel plate, see chapter 4). The corresponding model parameters can be found at the end of this thesis.

$$\begin{aligned} P(z_s) &= H_{IP}(\zeta) P_u(z_s) \\ H_{IP}(\zeta) &= \frac{\zeta}{\zeta + 1} \\ \zeta &= \frac{z_s}{B/K_{max}} \end{aligned} \tag{3.6}$$

3.3.3. Settlement depth

The settlement depth of the object is based on the soil bearing capacity and submerged weight of the object. The soil penetration resistance is the bearing capacity of the soil times a hyperbolic factor. A larger settlement depth results in a higher penetration resistance. When the object rests on the soil it applies a pressure, the soil penetration resistance applies a counter force. A simplistic way of modeling the soil penetration resistance is with a linear spring. To test if the soil penetration resistance force acts similar as the linear spring soil model some basic tests are done, which are shown in figure A.8 in Appendix A.
The difference between the model with and without soil penetration resistance is shown in figure 3.3 for the experimental sample. The blue line displays the displacement of the sample until the maximum length of the cable is reached, without any resistance. The red line shows the frame settlement when the soil penetration resistance is added. A settlement depth of 0.08 m is measured for sample 1. In section 4.7 the results of the experiments and the model are compared.

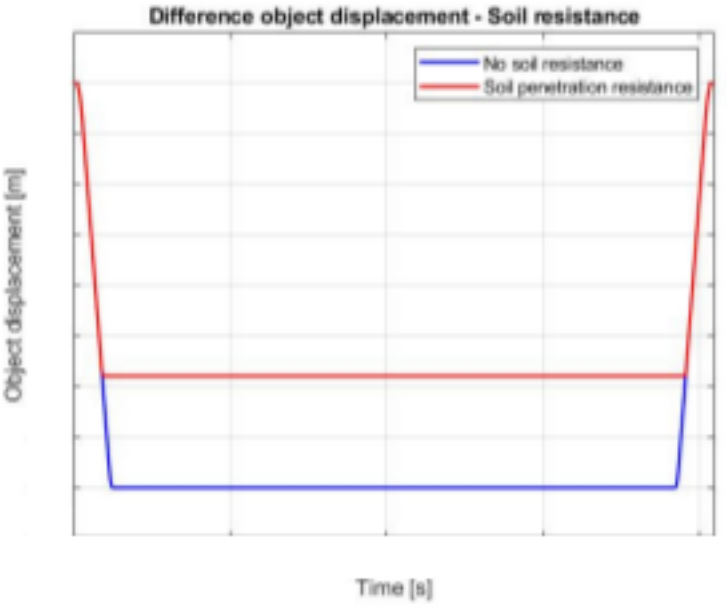

Figure 3.3: Sample 1 displacement with and without soil resistance. Soil penetration resistance based on Quiggin and Randolph model.

3.3.4. Soil suction resistance

In the uplift mode the soil resistance becomes negative, i.e. soil suction. This is also observed in other literature studies and defined as the reverse end bearing capacity mechanism. The process starts at P_0, which is the latest value of the soil resistance in initial penetration mode (see figure 3.2). When the soil depth decreases compared to the maximum settlement depth (z_{P_0}) the uplift mode begins. The suction increases during the lift and approaches the ultimate suction resistance. Figure 3.4 shows the suction resistance for the stainless steel sample 1.
The soil suction resistance from the model is compared with the results of the Excel file, to check if the results match (Appendix A figure A.9). Equation 3.7 is used to determine the soil suction resistance ($P_{suc}(z_s)$). The hyperbolic factor ($H_{UL}(\zeta_0 - \zeta)$) is zero at the start of the uplift and approaches 1.0, when ($\zeta_0 - \zeta$) gets large compared to the resistance ratio $A_{UL}(z_s)$.

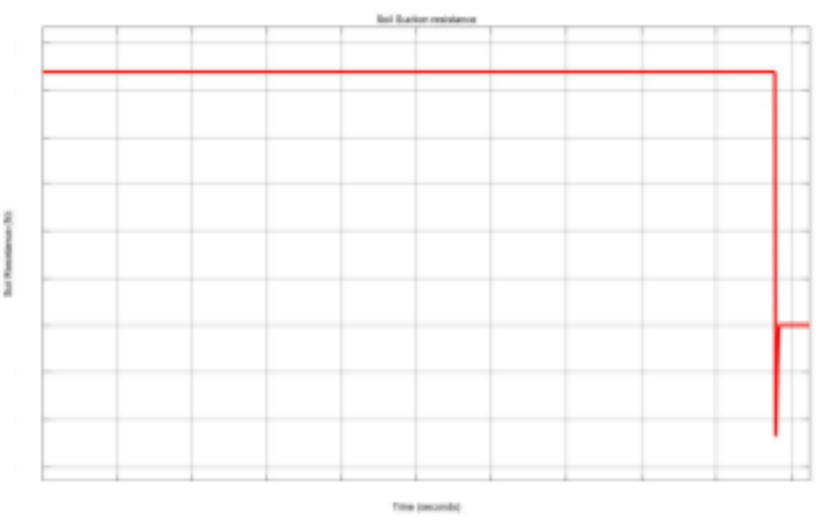

Figure 3.4: Soil suction for the experimental sample 1.

$$
\begin{aligned}
P_{suc}(z_s) &= P_0 - H_{UL}(\zeta_0 - \zeta)(P_0 - P_{u-suc}(z_s)) \\
H_{UL}(\zeta_0 - \zeta) &= \frac{\zeta_0 - \zeta}{A_{UL}(z_s) + (\zeta_0 - \zeta)} \\
A_{UL}(z_s) &= \frac{P_0 - P_{u-suc}(z_s)}{P_u(z_0)}
\end{aligned} \tag{3.7}
$$

According to the literature [41] the suction resistance can only be sustained for a limited displacement past the point where the net resistance becomes negative, after this point the suction decays while the uplift continues (green line in figure 2.19). This limitation on the suction resistance is implemented by using equation 3.8. The exponential factor $E_{UL}(z_s)$ depends on the actual settlement depth and the largest settlement depth during uplift (z_{P_0}). It limits the suction resistance to be no more than the ultimate suction resistance at the start of the uplift. As the uplift continues this exponential factor limits the suction even more.

$$
\begin{aligned}
P_{suc-lim}(z_s) &= E_{UL}(z_s) P_{u-suc}(z_s) \\
E_{UL}(z_s) &= exp(\frac{min(0, (z_s - z_{P_0})}{\lambda_{suc} z_{P_0}})
\end{aligned} \tag{3.8}
$$

3.3.5. Soil resistance over settlement depth

Figure 3.5 gives an overview of the soil penetration and suction resistance versus the settlement depth. The soil resistance is multiplied by the length of the object, in this case sample 1, to get the corresponding soil resistance of that geometry. The blue line is the soil penetration resistance, which increases with depth. It approaches the ultimate penetration resistance, which is displayed as a black dashed line. The soil suction resistance (red line) begins at the latest value of the soil penetration resistance, when the maximum settlement depth is reached and the uplift starts. The steep increase to the ultimate soil suction resistance followed by the decrease due to the limiting exponential factor is clearly shown. Comparing the graph to figure 2.19 confirms that the soil model behaves similar to the model of Quiggin and Randolph.

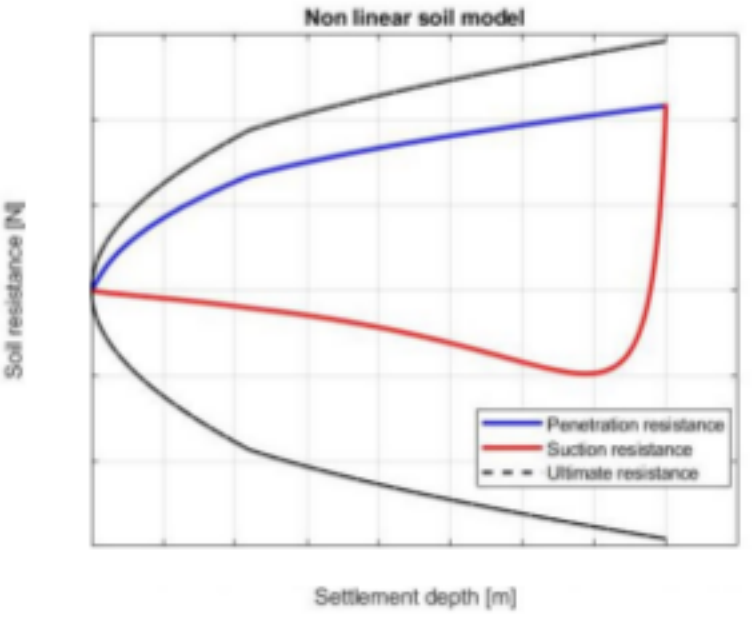

Figure 3.5: Non linear soil model overview. Soil penetration and suction resistance for sample 1.

3.4. Lifting force

The lifting force is the force the cable should apply to the object in order to release it from the soil. During the uplift the submerged weight of the object, suction resistance, adhesive force and added soil weight create a counter force, which the cable should overcome. At first, only the Quiggin and Randolph model was implemented in the Simulink model, which means only the submerged weight and soil suction created a counter force. As explained in section 4.7, this underestimated the required lifting force, since the adhesive force and added soil weight are missing. How these counter forces are added to the model is explained in the following subsections. In section 4.7, the estimated lifting force for sample 1 is determined using the Simulink model and compared to the experimental results. The model parameters are calibrated based on the results, resulting in a similar lifting force for the model and experiment. Now the model is validated, an estimation of the lifting force for the collector is made in section 3.5.

3.4.1. Adhesive force

Equation 2.15 is used to determine the adhesive force. The equation contains an adhesion factor (α), which depends on the material and type of soil. In table 3.1 the adhesion factors for this study are shown. The adhesion factors are based on the research of Bitar [59], who investigated the adhesion of the artificial and actual CCZ soil.

For the experimental sample the second part of equation 2.15 is neglected, because there are no grousers present. For the collector it is assumed that grousers (height m) interact with the soil during uplift. The

undrained shear strength and contact area also differ for the experiment sample and collector. These parameters can be found in an overview at the end of this thesis.

Table 3.1: Adhesion factors for the stainless steel sample 1 and the track rubber belt.

Interaction material surface - soil	Adhesion factor (α)
Stainless steel - Artificial CCZ soil	
Stainless steel - CCZ soil	
Track rubber belt - CCZ soil	

3.4.2. Added soil weight

The CCZ soil will flow on top of the tracks, when the tracks sink in the soft cohesive soil. During uplift a part of the soil stays on the tracks, this is called the added soil weight. The tracks are made out of multiple rubber belts with an open space in between them. These open spaces reduce the added soil weight, since a part of the soil can flow from the belts through these spaces. Equation 2.3 is used to determine the added soil weight, but since the open spaces are not considered in this equation a reduction factor is added. The reduction factor is based on the amount of soil that remained on top of sample 3 after it was lifted. Sample 3 has the same width as one track belt, so a similar amount of added soil weight per the length of sample 3 is assumed. This results in a reduction factor of % for the added soil weight of the tracks.

3.5. Required lifting force collector

Determining the required lifting force for the collector is essential to determine if the collector can be retrieved with the umbilical. As mentioned in chapter 2, the load limit of the umbilical is kN, which may not be exceeded. The model parameters are adjusted for the collector and the actual CCZ soil, these values can be found in chapter 9. Two scenarios are modelled; the short term and long term breakout. In both scenarios the adhesive force and added soil weight are equal. Figure A.11 and A.12 in Appendix A show the adhesive force and added soil weight for the tracks of the collector. According to the model, the collector settles about m into the soil, as shown in figure A.10 in Appendix A.

3.5.1. Lifting force - short term breakout

It is desired to avoid the short term breakout scenario, since a quick breakout results in a higher breakout force, as shown in literature and the experimental results. However, if a very quick retrieval is required for whatever reason, this should have been examined. Figure 3.6 shows the estimated required lifting force of the collector for a short term breakout. The same time interval as for the experiments is taken, which is within 15 seconds for a short term breakout. The lifting force increases when the uplift starts until the tracks start moving upwards from the soil. When the settlement depth decreases the lifting force also decreases, because the suction reduces for a lower depth. A small kink is observed just after the peak, this is the adhesive force becoming zero when the tracks are no longer in contact with the soil. The final lifting force is the submerged weight of the collector plus the added soil weight. An estimated required lifting force of kN is measured for the short term breakout, which exceeds the umbilical limits.

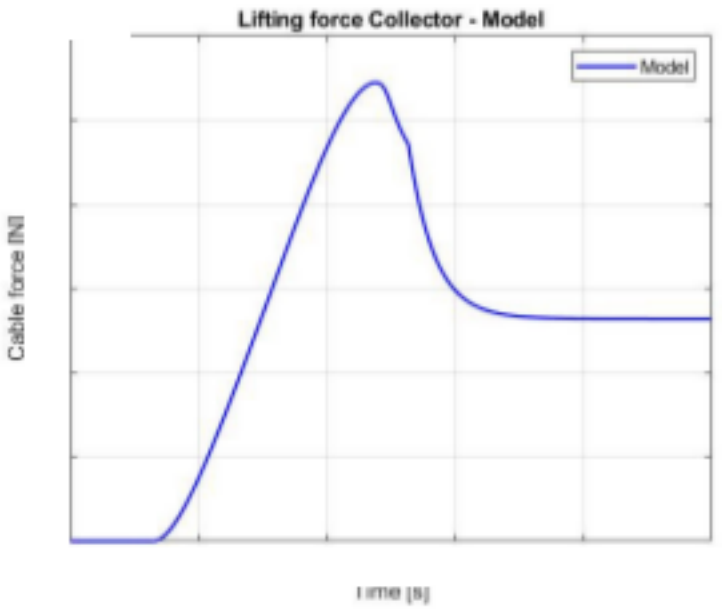

Figure 3.6: Required lifting force of the collector for a short term breakout.

3.5.2. Lifting force - long term breakout

The long term breakout is a more plausible scenario for the retrieval of the collector. The passive heave compensation (PHC) system is the reason why this is possible, despite the sea environment. Figure 3.7 shows the estimated required lifting force of the collector for a long term breakout. A breakout time of approximately 45 seconds is measured, which corresponds to the long term breakout time of the experiments. The lifting force slowly increases, due to the lower lifting velocity, until the tracks start moving out of the soil. Then, the lifting force reduces to the submerged weight plus the added soil weight. The estimated required lifting force of the collector during a long term breakout is kN, which is below the umbilical's load limit. This means that the collector can be retrieved using the umbilical, if a long term breakout is applied.

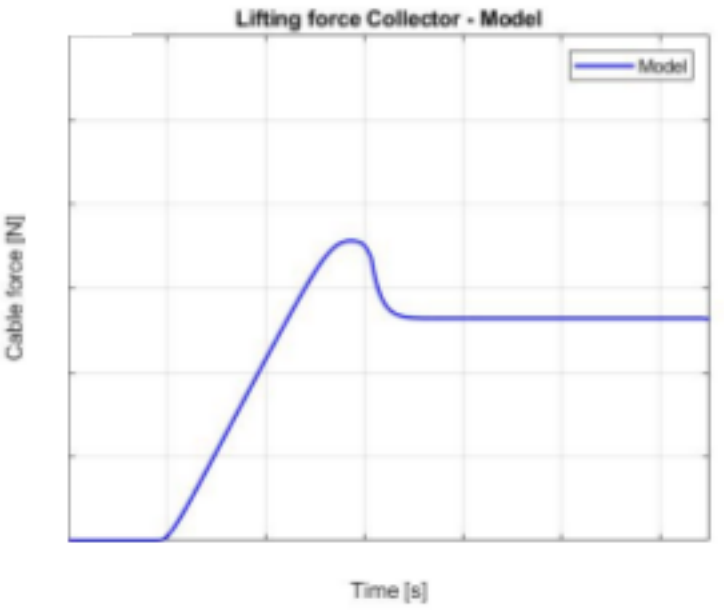

Figure 3.7: Required lifting force of the collector for a long term breakout.

3.6. Object design

The model discussed above gives an estimation of the breakout force of a rigid object. In order to add flexibility to the object, several blocks of the same model are connected by vertical springs. Figure 3.8 shows a schematic model of the flexible object. The long rectangular block represents the experimental frame or track suspension system. The outer blocks are connected with this suspension block through springs. In between the outer blocks, multiple blocks (2 to N-1) are connected by vertical springs. This way the created object can deflect in z-direction. The stiffness of the vertical springs determine how stiff the object becomes. Figure 3.8 shows two position: 1. when the object rests on the soil and 2. when the object is lifted.
Due to the lack of time, the flexible model is not built during this graduation project. However, for future research the rigid model described in this chapter can be used to built the flexible model as described in this section. It is assumed that the flexible model will generate a lower breakout force. This is observed during the experiments and is explained in chapter 4. The sides of the flexible object will release first due to deformation, so the suction and adhesive force reduce at the sides. Resulting in a lower total suction and adhesive force, thus a lower lifting force.

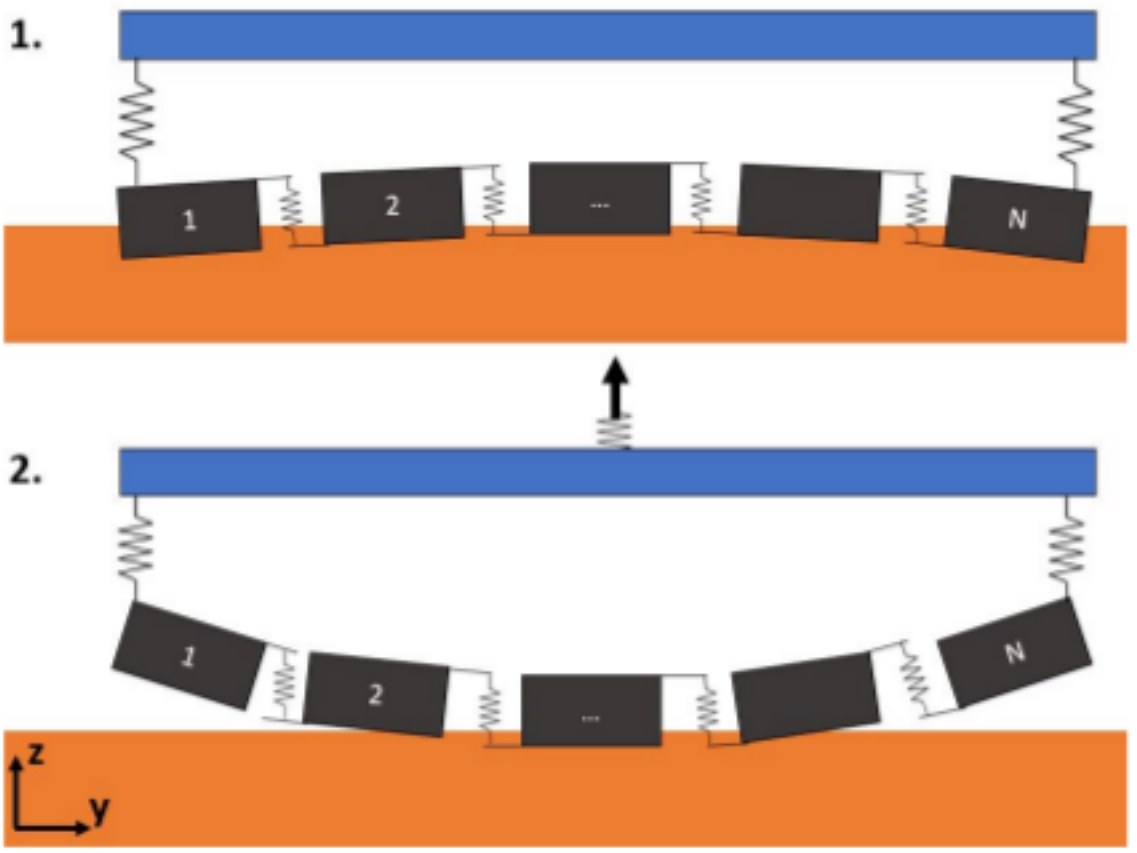

Figure 3.8: Schematic overview of the simulation of a flexible object in the model.

4

Experiments

Many experimental studies on the breakout of an embedded object are done, but none of them consider a flexible object. The flexibility is an interesting property and could affect the breakout mechanism and breakout force. The tracks of the collector consist out of multiple parallel rubber belts, which are flexible to some extent. To get a clear view on the effect of the flexibility on the breakout, experiments are conducted. Also, the design of the tracks and the amount of load reduction due to eccentric lifting are investigated by conducting experiments. The experiments will be discussed in detail in the following sections.

4.1. Introduction experiments

Multiple experiments are conducted, focusing on two main topics; flexibility and the breakout force. The goal of the experiments is to study the effect of a flexible object, in comparison to a rigid object, on the breakout force. To study this effect and to determine the required breakout force four experiments are performed, using five different test samples. The test samples are: a stainless steel plate (sample 1), a flexible rubber belt (sample 2) and the actual rubber belt from the tracks, in three different sizes (sample 3-5). In section 4.2 the test samples will be further discussed.
The first experiment focuses on the flexibility. The test samples, all with a different out of plane stiffness, are lowered into and extracted from the artificial CCZ soil. This process is repeated for a short term, intermediate and minimum breakout. The results of the different samples are compared and show the effect of flexibility on the breakout force. After the flexibility experiments, grousers are mounted on the belt sample and the assembly is tested. Sample 4 is used for these tests, since the sample size matches the grouser size. According to the literature survey, adding grousers increases the required breakout force. To investigate if this is true and how large the increase will be for a flexible object, the grousers experiment is conducted. The next type of experiment considers eccentric lifting. It has been shown in previous studies that an eccentric lift will reduce the breakout force. To investigate the effect of eccentric lifting of the tracks, a lift from the edge of the frame is conducted for samples 1 to 4. The final experiment will look into the effect of in situ time on the breakout force. Sample 3 is placed on the soil with different in situ times to see if it has an impact on the breakout force. All experiments will be discussed in more detail further along this chapter. A clear overview of the experiments and their goal can be found in table 4.1.

By lowering and extracting the different test samples from the artificial CCZ soil, the settlement depth, sample deflection, breakout time and breakout force are determined. By analyzing the results the effect of the flexibility on the breakout can be determined and an estimation of what will happen in the actual deep sea mining situation can be made. The results are used to calibrate and validate the Simulink model, this is discussed in section 4.7.

Table 4.1: Overview of the experiments, their goal and the samples that are used in each experiment.

Experiment	Goal	Samples
1. Flexibility	Investigate the effect of flexibility on the breakout force.	Sample 1-5
2. Grousers	Investigate the effect of grousers on the breakout force.	Sample 4
3. Eccentric lift	Investigate the effect of eccentric lifting on the breakout force.	Sample 1-4
4. In situ time	Investigate the effect of different in situ times on the breakout force.	Sample 3

4.2. Test samples

There are five samples that will be tested. The samples are picked based on their flexibility and size. In figure 4.1, the test samples are shown along with the number to which the sample will be referred in this thesis. Sample 1, 2 and 3 are made out of different materials, namely: stainless steel, reinforced rubber and EPDM (Ethyleen-Propyleen-Dieen-Monomeer) rubber. All samples have a different stiffness. If the stiffness of a sample is mentioned in this thesis the out of plane stiffness is meant.

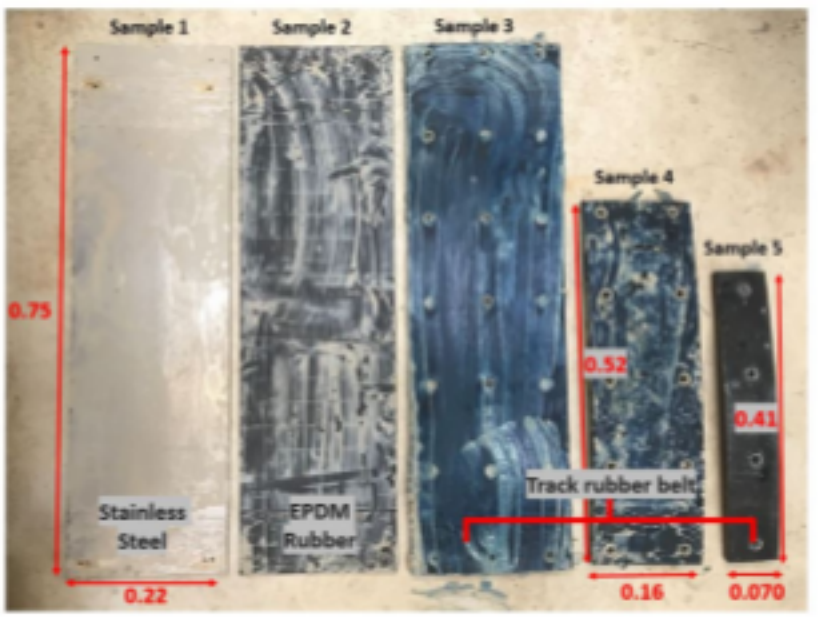

Figure 4.1: From left to right: 1) stainless steel plate, 2) EPDM rubber belt, 3) track rubber belt Allseas large, 4) track rubber belt Allseas medium, 5) track rubber belts Allseas small.

Sample 1 and sample 2 are the two extreme samples, a stainless steel plate and flexible rubber belt. They will clearly show the effect between rigid and flexible. Sample 3 is the sample of interest for Allseas and has an out of plane stiffness in between sample 1 and 2. To see how the stiffness of the belt changes over size and what impact a smaller contact area has on the breakout force, sample 4 and 5 are picked to test. As shown in figure 4.1, the samples from Allseas have perforations. The perforations are for the attachment of the grousers.
In table 4.2 the dimensions of the samples and their (dry) mass is shown. The samples are weighed with and without the sample attachment frame of 18.4 kg, since the weight is an important parameter when determining the breakout force. The length of the largest samples (1-3) is based on the boundaries of the container. They are about 3 track segments long (one segment is cm, see figure 2.3). Sample 4 is a smaller variant of the rubber belt from Allseas, which was already available at the company. Sample 5 is cut from the same belt sample 3 is taken from, but it is cut over its length in three equal parts to get a smaller belt. The length of sample 4 and 5 is based on the position of the perforations, such that it could be attached to the frame.
The variety of the samples will be used to gain insight into the effect of flexibility on the breakout. With the experimental results and the Simulink model, an estimation of the behaviour of the full size tracks can be made.

Table 4.2: Overview of the dimensions, contact area and mass of the samples.

	Dimensions (length x width x thickness) [m]	Contact area [m^2]	Mass sample [kg]	Mass sample plus frame [kg]
Frame	0.16 x 0.75 x 0.3	0.048	18.4	-
Sample 1	0.005 x 0.75 x 0.22	0.17	6.45	24.85
Sample 2	0.005 x 0.75 x 0.22	0.17	1.2	19.60
Sample 3	0.015 x 0.75 x 0.22	0.17	3.0	21.40
Sample 4	0.015 x 0.52 x 0.16	0.080	1.35	19.75
Sample 5	0.015 x 0.41 x 0.070	0.028	0.50	18.9

4.3. Test setup

The test set up that is schematized in figure 4.2 has been used in this study, since it enables to use a range of sample sizes, parameter control during testing is straightforward and last but not least the test setup is simple and its construction was at low cost. The test setup consists of three main components. In this section the design of the test setup is discussed and some of the parts are explained in more detail.

4.3.1. Design test setup

The test setup consists of three main components: a container with soil, a sample attachment frame and a lifting mechanism (figure 4.2). The function of the test setup is to lower and extract a frame that holds the test samples, from a container with artificial CCZ soil. The container (2.) is filled with the artificial CCZ soil and water. A lifting beam (5.) is assembled above the container and multiple pulleys (8.) are attached to it. Two steel cables (10.) with no stretch follow the pulleys, one to the winch and one to the bucket, which will be used to lower and extract the frame (9.). The load cell (7.) is attached underneath a pulley and connected to the frame to measure the load that the cable applies to the frame. The deflection sensor (3.) is assembled in the centre of the frame to measure the deflection of the different samples. Four displacement sensors (4.) are attached at the lifting beam and connected to the corners of the frame to measure the displacement and consolidation settlement of the sample and frame.
The winch (11.) is used to lower and haul in the frame. When hauling in the frame the winch is turned manually with a constant pace, this releases the frame from the soil. Another mechanism to create a breakout is the bucket (1.). First the frame is lowered onto the soil with the winch. Then the second steel cable is attached to the bucket. The pallet truck lifts the loaded bucket, which is connected to the frame by the steel cable. When the breakout starts the pallet truck is lowered, such that the bucket floats till the frame and sample break free.

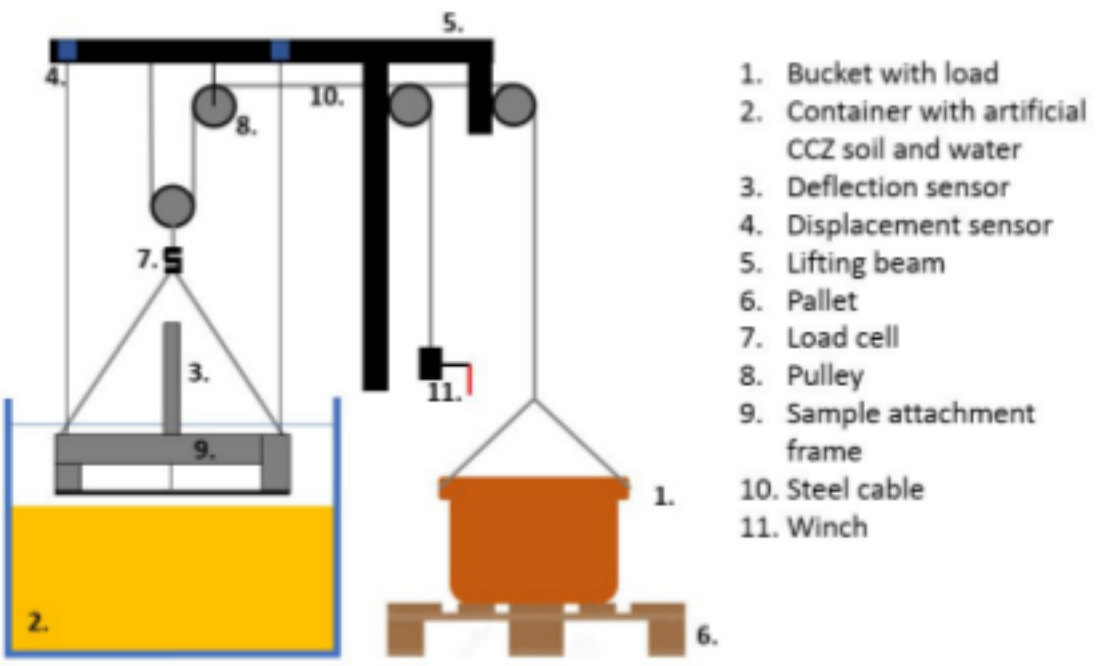

Figure 4.2: Test setup design. Side view.

Figure 4.3: a.) Design of the sample attachment frame, with the left beam still open and the right beam closed of with a plate. b.) Sample 3 attached to frame. c.) Sample 5 attached to frame, right beam slides to the left.

Sample attachment frame

The sample attachment frame is designed such that it can hold the different test samples. It is made out of multiple aluminum strut profiles and two threaded rods. The aluminum strut profiles have the advantage that parts can be easily assembled on them. If necessary the whole frame could be taken apart piece by piece. This makes it also possible to move the lower right beam horizontally along the frame, such that samples of different sizes can be attached, figure 4.3. Since the open sides of the strut profiles will cause more resistance, they are closed with plates. The small plates contain holes, such that the strut profiles still fill up with water.
The samples have holes near the edges, with long countersunk bolts the samples are attached to the frame. By tightening or loosening the threaded rods in the centre of the frame a tension can be applied to the sample. The sample attachment frame is 0.75 meter long, 0.30

meter wide and has a height of 0.16 meter. At each corner of the frame a ring is attached, such that a stable lift can be executed with the steel cables. As the samples do not differ much in weight, the lift is always applied from the centre without the frame tilting. A smaller aluminum strut profile is vertically assembled to the frame, such that the deflection sensor can be attached.

Artificial CCZ soil

The amount of CCZ soil was limited available at Allseas, so an artificial soil is made from kaolinite clay with similar characteristics for testing. The soil characteristics for the artificial soil can be found in figure B.4 and B.5 in Appendix B. This artificial CCZ soil is placed in the container and mixed with water. A soil strength of 1.2 kPa at the surface and 2.0 kPa a few centimeters below is achieved by mixing the artificial soil, this is measured with a miniature vane test. How the soil tests are conducted will be discussed in section 4.4.1.
When applying a pressure on the soil with the frame, the soil stress distribution must be considered. The soil stress distribution shows the range to where the pressure has an impact in the soil. It must be taken into account to prevent the boundary effect of the container walls to affect the test results by altering the stress field. To determine the dimensions of the soil layer the soil stress distribution graph in figure 4.4 is used. The frame and samples are rectangular shaped but the graph considers square footings and infinite strip footings, so a red line is drawn in the figure which is an estimation of the soil stress distribution for a rectangular footing. Following the red line in the graph shows that the width of the container in x-direction must be approximately 1.2 times the width of the sample, thus at least 0.26 meter at each side of the sample. The container has to have a minimum depth of 2.7 times the width of the sample. Taking this into account, results in a required soil layer of 0.60 meter high and 0.75 meter wide for the largest sample with a width of 0.22 meter. The width of the samples is the dominant parameter, since a large part of the load acts on the sides closest to the centre, as shown in figure 4.4.
The selected container for the experiments is 1.25 meters wide, 0.80 meters long and has a height of 1.00 meter, so it meets the requirements. On top of the soil a layer of water is added to fully saturate the soil.

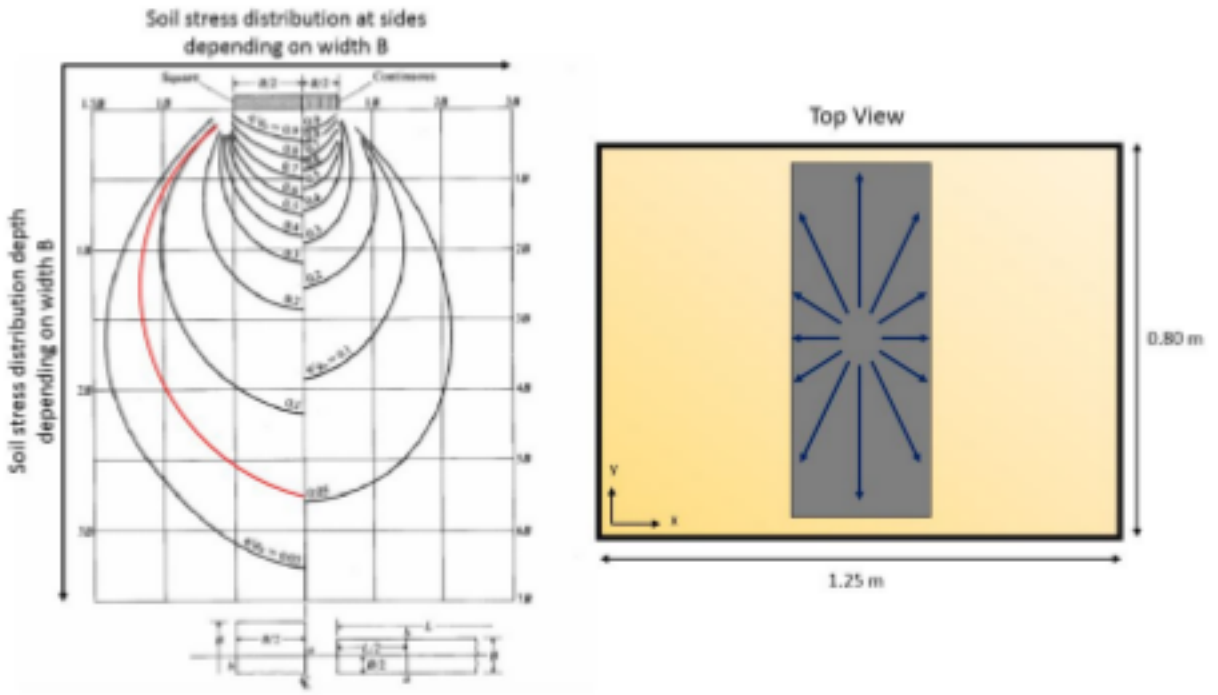

Figure 4.4: Left: soil stress distribution graph. Right: top view of the container with sample.

Breakout using the winch

The winch is used to find the required breakout load of the sample. By manually hauling in the frame at a constant pace, a load is applied on the frame. The load cell measures the applied load over time. For the breakout with the winch, the breakout time will be short term. The breakout time is defined as the time between the breakout force increasing till the object is extracted. In the experiments a short term breakout time interval of approximately 8 to 15 seconds has been observed. All breakouts that happen within 15 seconds are considered as a short term breakout. During the short term breakout, undrained conditions are expected.

Breakout using bucket mechanism

The bucket mechanism is used to find the minimum breakout force and to investigate the time dependent behaviour. The minimum breakout force is the least amount of force that is required to release the object from the soil. To find the minimum breakout force, the bucket is filled with sand till it is equal to the sub-

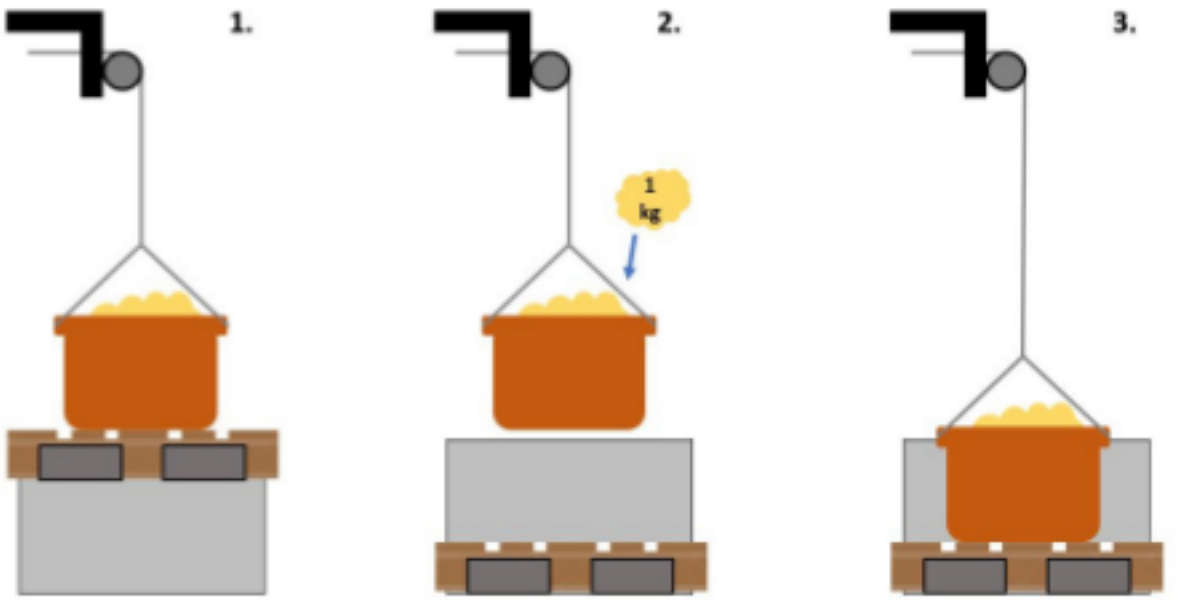

Figure 4.5: 1.) Bucket filled with sand and lifted with pallet truck (no load on frame). 2.) Pallet lowered, bucket floats and applies load on frame. Extra mass added with sand. 3.) Frame released from soil, bucket has fallen on pallet.)

merged mass of the sample and frame. First, the frame is lowered onto the soil using the winch. Then, when it is time to retrieve the frame, the bucket is lifted with the pallet truck and is attached to the steel cable (figure 4.5 - 1.). The pallet truck is lowered such that the bucket floats. After one minute the first extra kilogram of sand is added to the bucket (figure 4.5 - 2.), this process is repeated till the bucket falls back on the pallet and the frame is released (figure 4.5 - 3.). The final measured value before the release is the minimum breakout mass, which can be translated to the minimum breakout force. The breakout time for the minimum breakout is defined as long term, which means the required time interval for the object to break free is larger than 15 seconds. A longer breakout time causes (partially) drained conditions, which lowers the breakout force.
Intermediate breakouts are also conducted with the bucket mechanism. The intermediate breakout is estimated by taking a load in between the minimum and the short term breakout. This load will be added to the bucket and the same process as the minimum breakout is repeated. Semi undrained conditions are expected to occur. The intermediate breakout, together with the minimum and short term breakout, shows the effect of time on the breakout force. The full scope of undrained to drained conditions are covered.

Load cell

A S-type load cell is used in the experiments. The load cell measures the load of the winch or bucket, acting on the sample attachment frame. It is placed directly above the frame where the steel cables of the frame meet. The load cell is calibrated by applying a known load and measuring this load on an external device along with the corresponding voltage. These values are implemented in a Virtual Instrument (VI) in the program Labview. Via this VI in Labview the load can be measured, stored and analysed. Figure B.1 in Appendix B shows the calibration graph of the load cell. The load cell has an accuracy of approximately 1% of the capacity, which results in an accuracy of 2 kg. A precision of 0.3 kg is measured and the selected sample frequency during breakout is 1000 Hz. This means thousand data points are measured every second.

Figure 4.6: S-type load cell with a capacity of 200 kg.

Deflection sensor

At the centre of the frame the deflection sensor is attached to a vertical strut profile, as shown in figure 4.7. This sensor measures a change in displacement through a thin rod that can move in and out of a tube. The range of the sensor is limited to a 5.5 cm displacement. The deflection sensor needs to be assembled at a place where it will not go below the water, thus the thin rod is extended such that it can reach the sample from a higher position. Since the original thin rod was too thin and started bending, it is replaced with a thicker, stiffer aluminum rod. The rod is guided by a plate near the sample, to make sure the rod does not bend and remains in the same position. The deflection sensor shows how much a sample deflects at its center. This information is useful when investigating the behaviour of the flexible samples in the soil. The sensor is connected to the VI in Labview to measure and store the displacement.

Before doing tests with the deflection sensor it is calibrated. Different objects, of which the height is measured, are placed underneath the thin rod. The corresponding voltage is written down and added to the VI in Labview, such that it shows the correct value of the deflection sensor. The calibration graph can be found in figure B.2 of Appendix B. The deflection sensor has an accuracy of 0.02 mm and a precision of 0.01 mm.

Figure 4.7: Sensor that measures the deflection of the sample.

Figure 4.8: One of the four displacement sensors that measures the consolidation settlement.

Displacement sensor

Four displacement sensors are attached to the lifting beam and connected to the corners of the frame to measure the consolidation settlement and behaviour of the frame and sample. Figure 4.8 shows one of the sensors. The measurements of the sensors are used to make an estimation of the behaviour of the sample when it is lowered onto the soil and to determine the consolidation settlement over the settlement time. The cables of the sensors have a slight angle when connected to the frame, since the sensors are placed on the lifting beam. These angles are very small, between 1 and 2.5 degree, but to be as accurate as possible they are included when determining the displacement.

The sensors are calibrated by extracting the sensor's cable and measure how far it is extracted, together with the corresponding voltage (see figure B.3 in Appendix B). Again, these values are added to the VI in Labview, such that it shows the correct displacement via Labview. All four displacement sensors have an equal accuracy and precision of 0.7 and 1 mm. The sample frequency during settlement time is 10 Hz.

4.4. Test parameters

Before the start of the experiments a few test parameters should be investigated. If the test parameters are defined correctly the results will be more representative of the actual situation.

4.4.1. Soil shear strength

As earlier mentioned, the soil used for the experiments is an artificial soil with similar characteristics as the CCZ soil. The shear strength of the soil is a dominant parameter when determining the bearing capacity of the soil and settlement, which means that it will also affect the breakout. CCZ soil has a shear strength of approximately kPa. To measure the shear strength of the artificial soil, miniature vane tests are done. The miniature vane test device is shown in figure 4.9.

Figure 4.9: The miniature vane test device to measure the shear strength of the soil. The left picture shows one of the shear tests in the container.

First, the soil is placed in a steel watertight container till it has the required depth, as described in section 4.3.1. Then, the container is filled with water. The soil rested for one week, such that the soil settled and is fully saturated. Now, the first shear strength tests could be done. The water was removed such that the soil was better accessible. Different spots on the surface of the soil are tested (figure 4.9). The miniature vane device is placed on the soil and the red ring is twisted clockwise until the vanes turn loose. The pointer indicates the value of

the shear strength in kilograms per square centimeter. However, since a bigger vane with a diameter of 47.6 is used for the soft soil, a multiplier should be used. The multiplier for this type of vane is 0.2, to get the actual shear strength. All tests have the same result, namely a shear strength of 0.1 kg/cm^2. This value multiplied by 0.2 and converted to kPa, gives a shear strength of 1.96 kPa.

Besides doing shear tests on the undisturbed soil, the soil is also disturbed. The soil is remoulded by slicing through the soil and scooping out some pieces, afterwards the soil is flattened with a shovel or by hand. Then, the soil shear strength is measured again. The shear strength results of disturbed and undisturbed are similar, which means that the shear strength is not affected when disturbing the soil at the surface during a breakout. Thus, after a breakout the soil can be flattened and another experiment can be executed.

Before an experiment is executed the shear strength test is done at 3 different spots below the frame, two at the sides and one in the centre. This is done to confirm that the shear strength stays constant. When the water layer on top of the soil is added, it is observed that the top layer becomes softer. The layer has a measured shear strength of 1.2 kPa. The shear strength increases with depth, since a few centimeters below this measured layer the shear strength is approximately 2.0 kPa as earlier measured.

4.4.2. Translation bucket weight to load cell

The load in the bucket that is required to break the sample free from the soil can increase up to a high amount. For safety reasons, the extra pulley just above the load cell is added to the test setup. The basic theory of a pulley is that it halves the load, such that half of the required breakout load has to be applied to the bucket. However, this theory did not match practice, when looking at the results of the load cell. The load cell values where not doubled at all. The reason for this can be found in the efficiency loss of the pulley. To get an insight in the translation between bucket weight and the load cell a test is done.

The frame is loaded with multiple weights, such that it is very heavy and fixed to its position. When applying a load to the frame with the bucket, the frame will not move but the load cell does measure the applied load. Multiple loads are applied with the bucket and the corresponding values of the load cell are noted. The graph in figure 4.10 shows the measurements and the belonging equation. So when the bucket breakout mechanism is used, this equation shows how much the bucket should weigh to get the correct load on the frame.

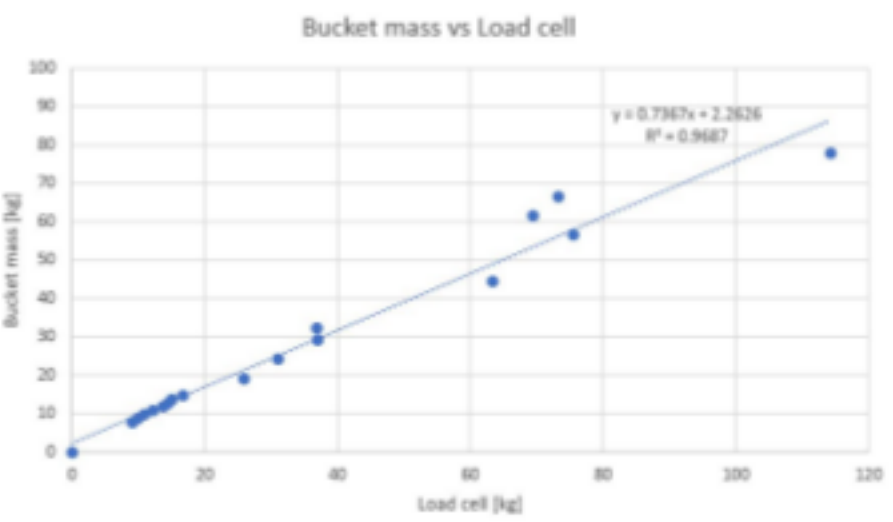

Figure 4.10: The relation between the bucket mass and load cell.

4.4.3. Pressure on the soil

The collector has a submerged mass of tonnes and applies a pressure of approximately kPa on the seabed. This pressure will cause the tracks to sink. To get accurate results, the pressure is simulated by adding weights on top of the sample attachment frame (figure 4.11), such that a similar pressure on the soil is created. In table 4.3 an overview of the required submerged mass per sample to get a pressure of kN per square meter is given. The final column shows the actual submerged mass of the frame and samples with the extra added weights. Before extracting a sample, the weights are removed for safety and to simulate the situation of the collector's frame mass being lifted before the tracks are released. The experimental submerged mass is created with weights of 12.3 and 5.6 kg, which were available in the laboratory. Adding these weights results in a submerged mass that is close to the required submerged mass to mimic the pressure. It is expected that the difference will not have a major affect on the breakout results.

Figure 4.11: Added extra weight to mimic pressure on soil. One blue weight has a mass of 12.3 kg.

Table 4.3: Overview of required extra added submerged mass to create a pressure on the soil of kPa.

Sample	Contact area [m^2]	Submerged mass of frame and sample [kg]	Required submerged mass of frame and sample to apply kPa [kg]	Experimental submerged mass of frame and sample with extra weight [kg]
1	0.17	15.8	100.51	97.55
2	0.17	12.3	100.51	94.05
3	0.17	12.8	100.51	94.55
4	0.080	12.4	47.30	43.06
5	0.028	12.0	16.55	16.50

4.4.4. Sample flexibility

Tests are conducted using five test samples with different out of plane stiffness in order to investigate the effect of flexibility. The out of plane stiffness depends on the material properties and sample dimensions. Applying a tension to the sample can also change the stiffness. The tracks of the collector are under tension during operation, but what if you reduce this tension? Will it have an effect on the breakout force? To see the effect, all samples are tested with an without tension. The sample attachment frame is built such that it can apply a tension to the sample by tightening the threaded rods in the centre of the frame, which allows testing of the individual samples with different stiffness.
To measure the out of plane stiffness of a sample, deflection tests are done. The samples are attached to the sample attachment frame with or without tension applied to it. Without tension the attachment points of the frame have the same distance as the length of the sample, so the frame does not apply a tension. When the sample is attached, it is placed on top of two beams, such that both ends of the sample are fixed. A load of 5.6 kg is placed at the centre of the sample and with the deflection sensor the deflection is measured. The 5.6 kg load is selected because of its size and load being suitable for all samples. The deflection test process is repeated every time a new sample is attached to the frame. In table 4.4 the results of the deflection tests can be found and the corresponding stiffness. The out of plane stiffness is calculated using equation 4.1.
The results of sample 2 with and without tension in table 4.4 show no difference, due to the boundary conditions of the test setup. Therefore, sample 2 is cut smaller, such that it can extend further. For comparison purpose it is cut in the same dimensions as sample 4. In the thesis there will be referred to sample 2 long and short, to define which of the two is used.

$$k = \frac{F_{load}}{\delta} \tag{4.1}$$

Table 4.4: Deflection at centre of sample and corresponding out of plan stiffness.

Sample		Deflection [m]	Out of plane stiffness [kN/m]
1	No tension	0.00100	54.94
1	Tension	0.00100	54.94
2 (long)	No tension	0.0255	2.15
2 (long)	Tension	0.0255	2.15
2 (short)	No tension	0.0178	3.09
	Tension	0.0122	4.50
3	No tension	0.0155	3.54
	Tension	0.00620	8.84
4	No tension	0.0110	4.99
	Tension	0.00204	26.93
5	No tension	0.00502	10.94
	Tension	0.00130	42.26

4.5. Test procedure

In the following section, the test procedures of the four experiments types is discussed. The basic test procedure is explained in section 4.5.1, for the flexibility experiment. The other experiments have broadly the same procedure but with slight adjustments.

4.5.1. Flexibility experiment

The goal of the flexibility experiment is to investigate the effect of flexibility on the breakout force compared to a rigid object. The five different samples are used to show this effect. As earlier mentioned, all five samples have a different out of plane stiffness, which individually also varies when under tension or not.

At the start of an experiment, the to be tested sample is attached underneath the sample attachment frame. Tension is applied if required and a deflection test is done. The frame is installed underneath the load cell, as shown in figure 4.12 for sample 3. To mimic the pressure on the soil the extra weights are added to the frame. Then, the soil is flattened and shear strength tests are executed. When everything is ready, the winch lowers the frame onto the soil. Labview, the digital measuring software, is started at the moment the sample is lowered, and measures the displacement. When the frame rests on the soil, the immediate settlement has already taken place. Each sample will settle for half an hour. After half an hour the extra added weights are removed and the sample is extracted from the soil. The extraction can be done via two methods; the winch or the bucket mechanism. The winch will haul in the frame at a constant pace till it is released. It is a short term breakout, so within a time interval of 15 seconds the sample breaks free. The measured load in the load cell shows the maximum required breakout load for that sample.

Figure 4.12: Sample 3 attached to frame to conduct flexibility tests.

The other breakout mechanism is the bucket. It will be used to find the minimum breakout and to do an intermediate breakout test. As explained in section 4.3.1, the bucket is filled with sand corresponding to a specific load and lifted with the pallet truck. It is attached to the steel cable and thus the frame. When the pallet truck is lowered, the bucket will float till the sample is released from the soil (figure 4.5). In case of the minimum breakout, the submerged mass of the frame plus sample will be added to the bucket and every minute an extra 1 kg of sand is added until the sample breaks free. For the intermediate breakout, a load between the minimum and short term breakout load is added to the bucket. These three breakouts (i.e. short term, minimum and intermediate breakout) are conducted for all samples. The results are shown in section 4.6.

4.5.2. Grousers experiment

The pistenbully tracks contain grousers, which have a similar design as skirts. From literature studies it is known that adding skirts to a foundation, results in a higher breakout force. To get an insight into the effect the grousers have on the breakout force, this experiment will be conducted. To recreate the grouser a simple L-shaped stainless steel profile is used. It is recycled from another experiment done at Allseas so the size was already determined. However, the two L-shaped profiles fitted perfectly on sample 4, so the grousers experiment is executed using this sample. Sample 4 is already tested with and without tension in the flexibility experiment, so these results are available to compare with. Now, the results of sample 4 with the two grousers attached has to be generated. The tests with the grousers are also conducted with and without tension. The tension is kept the same as sample 4 without grousers (27 kN/m), so it is easier to see what the effect of the grousers on the breakout is. Figure 4.13 shows what sample 4 looks like when the two grousers are attached. When sample 4 with grousers is attached to the frame, the same basic procedure as described in the flexibility experiment is followed. Only the winch is used, since these results are easier to compare with the already generated results from the flexibility experiment due to the similar breakout time. Sample 4 with and without the grousers is also tested during an eccentric lift. The eccentric lift experiment is further explained in the next section.

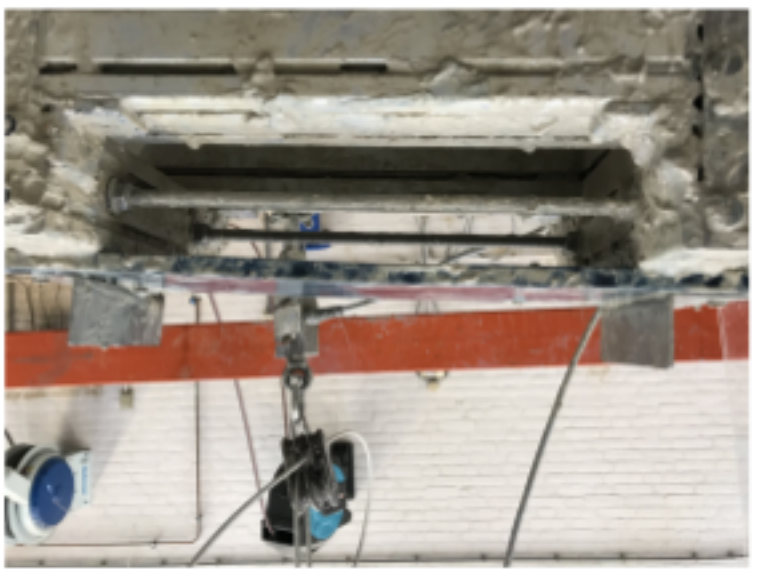

Figure 4.13: Grousers attached to sample 4.

4.5.3. Eccentric lift experiment

Literature studies show that an eccentric lift can reduce the required breakout force. However, this is tested with rigid objects, thus to test the effect of eccentric lifting on flexible objects this experiment is executed. The results show the amount of load reduction, which could be useful if the umbilical limits are exceeded.

Sample 1, 2, 3 and 4 are tested in this experiment, also with and without tension. The same basic procedure as in the flexibility experiment are followed, but this time the steel cables of the frame have a different configuration. Figure 4.14 shows the new setup. The right cables are shorter (42 cm) than the cables on the left (61 cm), so first the right side of the frame is lifted, followed by the left side. The behaviour of the frame and the attached sample during an eccentric lift is further discussed in section 4.6.2. The eccentric lift is conducted by applying a lifting force with the winch.

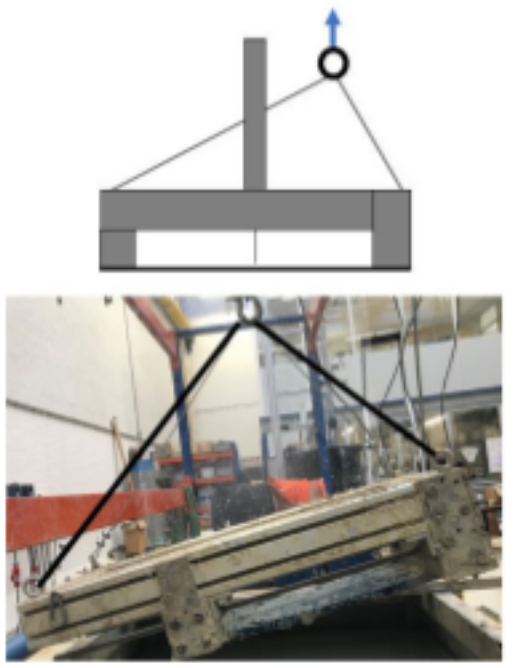

Figure 4.14: Setup of frame for eccentric lifting.

4.5.4. In situ time experiment

The in situ time is the amount of time an object spends at the seabed until it is extracted. The longer the in situ time the harder it is to extract an object, according to the literature survey. This is because the soil can regain its strength, excess pore pressures have time to diffuse and the soil flows back around the object.

Again, the same basic procedure as in the flexibility experiment is followed, but with different settlement times. Only sample 3 will be tested in this experiment due to the lack of time. To use time efficiently, sample 3 is placed on the soil at the end of the day, left there for the night and extracted the next morning. This is an in situ time of approximately hours. To get the results of a more extremer case, sample 3 is also put in the soil for one whole weekend (hours). Unfortunately, this test can only be done once due to time. The in situ time experiments are conducted with the winch.

4.6. Results

The results of the experiments are shown in this section. There are many results, so in order to keep it structured sample 3 is focused on. The results of the other samples can be found in the Appendix B.
There is no tension applied to the samples, unless else is stated. The breakout force to which is referred in this section, is the measured breakout load minus the submerged weight of the frame and sample.

4.6.1. Soil behaviour

There are three different layers of soil observed, as shown in figure 4.15. The first layer is fluidized soil, the soil is very soft and feels almost as a fluid. Based on the amount of movement in the container and the settlement time, the layer changes in thickness between approximately to cm. The second layer is the soft cohesive soil, that feels like mud. It adds some resistance to the frame, but during the immediate settlement the frame and sample sink easily through this layer. It is difficult to measure the thickness accurately but an estimation of to cm is made. The shear strength of the second layer is approximately 1.2 kPa. The final layer is the more solid artificial CCZ soil (2.0 kPa), which is the layer the frame and sample are able to rest on. When the frame stands on this layer during the half hour settlement time it does not settle further, according to the consolidation settlement measurements.

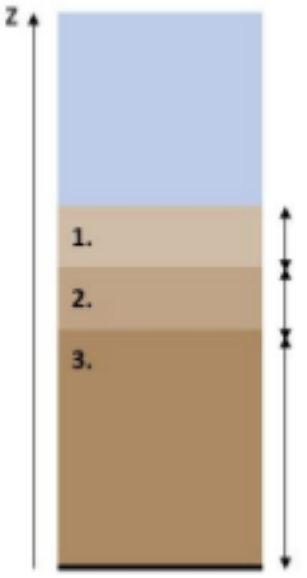

Figure 4.15: Three types of soil layers are observed in the container, as shown in this figure.

4.6.2. Behaviour of frame and sample

To determine the behaviour of the frame and sample, the deflection and displacement sensors are used. The displacement sensors measure the position of the frame and the consolidation settlement. According to the results, the consolidation settlement for all samples is very little for a settlement time of half an hour. Only about a few millimeters deep, which cannot be measured accurately with the selected displacement sensors. It is assumed that the consolidation settlement is approximately equal for all samples.
However, the results of the displacement sensors do show the position of the frame. The measurement starts when the frame is just above the soil and stops when it stands on the soil. The results show the pitch, roll, height and deflection of the sample. The yaw is zero in all cases. Figure 4.16 shows the coordinate system of the frame, based on this coordinate system the results are shown. The corners of the frame, where the displacement sensor cables engage with the frame, are labelled such that the results are easier to read. The results of one side on the y-axis (P4 to P1) and one side on the x-axis (P1-P2) are discussed in this section, because it is a rigid frame.

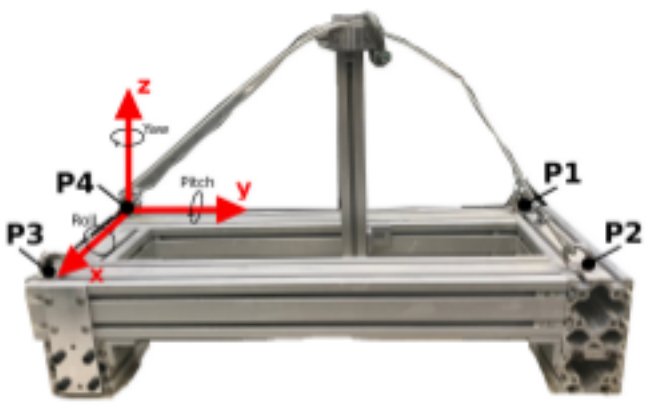

Figure 4.16: Coordinate system of the frame and labelled corners P1 to P4.

It is assumed that the displacement of the corners of the samples (where the sample is attached to the frame) is similar to the measured displacement of the corners of the frame. To determine the position of the frame in between the four measured points, linear interpolation is applied since the frame is rigid. The position of the samples in between the four measurement points cannot be determined with linear interpolation due to the flexibility. Further along this section, the behaviour for the flexible samples is discussed.
For each individual test the behaviour of the frame and sample are slightly different, but will not show extreme differences. Multiple measurements are done, but in this section only a single measurement of sample 3 is shown.

Figure 4.17 shows the pitch of the frame with sample 3 attached. The left figure shows the start position of the frame just above the soil (black circles) and the final position at the soil (red circles). On the right figure, the angle of the frame and the height over time is shown. The time interval is based on when the pitch angle

starts to increase. For sample 3, the pitch angle never exceeded a 7 degree angle. The pitch behaviour of the frame with the other samples attached is displayed in figures B.6, B.7, B.8 in Appendix B. Different heights can be observed in the graphs, because the start position above the soil differs per test. The pitch of the frame is measured all in the same direction, because the soil had a slight height difference which was observed when analysing the results. Thus all samples tilted to the same side.

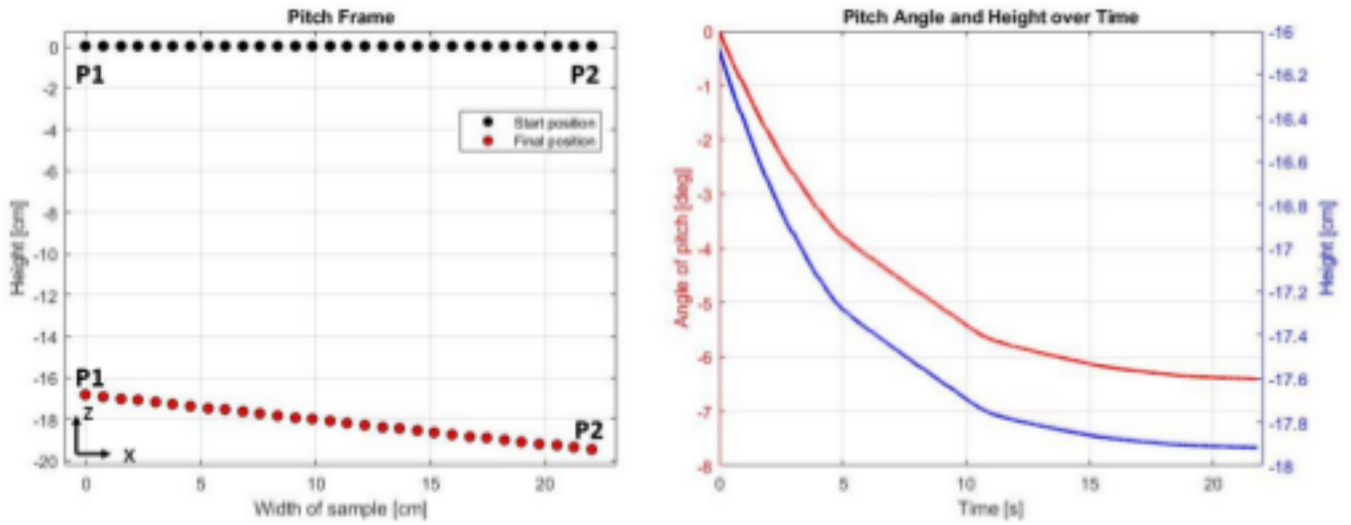

Figure 4.17: Sample 3. Left: Pitch position of the frame (side view) at start and final position. Right: Pitch angle and height over time.

The same graphs are made for the roll behaviour of the frame. Figure 4.18 shows the roll of the frame with sample 3 attached and the roll angle the frame experiences over time. The roll angle is always lower than the pitch angle, probably due to the structure of the soil surface and the smaller width. The graphs for the other samples can be found in Appendix B (figures B.9, B.10 and B.11).

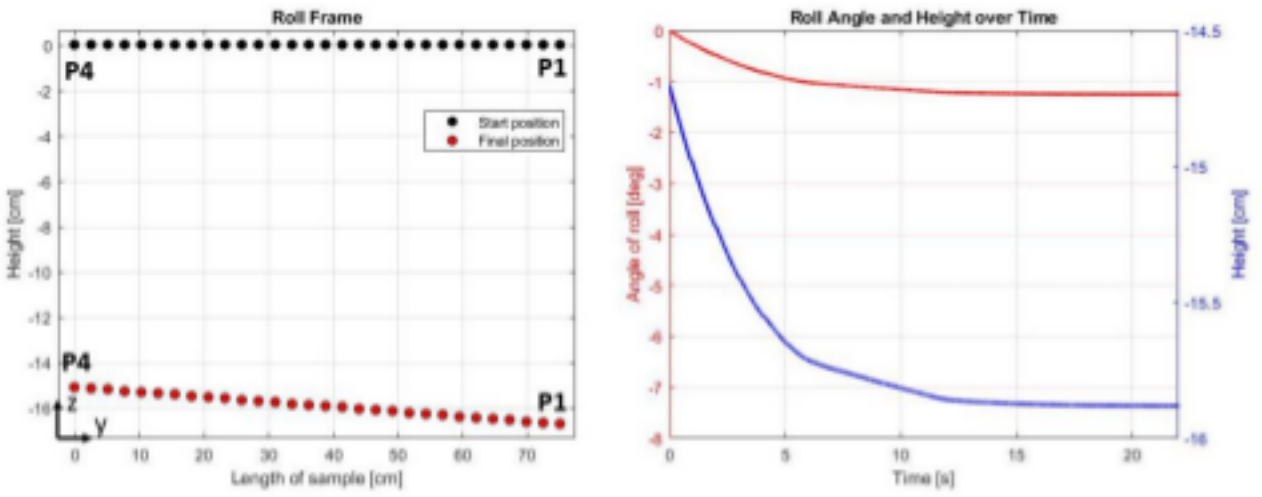

Figure 4.18: Sample 3. Left: Roll position of the frame (side view) at start and final position. Right: Roll angle and height over time.

The behaviour of the flexible samples in z-direction will be different from the frame, due to the flexibility. The deflection sensor measures how much the sample deflects at its centre. To make an estimation of the behaviour of the rest of the sample, the Lagrange interpolation method is used. The deflection of sample 3 when it rests on the soil is shown in the upper left graph of figure 4.19. Below zero height the soil starts, defined with a yellow/brown background. The dashed line is the initial condition of the sample, so when there is no deflection. The upper right graph in figure 4.19 shows the increasing deflection when it is lowered onto the soil. Due to the winch being jammed sometimes and the vibrations of the sample during lowering, there are some bumps in the graph.
It is also interesting to see the behaviour of the flexible sample when it is extracted from the soil. During the uplift of the frame (perfect centric lift), the flexible sample sticks to the soil while the frame is already released. The deflection of the sample just before breakout is shown in the bottom left graph of figure 4.19. The bottom right graph in figure 4.19 shows the deflection of sample 3 over time. In this graph the sticking behaviour is shown by the inverse peak. The sample deflects to the opposite side, then releases from the soil and goes back to its initial condition.
The deflection graphs for the other samples can be found in Appendix B (Figures B.12, B.13 and B.14). For some graphs the start position of the deflection sensor during breakout is different than the final position of lowering, this is because the deflection sensor is lowered before the breakout such that it can extend over

its full range. It happened often that the deflection sensor was too short to measure the full motion, so this is fixed by lowering the deflection sensor before a breakout. The small peaks, that look like noise, are the vibrations of the sample.

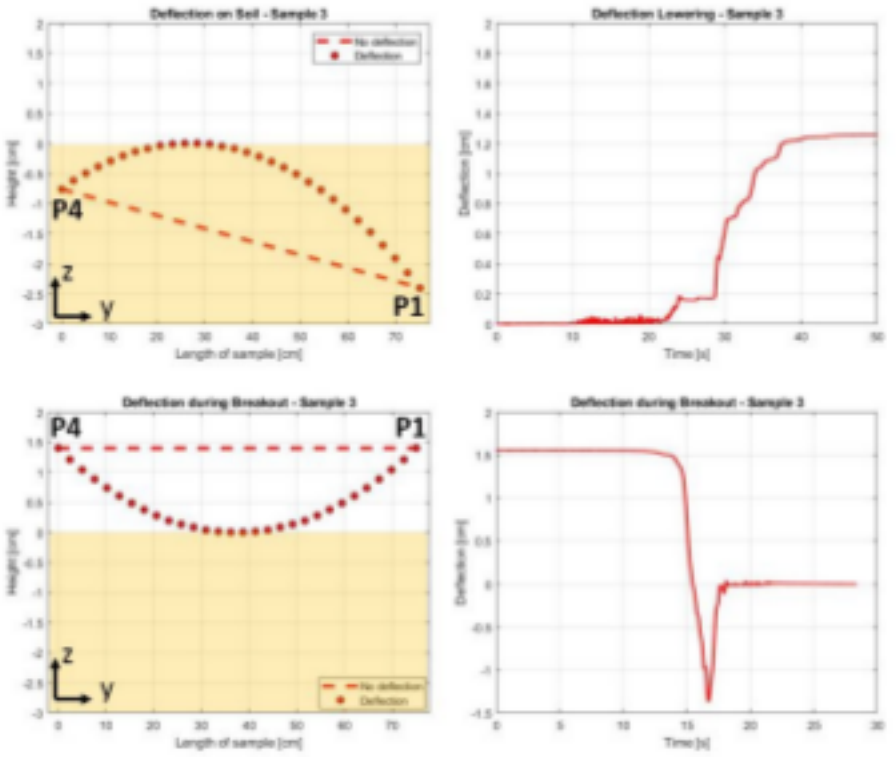

Figure 4.19: Top left: Deflection of sample 3 on soil (side view). Top right: Deflection of sample 3 over time, when lowering the frame onto the soil. Bottom left: Deflection of sample 3 just before breakout (side view). Bottom right: Deflection of sample 3 over time, during breakout.

The behaviour of the frame and sample when it is lowered onto the soil is discussed above. Now, the behaviour of the frame and sample during breakout will be discussed. There are two mechanisms to create a breakout; the winch and bucket mechanism. The breakout with the winch for sample 3 is shown in figure 4.20 on the left and the breakout using the bucket mechanism on the right. As shown in the graphs, the winch is a short term breakout (breakout time below 15 seconds) and the bucket mechanism creates a long term breakout. The long term breakout shows small steps in applied load, which are the extra added one kilograms of sand. Adding the extra load to the bucket continues till a breakout occurs and the minimum breakout load is found. In the short term breakout graph of sample 3 two peaks are observed, this is due to one side breaking out first followed by the other side (second peak). This behaviour repeated in multiple tests also for other flexible samples, probably because of the ability to deform. If one side releases first, the rest of the sample follows piece by piece just like velcro. The first peak is taken as the required short term breakout mass. The applied mass is measured by the load cell. The behaviour during breakout for the other samples can be found in figures B.15, B.16, B.17 and B.18 in Appendix B.

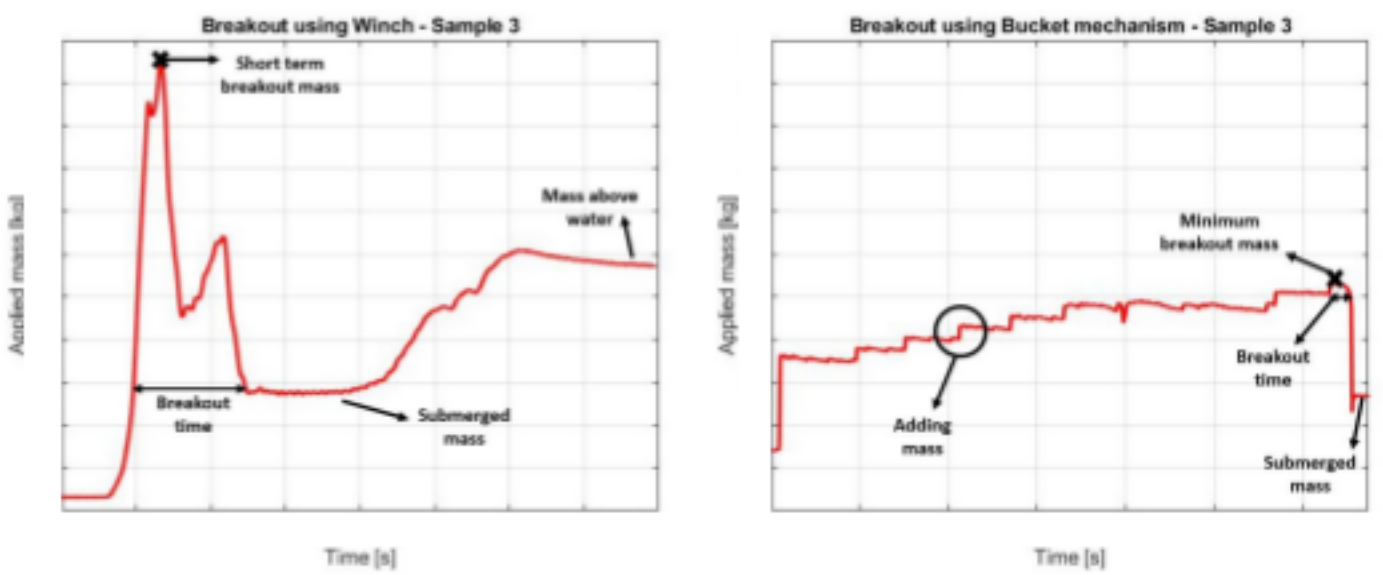

Figure 4.20: Left: Breakout using the winch, short term breakout. Right: Breakout using the bucket mechanism, long term breakout.

4.6.3. Breakout force and flexibility

All test results from the short and long term breakouts of one sample are merged in a graph, to get an overview of the required breakout force over time. This graph can be compared with the graphs of other samples, to see the effect flexibility has on the breakout force.
Figure 4.21 shows the breakout force versus time for sample 3, that has an out of plane stiffness of 3.54 kN/m. The breakout force is the measured breakout load minus the submerged mass of the frame and sample, converted to Newtons. Some of the bucket mechanism measurements turned out to be short term, so this explains the circles close to the winch measurements. One of the winch measurements is much higher, than the other measurements at the same breakout time. This is because the frame was stuck behind the container, so it is a measurement error. The bucket measurement at approximately 87 seconds breakout time is too low, since the frame was bumped with a weight just before breakout so the suction resistance already decreased. Thus, this value should also not be taken into account.

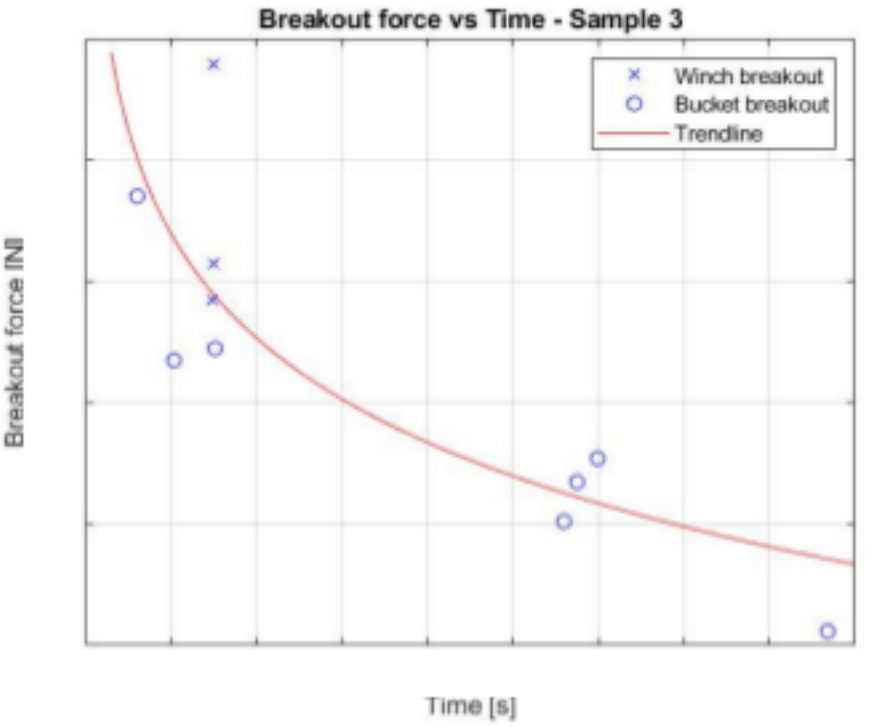

Figure 4.21: Breakout force for sample 3 over time. Trend line: $F =$

A trend line is plotted in the graph to show the estimated breakout force over time. The trend line is based on the findings of the literature survey, i.e. a higher breakout force for a smaller breakout time and a lower breakout force for a larger breakout time. This results in a logarithmic line that decreases over time. The trend line reliability, R^2, is 0.73. If the trend line reliability value is at or near 1, the trend line is considered reliable. More results will contribute to a more reliable trend line.
The same graph as in figure 4.21 is made for sample 1 and 2, which have the same contact area as sample 1. The graphs are shown in figure B.19 and B.20 in Appendix B. All graphs confirm the findings from the literature survey, namely that the breakout force is higher for the short term breakout and decreases for the long term breakout. This is due to the fact that suction decreases with an increase in breakout time, since (partially) drained conditions are achieved. During a short term breakout, undrained conditions are the cause for a higher suction force.

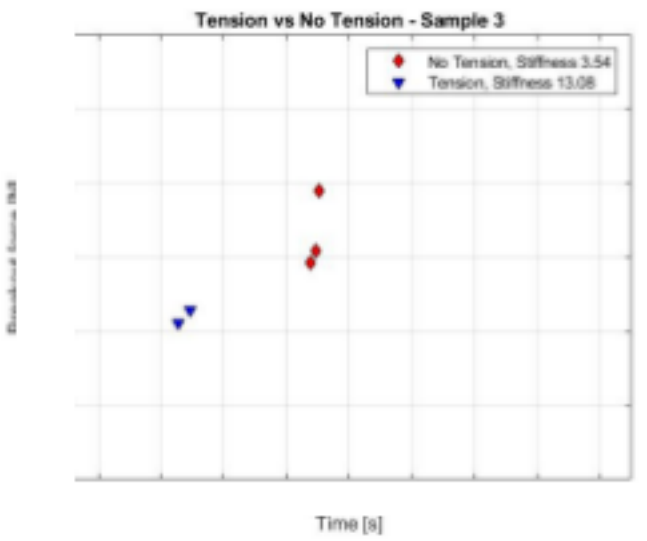

Figure 4.22: Breakout force of sample 3, with and without tension applied.

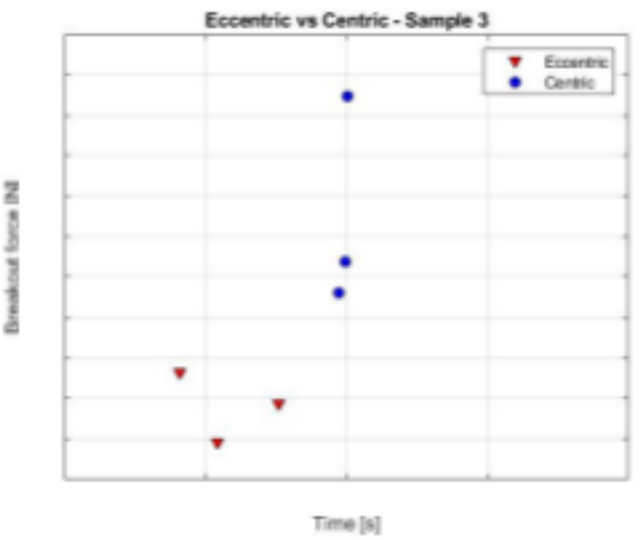

Figure 4.23: Breakout force of sample 3 during a centric and eccentric lift.

Breakout force - with and without tension
To test if applying a tension to the sample has an effect on the breakout force, all flexible samples are tested with and without tension. In figure 4.22 the difference in breakout force between sample 3 with and without tension is shown. With tension, sample 3 has a stiffness of 13.08 kN/m according to the deflection tests. It was not possible to get the breakout time exactly the same for every test, so to compare approximately the same breakout times are considered. The graphs of the other flexible samples are shown in Appendix B (figures

B.21, B.22 and B.23). There is a clear trend between tension and no tension for all samples. Namely, the sample without tension has a higher breakout force than the same sample with tension. The breakout force is reduced up to % for the samples with tension. Sample 5 is an exception and has a higher breakout force when tension is applied. This might be due to the size of the sample, since it is very small compared to the frame.
A plausible reason for the higher breakout force, when there is no tension applied to the sample, is because the sample stays longer in the soil due to the larger deflection thus experiences more soil resistance. If tension is applied, the samples are still able to deform to a certain extend. The sample will have a small deformation and the release of the rest of the sample follows faster.

4.6.4. Eccentric lift

The cable configuration on the frame is adjusted to make the eccentric lift possible. As shown in figure 4.14, the cables on the right are shorter than the cables on the left. This causes the frame to tilt when it is lifted, such that one side breaks free first followed by the other side. The roll angle of the frame is clearly shown in figure 4.24, which are the measurements of the displacement sensors. A roll angle of approximately 25 degrees is measured. The large roll angle confirms the eccentric lift of the samples.
According to the literature survey, an eccentric lift reduces the breakout force. The results confirm this, as shown in figure 4.23. A reduction of the breakout force up to % for sample 1 is measured. All samples experience a reduction of the breakout force during the eccentric lift, see figures B.24, B.25 and B.26 in Appendix B. An eccentric lift reduces the suction force, since a portion of the frame is still supported by the soil. This creates negative pore pressure at one side and positive pore pressure at the other side.

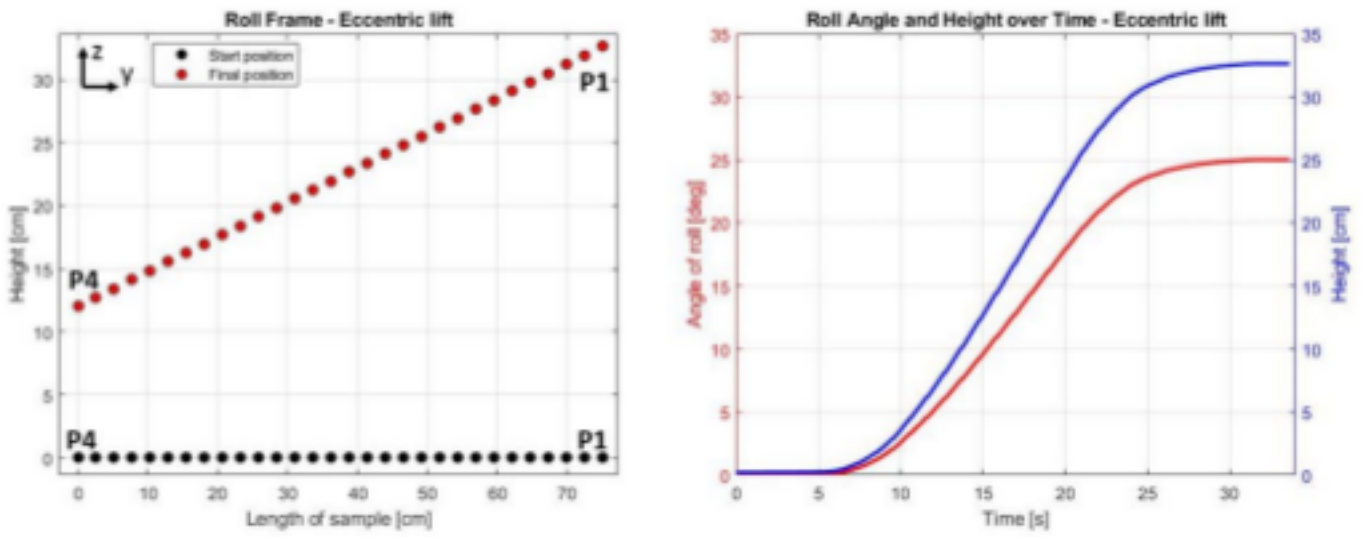

Figure 4.24: Left: Position of frame before and after the eccentric lift. Right: Roll angle and height of the frame over time.

4.6.5. Grousers

Grousers are part of the pistenbully tracks and will have an impact on the breakout force. To investigate this impact, the grousers are attached to sample 4 and the grouser experiment is conducted as explained in section 4.5.2. Figure 4.25 shows the breakout force of sample 4 with and without the grousers attached. As expected, the breakout force for sample 4 with grousers is higher due to more soil resistance. The breakout force increases with approximately % when the grousers are attached.
The results in figure 4.25 are of sample 4 without tension applied. To see if the tension on the belt together with the grousers will have a different outcome, the same tests are done with tension applied. Figure 4.26 shows the results of these tests. The same tension as sample 4 without grousers is applied to the belt, to focus on the effect the grousers have on the breakout force. Remarkable is that the sample with tension applied has a higher breakout force, this is the opposite of the tension versus no tension results of sample 4 without grousers. The reason for this

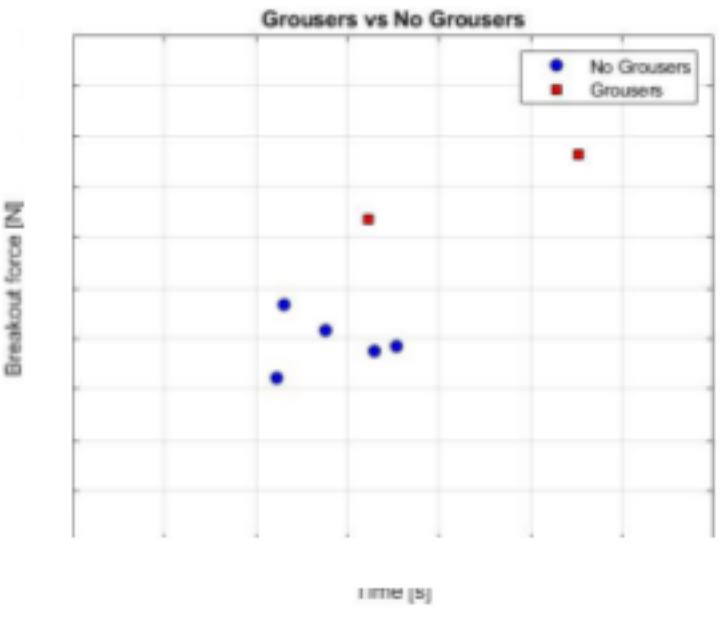

Figure 4.25: Breakout force of sample 4 with and without the grousers attached.

behaviour is that the grousers can create an angle when there is no tension applied to the sample, such that it has less soil resistance. When there is tension applied the position of the grousers is almost fixed and they experience more soil resistance. It is plausible that the grousers also affect the flexibility of the tracks, but to investigate this another research has to be done.
The effect of the grousers during an eccentric lift is also tested. Figure 4.27 shows the results of the eccentric lift versus centric lift for sample 4 with grousers attached. The results show the same behaviour as the eccentric experiment tests for the other samples, namely a reduction in breakout force.

Figure 4.26: Breakout force of sample 4 with grousers, with and without tension applied.

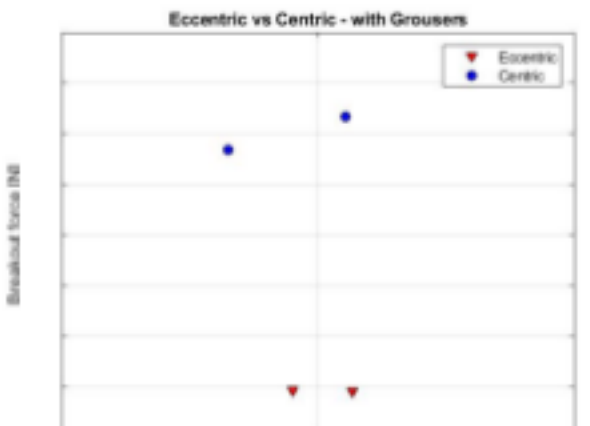

Figure 4.27: Breakout force of sample 4 with grousers during a centric and eccentric lift.

4.6.6. In situ Time

The in situ time has an impact on the breakout force, according to the literature survey the required breakout force increases with a longer in situ time. In the executed in situ experiments, sample 3 has been tested for several in situ times. The tested in situ times are: | hours. Figure 4.28 shows the required breakout force for the different in situ times. In the first hours a steep increase can be observed. A trend line is plotted based on the expectations of the literature survey, thus an increasing logarithmic line that flattens over time. The trend line reliability (R^2) is |

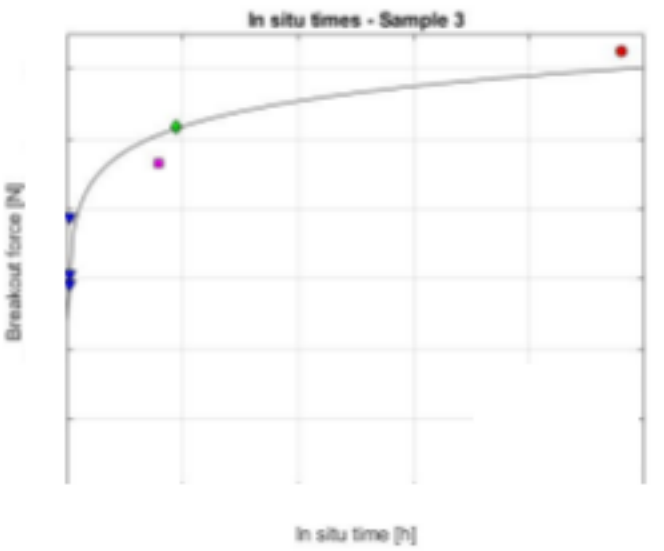

Figure 4.28: Breakout force of different in situ times for sample 3. Trend line: $F =$

4.7. Validation model

To calibrate and validate the Simulink model, the results of sample 1 are used. Sample 1 is chosen, since it is a rigid object. In this section the experimental parameters of sample 1 are implemented in the model and the results are compared. If the model generates reliable results, estimations about the collector can be made (see chapter 3 section 3.5).

4.7.1. Initial conditions for model

First, the initial conditions of the model should match with the experiment. The undrained shear strength of the artificial CCZ soil is measured during the experiments. The more solid layer 3 (see figure 4.15) has an undrained shear strength of approximately 2.0 kPa. However, the second layer, which is the layer the sample settles in, has an undrained shear strength of approximately 1.2 kPa. In the model the surface undrained shear strength parameter is taken as 1.2 kPa and the shear strength gradient is 2.0 kPa. Sample 1 has a contact area of 0.165 m^2 and, with the extra added weights, a submerged weight of 956.97 N. This results in a settlement depth of

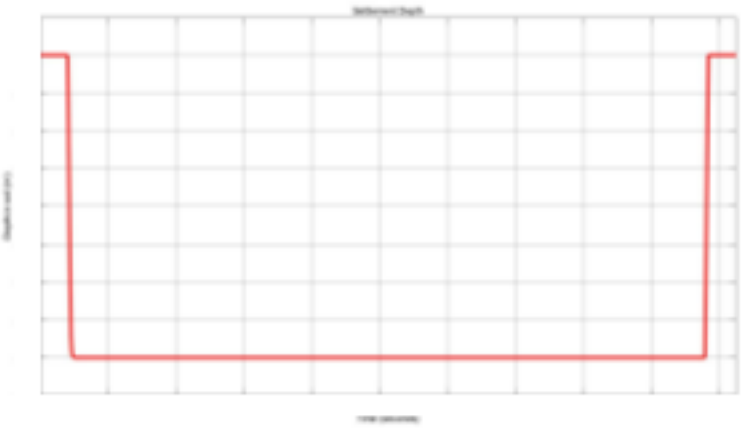

Figure 4.29: Soil depth of sample 1 with the extra weights.

m, as shown in figure 4.29. The settlement depth of the sample could not be measured accurately in the experiments, but a settlement depth between cm is estimated. This corresponds to the measured settlement depth of the model. When the maximum settlement depth is reached, the uplift can start.

4.7.2. Lifting force

The experiments are executed for a short term and long term breakout with the winch and the bucket mechanism. In the model the short and long term breakout are also implemented, by varying in the payout and hauling in velocity of the cable. The cable applies a force on the sample during uplift, this force is the lifting force. For the experiments the lifting force is measured with the load cell and for the model it is determined with the mass spring damper system. Before measuring the lifting force with the model the extra applied weight is removed, just like in the experiments.

Initial model - short term breakout

The initial model is based on the Quiggin and Randolph model [41], which models the soil penetration and suction resistance as explained in chapter 3. The model parameters for sample 1 can be found at the end of this thesis in chapter 9. For the short term breakout, the suction resistance ratio is estimated at . Figure 4.30 shows the difference between the experimental measurements and the estimated lifting force of the model for sample 1, during a short term breakout. The hauling in velocity of sample 1 in the model is m/s for a short term breakout, which is an estimation based on the average velocity of the experiments. A steep increase in the lifting force is observed when the uplift starts, this is also the case in the experimental measurements. The steepness of the increasing lifting force for the experiment depends on the rotational speed of the winch, this is done manually so it varies per experiment. After the peak when the sample starts moving upwards, the model lifting force has a slower decrease in lifting force compared to the experiment. This is because sample 1 moves slower to the surface in the model than in the experiments. When sample 1 is completely extracted from the soil the submerged weight remains to be lifted. For the short term breakout the damping is higher, due to the higher hauling in velocity, so the final lifting force is also higher compared to the long term breakout.

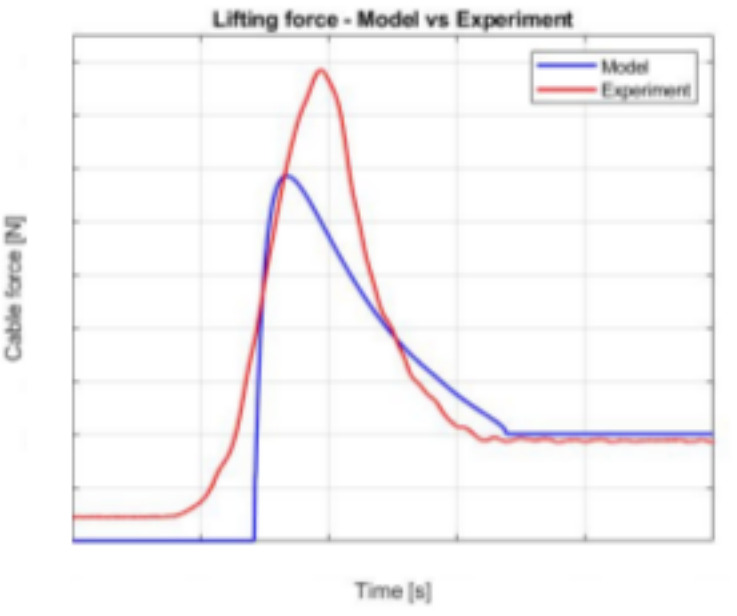

Figure 4.30: Difference in lifting force between the initial model and experimental measurements for sample 1 during a short term breakout.

It is clearly visible that the model underestimates the lifting force. This is because only the soil suction and submerged weight are considered as resisting forces in the initial model. The adhesive force and added soil weight are also acting on the sample, as known from literature. These extra forces are added to the adapted model, which is discussed below.

Initial model - long term breakout

For the long term breakout the hauling in velocity is adjusted to m/s and the suction resistance ratio is estimated to be . Figure 4.31 shows the difference in lifting force between the model and experiment for a long term breakout of sample 1. The main difference between the model and experiment is the decrease of lifting force over time. This is because in the experiments a constant load is applied to the sample with the bucket mechanism. Apparently, the sample remains at the same soil depth and then releases instantly. While in the model, the sample slowly moves toward the surface over time. The suction decreases when the sample is less deep in the soil, thus a decrease in lifting force over time is observed in the model. Again, the model lifting force is an underestimation, due to the missing adhesive force and added soil weight.

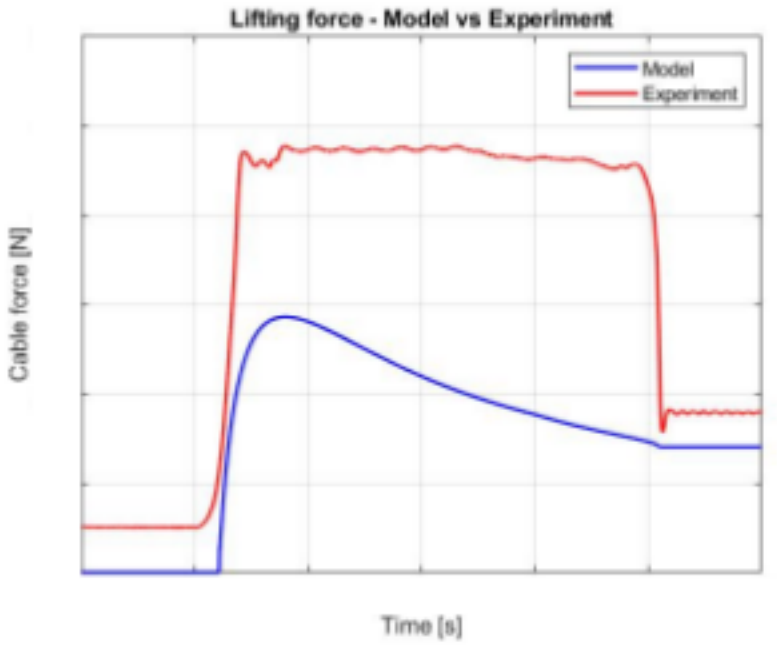

Figure 4.31: Difference in lifting force between the initial model and experimental measurements for sample 1 during a long term breakout.

Adapted model

The initial model underestimates the required lifting force, this is fixed by adding the adhesive force and added soil weight to the model. How the adhesive force and added soil weight are added is discussed in chapter 3 section 3.4. Figure 4.32 shows the lifting force of the model for sample 1 (short term breakout), when the adhesive force and added soil weight are implemented. As can be seen, the lifting force matches the peak value of the experimental lifting force. This peak value is the most important value, since this is the required force to extract the sample. After the peak, the same behaviour as in the initial model is observed, namely a slower decrease of lifting force for the model compared to the experiment. The steep drop, which was not present in the initial model, is the adhesive force that drops to zero when it is no longer in contact with the soil. The final value of the lifting force is the submerged weight plus the added soil weight. Again, the final lifting force for the short term breakout is higher, compared to the long term breakout, due to the larger damping. The final lifting force will be equal when there is no movement.
Figure 4.33 shows the adapted model for the long term breakout. The peak lifting force of the model matches with the experimental lifting force. After the peak is reached, the same behaviour as in the initial model is observed. The lifting force slowly decreases until the sample breaks free from the soil. When the sample is not in contact with the soil, the adhesive force drops to zero.

In both scenarios, the peak lifting force matches with the experimental results. The peak value is the most important value, when determining the required force to extract an object from the soil. After this peak, the lifting force only reduces since the object start moving to the surface. Therefor, the model is assumed to make a proper estimation of the required lifting force. Thus, an estimation of the collector can be made, which is discussed in chapter 3.

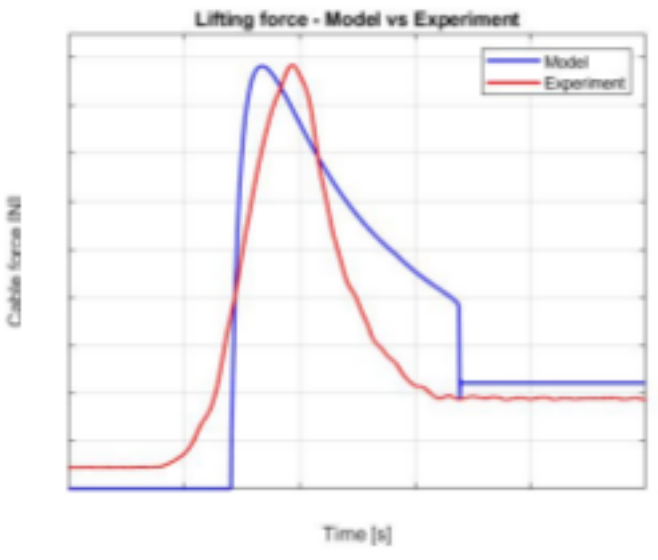

Figure 4.32: Difference in lifting force between the adapted model and experimental measurements for sample 1 during a short term breakout.

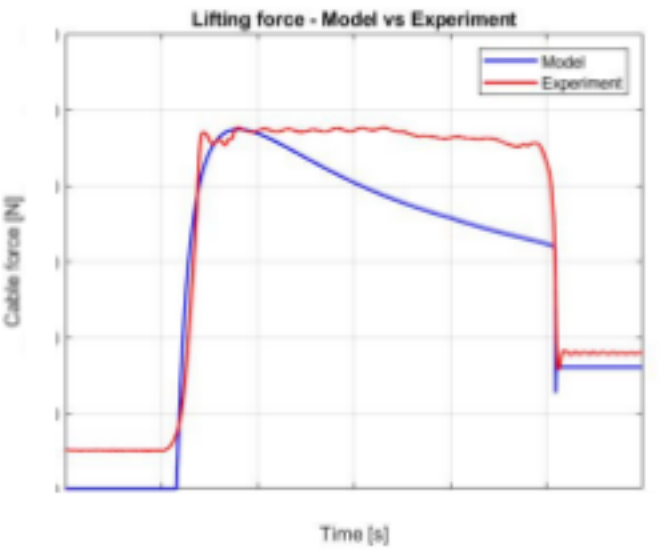

Figure 4.33: Difference in lifting force between the adapted model and experimental measurements for sample 1 during a long term breakout.

5

Analysis and discussion

This chapter covers the analysis and discussion of the results from the experiments and model. The analysis and discussion of the results gives answers to the research questions stated at the beginning of this thesis. Based on all the results, estimations about the collector and the breakout force are made. Can the umbilical retrieve the collector when it is stuck in the seabed? Or is a load reduction option necessary to succeed? In this chapter all important subjects are discussed.

5.1. Experiments

5.1.1. Test setup limitations and samples

The test setup was designed such that it could execute the desired experiments. It succeeded in doing this, but also came with some flaws. One of the flaws was the bucket breakout mechanism. Connecting the cable to the bucket created a load on the frame before the actual breakout test started, this was not desired. Also, the range of the pallet truck was too small, so the bucket had to be placed on top of multiple wood beams. Every time the pallet truck was lowered the wood beams had to be removed really quick for the short term breakouts, else the bucket would get stuck on the beams. A hydraulic lifting table would be a good replacement for the pallet truck, since it has a larger lifting range.

Another part of the test setup that needs improvement is the deflection sensor. The deflection sensor has a range of 5.5 cm, this was too little for some of the samples. To fix it the sensor was moved up and down in between the settlement en breakout tests. This was not ideal, so for future experiments the deflection sensor has to be replaced for another sensor with a larger displacement range, or it should be applicable under water.

Replacing the selected container with a container with transparent walls could be useful to see the behaviour of the samples and soil. However, the water gets blurry fast and the visibility will be little. But when longer in situ times are used the water clears up and this could be a good adjustment.

The test samples covered quite a good range of properties for the goal of the experiments. However, an extra sample could be added to the collection, that has an out of plane stiffness in between sample 1 and 3 with the same contact area. The results show a gap in between these two samples, since sample 3 was expected to be stiffer. A material with an out of plane stiffness between kN/m would satisfy.

Sample 3 has perforations to assemble the grousers, but these perforations also reduce the breakout force according to the literature. A sample of the same rubber belt as sample 3 but without the perforations would be interesting to test. It will also show the effect of the perforations on the breakout force. Unfortunately, there was no such sample available.

5.1.2. Behaviour of frame and sample

It is difficult to get a visual on the behaviour of the frame and sample, due to the water getting blurry and the non-transparent walls of the container. Therefor, the sensors are crucial to make an estimation of the behaviour of the frame and samples. The estimation is expected to be more accurate when multiple sensors are used, but for this research the selected amount of sensors is sufficient.

Initial condition before breakout
When the collector must be retrieved from the seabed, it is useful to know what the initial condition of the collector is. During the experiments the frame and samples applied an equal amount of pressure to the soil as the collector, due to the extra added weights. The frame is lowered onto the soil and goes through very soft soil layers before it touches the more solid soil. It rests on the soil for half an hour before it is extracted. The moment just before the breakout is considered as the initial condition. According to the results, the consolidation settlement for all samples is very little (few millimeters) and could not be measured accurately.
The soft mud-like soil layer thickness is difficult to measure, since there is no visual and it hardly adds any resistance to the frame and sample during lowering. It is estimated that the soft soil layer starts cm above the more solid soil layer, based on the results from the deflection and displacement sensors. The immediate settlement takes place when the frame sinks through the soft soil layer. During the settlement time, the soft cohesive soil starts to flow around the frame and sample. It is assumed that the collector will experience a similar interaction with the seabed.
In the results the frame and sample have a small angle in pitch and roll direction during most of the tests. This is because the soil is not perfectly flat, but this is also not the case on the seabed. The initial condition of the collector during a blackout depends on the period it is stuck on the seabed. If this period is relatively short, as during the experiments, only the immediate settlement takes place and the consolidation settlement is negligible. The soft soil layer will flow around the tracks and add more resistance. How large the roll and pitch angle of the collector is depends on the seabed conditions were the collector gets stuck.

Behaviour during breakout
One remarkable thing that happened during the breakout of the flexible samples,

When the sample is released, some of the soil flows of the sample and a part remains on top of it. Underneath the sample a bit of soil adheres to the surface, but not much. The samples with perforations have . Some of the perforations get clogged, so bigger perforations allow more soil flow. Figure 5.1 shows the soil on top of sample 3 after retrieval.
The tracks of the collector consist out of :

them. As earlier mentioned, the open spaces cause the soil to flow of the tracks more easily during uplift. Thus, less added soil weight needs to be lifted. The contact area of the tracks is reduced due to these open spaces, which means the tracks also experience less soil suction resistance.

Figure 5.1: Soil on top of Sample 3 after retrieval.

5.1.3. Flexibility
The results of the flexibility experiments give an insight into the effect of flexibility on the breakout force. In section 4.6.3 the individual results of the samples are discussed. In this section, the results are compared to see the impact of the flexibility. Figure 5.2 shows the trend lines for the breakout force of sample 1, 2 and 3 in the same time interval. These samples have the same contact area, but a different out of plane stiffness. The submerged weight of the frame and sample is extracted from the breakout force, such that the different masses of the samples do not have an impact. The results in figure 5.2 show that
As known from this study, the breakout force consists of the suction resistance, adhesive force and added soil weight. The samples are made out of different materials, so the adhesive force and added soil weight will differ for each sample.

It is assumed that this doesn't cause the large difference in breakout force. The added soil weight on the other hand is larger for sample 1 compared to the flexible belts. This is because sample 1 cannot deform, so the soil flows less easily of the sample compared to the flexible belts. Sample 3 has perforations, which reduce the added soil weight even more. However, the difference in added soil weight between sample 1 and sample 2/3 is approximately N according to the results, which has a limited impact looking at the total difference in breakout force. Assuming the adhesive force and added soil weight have little impact on the difference in breakout force, the suction resistance remains. The suction resistance depends on the soil properties and contact area of the sample. Since these parameters are equal, the solution can be found in the flexibility.

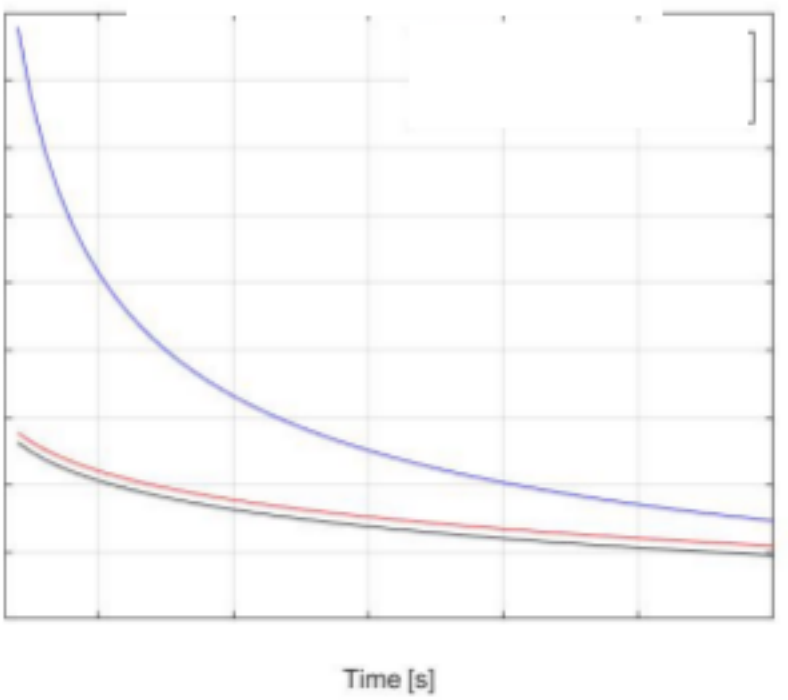

Figure 5.2:

since water can flow underneath the sample and drained conditions are achieved.

The smaller difference between sample 2 and 3 is due to the different stiffness, but also the fact that sample 3 has perforations. Perforations reduce the breakout force according to the literature, so sample 3 without perforation has probably even a higher breakout force.
For the short term breakout the difference between the rigid and flexible samples (sample 1 and 2/3) is large, while for the long term breakout this difference gets smaller. This is because a shorter breakout time results in a higher amount of suction, since it has no time to achieve (partially) drained conditions. The flexible samples experience less suction than the rigid sample, because they can deform themselves as mentioned above. During
thus the breakout force results are closer to each other and so is the difference.

The results for a sample with and without tension showed that a
Namely, the
The main difference between these results is; for the tension experiments the results of the same sample are compared, while for the flexibility experiment the results of different samples are compared.
When there is tension applied to the sample, there is still some space for deformation left. A small deformation can significantly reduce the soil suction, since water can flow underneath the sample. Because there is tension applied to the sample, the remaining part of the sample in the soil follows more rapidly. In case there is no tension applied the deformation might become too large, resulting in a longer interaction with the soil. This could be a possible reason for the higher breakout force, when no tension is applied to the sample. However, the difference between the amount of tension and no tension is small, because the tension is manually applied by tightening the bolts of the threaded rods. Additional research should investigate if this trend (lower tension, higher breakout force) remains when a larger tension is applied to the belts. There might be a transition, when the sample cannot deform anymore because of the tension.
Assuming that applying tension results in a lower breakout force, the collector should be retrieved when there is still a tension applied on the tracks. If the tension on the tracks should be equal as during operation or lower should be investigated in the additional research.

5.1.4. Contact Area

Sample 3, 4 and 5 are made out of the same material, but are different sizes. Sample 3 has three rows, sample 4 two rows and sample 5 has one row of perforations, as shown in section 4.2. The perforation ratio is approximately so this will not affect the results. To focus on the effect of different contact areas, the stiffness is kept equal for each sample. The breakout time is also similar for the results. Figure 5.3 shows the breakout force of the samples for the different contact areas. The average breakout force of all tests are displayed with the belonging error bars. An increasing linear trend is observed, which is expected since a larger contact area experiences more soil resistance. Since the belts are not equally scaled, an accurate estimation for larger contact areas cannot be made. However, it can be expected that the breakout force increases for larger contact areas.

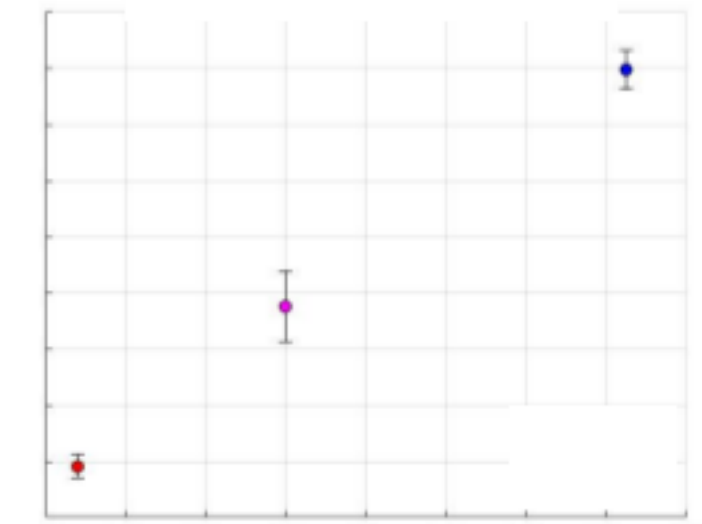

Figure 5.3: Breakout force

5.1.5. Effect eccentric lift

Both the results of the eccentric experiment and the literature show a force reduction during an eccentric lift. Figure 5.4 shows the difference between a centric and eccentric lift for sample 1 to 4. The mean breakout force is displayed with the belonging standard error for each sample. In these tests, the winch is used to extract the samples.

Table 5.1: Breakout force reduction percentage per sample for an eccentric lift.

Sample	Force reduction [%]
1	%
3	%
2 (Short)	%
4	%

Sample . Table 5.1 shows the reduction percentage of the other samples. There is a clear difference between samples 1 and 2 (short), and sample 3 and 4. The main difference between these samples is the surface, since sample 3 and 4 have perforations. Perforations reduce the suction force, as known from literature. Therefor, the suction resistance is already reduced and the impact of eccentric lifting will be less. While for sample 1 and 2 (short) the suction resistance is mainly reduced by the eccentric lift. Thus a larger difference in breakout force is observed.

The samples are also tested when tension is applied, to see if tension has an effect on the breakout force for the eccentric lift. According to the results, the force reduction is larger for the samples with tension (except for sample 2 (short)).

while with tension the sample deforms less and releases earlier from the soil. The results of an eccentric lift for the samples with tension can be found in figure B.27 in Appendix B.

Eccentric lifting is a proven approach to reduce the breakout force and might be a crucial load reduction option during the retrieval of the collector. Adjustments to the collector have to be made in order to create an eccentric lift. It is important to take into account that there is no power supply during the eccentric lift. Also retrieving the collector on the vessel might be difficult when under an angle, this has to be considered when a design for the eccentric lift is made.

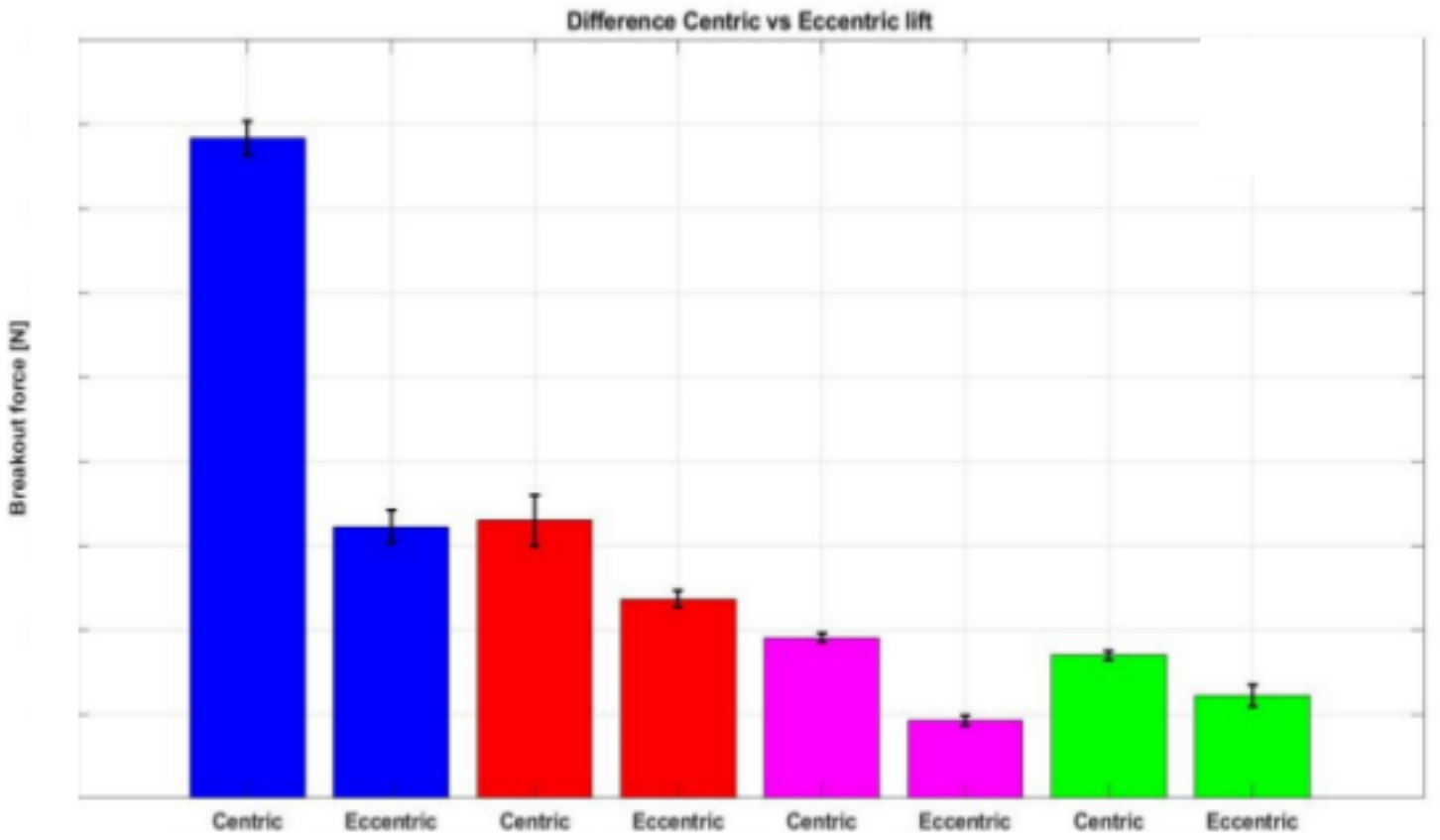

Figure 5.4: Difference in breakout force for centric and eccentric lift per sample.

5.1.6. Effect of grousers

The breakout force of sample 4 increases when the grousers are attached, as discussed in section 4.6.5. There are three reasons that could explain the increasing breakout force. First, the increasing soil side resistance due to the larger contact area of the grousers. Second, the increasing soil shear strength with depth, since the grousers sink deeper into the soil. And finally, the increasing soil suction, which has the largest impact. According to the literature, the soil suction is sustained for a longer time when grousers are attached. This is due to the increased length of the drainage path, which prevents the soil from becoming (partially) drained. The impact of the grousers on the flexibility is not investigated, but should be investigated in a future research. It is plausible that the grousers make the belts stiffer in multiple directions, which affects the breakout. However, the actual grousers are relatively small (meter high) compared to the size of the tracks (approximately meter long). Therefore, it is expected that the grousers have a small impact on the breakout force of the collector. To confirm this further, more detailed research about the grousers has to be done.

5.1.7. Effect longer in situ time

According to the literature and experimental results, a longer in situ period results in a higher breakout force. This is because the soil can regain its strength, the excess pore pressures have time to diffuse and the soil slowly flows around the collector, which increases the resistance. The in situ experiments with sample 3 show a , then flattens for longer in situ times.
When the collector is stuck on the seabed during a blackout, . The best option is to immediately start the retrieval when a blackout is noticed. Lifting the collector just above the soil is already enough, because then the soil resistance cannot increase. The problem can be fixed (if possible) and the operation can be continued, without hauling in the umbilical all the way to the vessel.

5.2. Model

The model is developed to make an estimation of the required lifting force for the collector. In this section, the model is analyzed and the reliability of the estimated lifting force is discussed.

5.2.1. Model compared to experiment

The soil resistance parameters are calibrated based on the experimental results. With the correctly calibrated parameters implemented, the peak lifting force of the model matches with the experimental results. After the peak a difference in lifting force is observed. This difference is due to the sample releasing instantly during the experiment, while in the model the sample slowly moves towards the soil surface. However, the peak lifting force is most important, since this is the required amount of lifting force to extract the sample. Since the peak in the model and experimental results match, it is assumed that the model gives a good estimation of the required lifting force.

5.2.2. Estimation lifting force collector

Before an estimation for the collector with the model was made, some calculations based on the experimental results are done. In Appendix A figure A.13 a rough estimation of the lifting force of the collector is made, based on the experimental results of sample 3. It is a rough estimation, since the flexibility is not taken into account for the increased length of the belt. The rough estimation results in a lifting force of kN for a short term breakout and kN for a long term breakout. The extra adhesive force that acts on the grousers is not considered in this estimation. The rough estimation can be compared to the model estimation, to determine if it is reasonable assumption.

Since the model is validated with the experimental results, an estimation for the collector is made using this model. The model parameters are adjusted for the collector as discussed in section 3.4. For the short term breakout, a lifting force of kN is estimated. This exceeds the umbilical limits (kN), which is not strange since the release is very quick. During the retrieval of the collector, such a quick release is not desired and will probably not be applied to the collector. However, if necessary, for whatever reason, a load reduction option should be applied to retrieve the collector in the short term breakout scenario.
The estimation for the short term breakout is an overestimation, since rigid tracks are considered. As known from this study, the flexibility will reduce the breakout force. The difference between the rough estimation and model estimation is large, this is due to the just mentioned rigidness of the model and because the model experiences a larger soil resistance (i.e. grousers included, greater suction resistance).

For the long term breakout a lifting force of kN is estimated. This estimation has a better match with the rough estimation based on the experimental results. Again, the model does consider the grousers, which are not taken into account in the rough estimation. And rigid tracks are considered, thus the lifting force is assumed to be an overestimation. However, it is in the same range as the rough estimation, which was not the case for the short term breakout. This is because during the long term breakout the suction does not have such a large impact as during the short term breakout. The long term breakout estimation is still an overestimation, but is assumed to be a good guideline for the actual retrieval of the collector.

6

Conclusion and recommendation

6.1. Conclusion

Research has been done to the retrieval of a stuck deep sea mining collector in a soft cohesive soil during a blackout. Retrieving the collector is of great importance, since losing such an expensive asset is not desired. The umbilical is intended to lift the collector from the soil. Nevertheless, the umbilical has a lifting capacity of kN, thus the breakout force may not exceed this limit. Literature studies give an insight into the breakout process of an embedded object from a soft cohesive soil. However, all studies consider a rigid object, which the tracks of the collector are not. Experiments are conducted to investigate the effect of flexibility on the breakout force compared to rigid objects. Also, plausible load reduction options are studied by performing experiments. To make an estimation of the lifting force of the collector, a model is developed. The model is calibrated and validated with the experimental results, such that a reliable estimation could be made. The combination of the literature, experiments and model provides sufficient information to determine if the collector can be retrieved. The conclusions based on the research are as follows:

- Soil suction, the adhesive force and added soil weight are soil resistance forces that act on the tracks. The suction is the dominant soil resistance, that affects the breakout force. The suction resistance is time-dependent and reduces for a longer breakout time.
- Due to the collector's submerged weight, the tracks will sink through the top layer(s) of very soft cohesive soil, this is considered as the immediate settlement. The consolidation settlement could not be measured accurately during the experiments, but is estimated to be very small especially in the first in situ hours.
- The open spaces between the track belts reduce the breakout force. The suction force is less due to the smaller contact area and the added soil weight reduces, since the soil can flow easily of the tracks through these open spaces. On the other hand, the grousers increase the breakout force, because of the increasing suction and adhesive force.
- The flexibility of the tracks can contribute to a reduction in breakout force. From the experimental results it is concluded that the flexible samples deform during breakout, which reduces the suction resistance.
- Applying tension to a flexible belt will result in a lower breakout force. The reason for this can be found in the decrease of belt-soil contact time. Additional research has to determine if there is a limit to the decreasing breakout force with increasing tension, for example when the belt cannot deform anymore.
- During a short term breakout of the collector from the soft cohesive CCZ soil, the lifting force exceeds the limits of the umbilical. To retrieve the collector, the load should be reduced by one of the load reduction options. For a long term breakout, the estimated lifting force of the collector is N. The lifting force remains within the umbilical limits. Therefor, a long term breakout is desired during the retrieval of the collector.
- Passive (i.e. no power supply required) load reduction options that are applicable to the collector are eccentric lifting, perforations, applying tension and/or an increased breakout time. Eccentric lifting can reduce the breakout force of the tracks up to %, according to the experimental results for sample 3.

6.2. Recommendations

6.2.1. Experiment

The test setup has some flaws, which should be adjusted or improved. One of the most important adjustments that should be made is the bucket mechanism. It did not function properly and was impractical to work with. The bucket can be replaced by another mechanism that creates a long term breakout or the bucket should be placed on a hydraulic table with a larger displacement range. The settlement depth of the samples was difficult to measure, since the start of the very soft top layer could not be indicated. A transparent container might help, but the blurry water has to be taken into account. Another flaw of the test setup is the deflection sensor. It should be replaced by a sensor with a larger displacement range or a sensor that is applicable under water.

Further research could be done to the effect of flexibility on the breakout force. There are way more flexible materials of different stiffness that could be tested. For this research an extra sample with an out of plane stiffness of 20-40 kN/m would be useful. But also samples with a lower stiffness than sample 2 are interesting to investigate. The tension tests done during this graduation should be extended. Testing one sample with different amounts of tension applied will show the effect of tension on the breakout force. It will also show if their is a limit to the decreasing breakout force with increasing tension.
Due to limited time, there are only basic tests conducted with the grousers. However, the grousers will probably affect the flexibility of the belts and also the behaviour during breakout. It is interesting to perform more detailed research to the effect of grousers.
The perforations in sample 3, 4 and 5 decrease the breakout force, which was also concluded from literature. Testing a similar sample without perforations would show the amount of reduction. The effect on the manoeuvrability of the collector when perforations are added to the track belts is also an interesting research topic.

6.2.2. Model

The model gives a good estimation for the peak of the required lifting force, but after this peak the behaviour differs from the experiments. Adjusting the breakout behaviour of the object in the model will probably fix this problem. The developed model could be used to make a model that also takes the flexibility into account. The flexible model will make a more accurate estimation for the required lifting force of the flexible samples and tracks.

Bibliography

[1] C. M. Ablow and S. Schechter. "Numerical simulation of undersea cable dynamics". Ocean Engineering 10.6 (Jan. 1983), pp. 443–457. ISSN: 0029-8018. DOI: 10.1016/0029-8018(83)90046-X.

[2] M.A. Alshamrani and S. Sture. "A Time-Dependent Bounding Surface Model for Anisotropic Cohesive Soils" (1998), pp. 61–76. DOI: 10.3208/sandf.38.61.

[3] C. P. Aubeny, H. Shi, and J. D. Murff. "Collapse Loads for a Cylinder Embedded in Trench in Cohesive Soil". International Journal of Geomechanics 5.4 (Dec. 2005). Publisher: American Society of Civil Engineers, pp. 320–325. ISSN: 1532-3641. DOI: 10.1061/(ASCE)1532-3641(2005)5:4(320).

[4] B. Bienen, C. Gaudin, and M.J. Cassidy. "The influence of pull-out load on the efficiency of jetting during spudcan extraction". Applied Ocean Research 31.3 (July 2009), pp. 202–211. ISSN: 0141-1187. DOI: 10.1016/j.apor.2009.09.001.

[5] Z. Bitar. "Reduction of adhesion in subsea operations" (2019).

[6] D. Bouwmeester et al. "Prediction of Breakout Forces for Deepwater Seafloor Objects" (2009).

[7] B.J.S. Breeveld. "Modelling the Interaction between Structure and Soil for Shallow Foundations" (2013).

[8] B.J. Buckham. "Dynamics modelling of low-tension tethers for submerged remotely operated vehicles" (2003).

[9] R. Chen, C. Gaudin, and M.J. Cassidy. "Investigation of the vertical uplift capacity of deep water mudmats in clay". Canadian Geotechnical Journal 49.7 (July 2012), pp. 853–865. ISSN: 0008-3674, 1208-6010. DOI: 10.1139/t2012-037.

[10] X. Chen, G. Hong, and S.A. Miedema. "A study on the clay adhesion factor" (2019).

[11] B.M. Das. "Bottom Breakout Of Objects Resting On Soft Clay Sediments". International Journal of Offshore and Polar Engineering 1 (Sept. 1991).

[12] B.M. Das. Shallow Foundations: Bearing Capacity and Settlement. Google-Books-ID: H9sNDgAAQBAJ. CRC Press, Feb. 2017. ISBN: 978-1-351-67244-3.

[13] E.H. Davis and J.R. Booker. "The effect of increasing strength with depth on the bearing capacity of clays". Géotechnique 23.4 (Dec. 1973). Publisher: ICE Publishing, pp. 551–563. ISSN: 0016-8505. DOI: 10.1680/geot.1973.23.4.551.

[14] R.C. DeHart and C.R. Ursell. "Force required to extract objects from deep ocean bottom" (Sept. 1967).

[15] "DNVGL-ST-N001 Guidelines for marine lifting & lowering operations" (2016). URL: http://rules.dnvgl.com.

[16] O.A. Eidsvik and I. Schjølberg. "Time Domain Modeling of ROV Umbilical using Beam Equations". IFAC-PapersOnLine. 10th IFAC Conference on Control Applications in Marine SystemsCAMS 2016 49.23 (Jan. 2016), pp. 452–457. ISSN: 2405-8963. DOI: 10.1016/j.ifacol.2016.10.447.

[17] Z. Fang. "A finite element cable model and its applications based on the cubic spline curve" (2012).

[18] A. Figenschou. "Umbilical". US7754966B2. July 2010.

[19] L.W.D. Finn and P.M. Byrne. "The Evaluation of the Break-Out Force For a Submerged Ocean Platform" (Jan. 1972). DOI: 10.4043/1604-MS.

[20] B. Freitas and T. Maria. "Numerical modelling of the time dependent behaviour of clays" (Jan. 2008). Accepted: 2011-10-10T13:40:34Z Publisher: Imperial College London (University of London).

[21] DNV GL. "DNVGL-RP-C212 Offshore soil mechanics and geotechnical engineering" (Aug. 2017).

[22] J.B. Hansen. "A revised and extended formula for bearing capacity" (1970).

[23] C. den Hertog. "Passive suction under mudmats" (2017).

[24] E.C. Hobaica and S.D. Cook. “The Characteristics of Syntactic Foams Used for Buoyancy”. Journal of Cellular Plastics 4.4 (Apr. 1968). Publisher: SAGE Publications Ltd STM, pp. 143–148. ISSN: 0021-955X. DOI: 10.1177/0021955X6800400405.

[25] S. Hong and J. Choi. “Experimental Study On Grouser Shape Effects On Trafficability of Extremely Soft Seabed” (Jan. 2001).

[26] A. Huang and H. Yu. Foundation Engineering Analysis and Design. Google-Books-ID: KtRBDwAAQBAJ. CRC Press, Dec. 2017. ISBN: 978-1-351-25539-4.

[27] DeepGreen Metals Inc. “DeepGreen and Allseas partner to harvest deep sea metals to meet skyrocketing growth in electric vehicle demand” (2020).

[28] G. Jun, W. Xiulun, and K. Kito. “Comparing tractive performance of steel and rubber single grouser shoe under different soil moisture contents”. International Journal of Agricultural and Biological Engineering 9.2 (Mar. 2016). Number: 2, pp. 11–20. ISSN: 1934-6352. DOI: 10.25165/ijabe.v9i2.1688.

[29] W. van Kesteren. “Numerical simulations of crack bifurcation in the chip forming cutting process in rock”. Fracture of Brittle Disordered Materials: Concrete, Rock and Ceramics (1995), pp. 505–524.

[30] H.J. Lee. “Unaided Breakout of Partially Embedded Objects from Cohesive Seafloor Soils”. NCEL-TR-755 (Feb. 1972).

[31] C.L. Liu. “Ocean sediment holding strength against breakout of embedded objects”. NCEL-TR-635 (Aug. 1969).

[32] C.M. Martin and E.C.J. Hazell. “Bearing capacity of parallel strip footings on non-homogeneous clay”. Frontiers in Offshore Geotechnics (2005).

[33] C.M. Martin and M.F. Randolph. “Applications of the Lower and Upper Bound Theorems of Plasticity to Collapse of Circular Foundations” (Jan. 2001), p. 13.

[34] G.G. Meyerhof. “Some Recent Research on the Bearing Capacity of Foundations”. Canadian Geotechnical Journal 1.1 (Sept. 1963). Publisher: NRC Research Press, pp. 16–26. ISSN: 0008-3674. DOI: 10.1139/t63-003.

[35] S.A. Miedema. The Delft Sand, Clay Rock Cutting Model, 3rd Edition. Jan. 2019. ISBN: 978-94-6366-132-4. DOI: 10.5074/t.2019.001.

[36] K.A. Miller et al. “An Overview of Seabed Mining Including the Current State of Development, Environmental Impacts, and Knowledge Gaps”. Frontiers in Marine Science 4 (2018). Publisher: Frontiers. ISSN: 2296-7745. DOI: 10.3389/fmars.2017.00418.

[37] Bruce J. Muga. “Ocean bottom breakout forces, including field test data and the development of an analytical method”. NCEL-TR-591 (June 1968).

[38] J.N. Newman. Marine Hydrodynamics. MIT Press, 1977. ISBN: 978-0-262-14026-3.

[39] P. Perzyna. “The constitutive equations for rate sensitive plastic materials”. Quarterly of Applied Mathematics 20.4 (1963), pp. 321–332. ISSN: 0033-569X, 1552-4485. DOI: 10.1090/qam/144536.

[40] M. Randolph. “Characterisation of soft sediments for offshore applications” (Jan. 2004). DOI: null.

[41] M. Randolph and P. Quiggin. Non-Linear Hysteretic Seabed Model for Catenary Pipeline Contact. ASMEDC, Jan. 2009, pp. 145–154. ISBN: 978-0-7918-4343-7. DOI: 10.1115/OMAE2009-79259.

[42] A. Roderick G.L. and Lubbad. “Effect of Object In-situ Time on Bottom Breakout” (1975).

[43] J. Salencon and M. Matar. “Bearing Capacity of Circular Shallow Foundations.” (Jan. 1982), pp. 237–267.

[44] M.A. Al-Shamrani. “Finite element analysis of breakout force of objects embedded in sea bottom” (1995), p. 18.

[45] L. Song et al. “Distribution of drag force coefficient along a flexible riser undergoing VIV in sheared flow”. Ocean Engineering 126 (Nov. 2016), pp. 1–11. ISSN: 0029-8018. DOI: 10.1016/j.oceaneng.2016.08.022.

[46] S.A. Suhail, F.A. Najam, and A. Nawaz. Modeling and Analysis of Soil-Pile Interaction for Dynamic Loading-A Review. Ed. by T. Abdoun and S. Elfass. Sustainable Civil Infrastructures. Springer International Publishing, 2018, pp. 128–148. ISBN: 978-3-319-63543-9. DOI: 10.1007/978-3-319-63543-9_12.

[47] K. Tani and W. Craig. “Bearing Capacity of Circular Foundations on Soft Clay of Strength Increasing with Depth”. 35.4 (1995), pp. 21–35. DOI: 10.3208/sandf.35.4_21.

[48] Karl Terzaghi, Ralph B. Peck, and Gholamreza Mesri. Soil Mechanics in Engineering Practice. en. Google-Books-ID: bAwVvO71FXoC. John Wiley & Sons, Feb. 1996. ISBN: 978-0-471-08658-1.

[49] M.A. Vaz and M.H. Patel. “Three-dimensional behaviour of elastic marine cables in sheared currents”. Applied Ocean Research 22.1 (Feb. 2000), pp. 45–53. ISSN: 0141-1187. DOI: 10.1016/S0141-1187(99)00023-1.

[50] A.B. Vesic. “Bearing capacity of deep foundations in sand”. Highway Research Record 39 (1963).

[51] A.S. Vesic. “Breakout resistance of objects embedded in ocean bottom” (May 1969).

[52] S.S. Vyalov. “Chapter 14 - Non-Linear Soil Models and Numerical Solutions of Problems”. Developments in Geotechnical Engineering 36 (Jan. 1986), pp. 481–556. DOI: 10.1016/B978-0-444-42223-1.50018-1.

[53] D.J. White et al. “An investigation into the vertical bearing capacity of perforated mudmats”. Frontiers in Offshore Geotechnics (2005), p. 459.

[54] E. Winkler. Die Lehre von der Elasticitaet und Festigkeit mit besonderer Rücksicht auf ihre Anwendung in der Technik. Google-Books-ID: IyZbAAAAcAAJ. 1867.

[55] L. Xiaojun et al. “Effect of perforations on uplift capacity of skirted foundations on clay” (2014).

[56] H. Xiaozhou and L. Shaojun. “Simulation and Calculation of Hydrodynamic Forces of Components of Deep Sea Mining System”. 2 (Dec. 2010), pp. 354–357. DOI: 10.1109/ICDMA.2010.129.

[57] B. Yenigul. “Summary of soil properties for Deltares” (2019).

[58] G. Yun and M. F. Bransby. “The Undrained Vertical Bearing Capacity of Skirted Foundations”. Soils and Foundations 47.3 (2007), pp. 493–505. DOI: 10.3208/sandf.47.493.

[59] Bitar Z. “Deep Sea Mining In Soft Clay: An Adhesion Problem” (Feb. 2021).

[60] A.R Zimnik et al. “The adherence of clay to steel surfaces” (2000), p. 7.

7

Definitions and Abbreviations

Definition	Description
Added soil mass	The amount of mass that sticks to the object after breakout
Bearing capacity	Maximum pressure that the object can sustain without soil failure
Breakout force	The soil resistance force required to break an object free from the soil. This is the lifting force without the submerged weight of the object.
Breakout time	The required amount of time to breakout an object from the soil
Centric lift	The object is lifted from the centre
Collector	The selected machine to collect the nodules from the seabed
Eccentric lift	The object is lifted from a different position than the centre
Grousers	Rigid bars attached to the rubber belts of the tracks, to improve traction
In situ time	Amount of time the object rests on soil
Intermediate breakout	Required force to break the object free from the soil in between the short term breakout and long term breakout
Lifting force	The required force to overcome all counter forces and extract the object from the soil. Includes the submerged weight of the object.
Long term breakout	Object releases from the soil in a time interval that is larger than 15 seconds
Minimum breakout force	The minimum required force to break the object free from the soil. This force is found by slowly increasing the applied mass.
Nodules	Rock-like deposits on the seabed that contain different minerals
Out of plane stiffness	The bending stiffness of an object in z-direction when it is clamped between to fixed points
Pistenbully tracks	Type of tracks, that have grousers attached to improve traction. Also used in snow areas.
Settlement time	Amount of time the object rests on soil
Short term breakout	Object releases from soil within a time interval of 15 seconds or less
Submerged weight	Weight of the object, when buoyancy force acts on it
Tracks	Mechanism for the propulsion of the collector
Umbilical	Cable for power supply, communication and lifting of the collector

Abbreviation	Description
CCZ	Clarion Clipperton Zone. Operational area for the deep sea mining project in the Pacific Ocean.
CRC	Cobalt Rich Crust
MV	Miniature Vane test. To measure the soil shear strength
PSV	Product Support Vessel. Vessel at surface connected to the collector.
SMS	Seafloor Massive Sulphides
SMT	Seabed Mining Tool. Other word for collector.
PHC	Passive Heave Compensation

8

Nomenclature

Symbol	Unit	Description
A	m^2	Cross sectional area
a	-	Fitting coefficient
α	-	Adhesion factor
a_{ad}	-	Adhesion of soil
A_d	m^2	Drag area
A_{max}	m^2	Maximum contact area
A_s	m^2	Effective soil-body contact area
a_t	kPa	Adhesive tensile strength
A_{tracks}	m^2	Contact area of the tracks
A_{UL}	-	Resistance ratio
B	m	Width of the tracks
b	-	Fitting coefficient
B'	m	Effective width foundation
c	kPa	Cohesion of soil
c	Ns/m	Damping. Contains cable and drag damping
c_{01}	kPa	Average undrained shear strength above base level
c_{02}	kPa	Undrained shear strength below base level
C_a	-	Added mass coefficient
C_d	-	Drag coefficient
C_m	-	Inertia coefficient
c_0	kPa	Undrained shear strength at surface
D	m^2/s	Pore pressure diffusion coefficient
δ	m	Deflection
ΔP	kPa	Pressure difference soil
Δs	m	Flow length
d_γ	-	Depth factor
d_c	-	Depth factor
D_f	m	Settlement depth
d_q	-	Depth factor
d_c'	-	Adjusted depth factor
DAF	-	Dynamic Amplification Factor
dL	m	Elongation of umbilical
E	GPa	Young's Modulus
E_s	GPa	Modulus of Elasticity Soil
E_{UL}	-	Exponential factor

Symbol	Unit	Description
$\dot{\epsilon}_{ij}$	s^-1	Total strain rate
$\dot{\epsilon}^{el}_{ij}$	s^-1	Elastic component strain rate
$\dot{\epsilon}^{vp}_{ij}$	s^-1	Visco-plastic component strain rate
F	N	Breakout force
F_{ad}	kN	Pulling force adhesion
F_{allow}	kN	Allowable lifting load for the umbilical
F_b	kN	Buoyancy force
F_{cable}	N	Force in cable
F_{cor}	-	Correction factor
F_{lift}	kN	Lifting force umbilical
F_{load}	N	Force of applied weight
F_{max}	kN	Maximum load acting on umbilical at water surface
$F_f(t)$	kN	External fluid force
g	m/s^2	Gravity
γ	kN/m^3	Unit weight of soil
γ'	kN/m^3	Submerged soil unit weight
H_g	m	Height of grouser
$H_{IP}(\zeta)$	-	Hyperbolic factor
$H_{IL}(\zeta_0 - \zeta)$	-	Hyperbolic factor
I_f	-	Influence factor
k	kN/m	Out of plane stiffness
k_l	m^2	Permeability soil
k_{cable}	kN/m	Axial stiffness umbilical
k_c	-	Rate of increase shear strength
k_r	$kN/m^2/m$	Modulus of sub-grade reaction
L	m	Length of the tracks
L_0	m	Length of umbilical
L'	m	Effective length foundation
m	kg	mass of object
m_{sub}	kg	Submerged mass of object
μ	-	Poisson's ratio
n	-	Number of rubber belts per track
N_γ	-	Bearing capacity factor
N_c	-	Bearing capacity factor
N_q	-	Bearing capacity factor
n_g	-	Number of grousers
P	kPa	Pressure of collector on seabed
p	kN/m^2	Pressure
ϕ	Deg	Internal friction angle
P_0	N/m	Latest value of soil resistance in previous mode
p_{excess}	Pa	Excess pore pressure
P_{soil}	kN/m	Soil resistance
p_{steady}	Pa	Pore pressure at end of consolidation
P_{suc}	N/m	Suction resistance
$P_{suc-lim}$	N/m	Limited suction resistance
P_u	N/m	Ultimate penetration resistance
P_{u-suc}	N/m	Ultimate suction resistance
P_w	kN	Suction force
$P(z_s)$	N/m	Resistance force soil
q	m^3/s	Specific flow
q_d	Pa or N/m^2	Bearing capacity
q_u	kPa	Ultimate bearing capacity
R	-	Slope of failure line
R^2	-	Reliability of trend line
R_v	kN	Soil resistance at sides of object
ρ_f	kg/m^3	Density of fluid
ρ_{sea}	kg/m^3	Density of seawater
ρ_w	kg/m^3	Density of water

Symbol	Unit	Description
σ	Pa	Soil stress
σ'	Pa	Effective soil stress
s_γ	-	Shape factor
S_c	m	Primary consolidation settlement
s_c	-	Shape factor
S_e	m	Elastic settlement
s_q	-	Shape factor
S_s	m	Secondary consolidation settlement
S_t	m	Total settlement depth
s_c'	-	Adjusted shape factor
t	s or min	Breakout time
t_0	s or min	Reference time
t_{insitu}	hour	In situ time
u	m/s	Velocity of object
v	m/s	Velocity seawater
$\dot{v}$	m/s^2	Acceleration seawater
V	m/s	Velocity
V_{disp}	m^3	Volume of displaced body of fluid
V_{obj}	m^3	Volume of object
V_{sea}	m^3	Volume of seawater above object
W	kN	Submerged weight of collector
w	m	Settlement
W_{dry}	kN	Dry weight
W_s	kN	Added soil weight
W_{sub}	kN	Submerged weight
W_{umb}	kN	Submerged weight of the umbilical
x	m	Length umbilical hauled in
ξ_{Pe}	-	Pore-Peclet number
z	m	Displacement of object
z_{soil}	m	Soil depth
ζ	-	Non-dimensionalized soil penetration
$\dot{z}$	m/s	Object velocity
$\ddot{z}$	m/s^2	Object acceleration

9

Model Parameters

Symbol	Unit	Description	Experiment	Collector
a	-	Coefficient		
α	-	Adhesion factor		
b	-	Coefficient		
B	m	Width of object		
Cd	-	Drag coefficient		
D	m	Cable diameter		
E	GPa	Young's modulus cable		
f_{suc}	-	Suction resistance ratio		
g	m/s^2	Gravity		
γ	N/m^3	Soil density		
γ_{sub}	N/m^3	Submerged soil weight		
H_g	m	Height of grousers		
k_c	-	Shear strength gradient		
K_{max}	-	Normalized maximum stiffness		
L	m	Length of object		
λ_{suc}	-	Normalised suction decay distance		
L0	m	Initial cable length		
m_c	kg	Mass of cable		
m_{frame}	kg	Dry mass of frame and sample		
m_{sub}	kg	Submerged mass of object		
n_{belt}	-	Number of belts		
n_g	-	Number of grousers		
ρ_{water}	kg/m^3	Density water		
s_u	Pa	Undrained shear strength		
V	m^3	Volume object		
v_{in}	m/s	Hauling in velocity		
v_{out}	m/s	Payout velocity		
z_a	m	Attachment point cable		

A

Appendix A - Model

A.1. Lifting mechanism

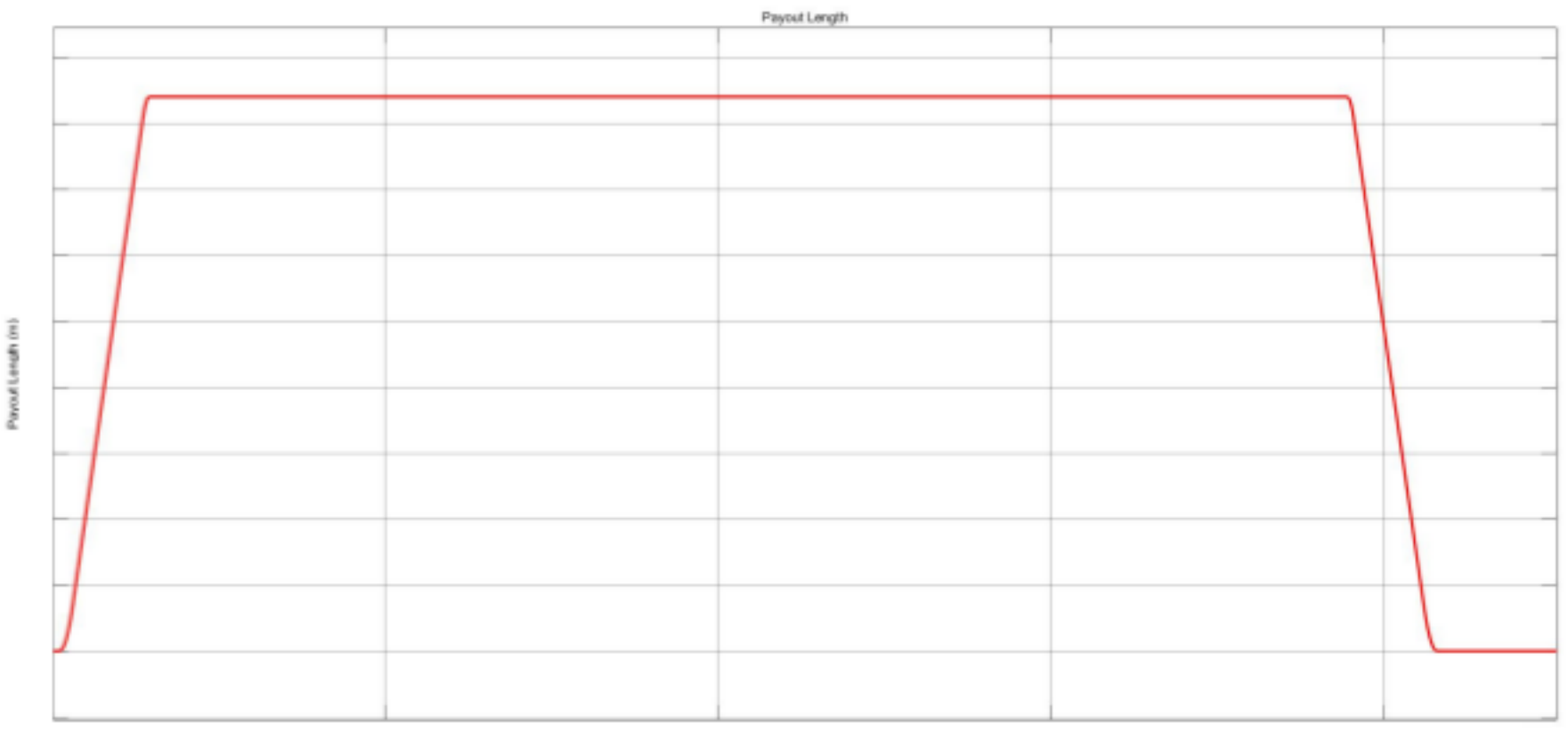

Figure A.1: The payout length of the cable (for experiment) with a payout velocity of m/s.

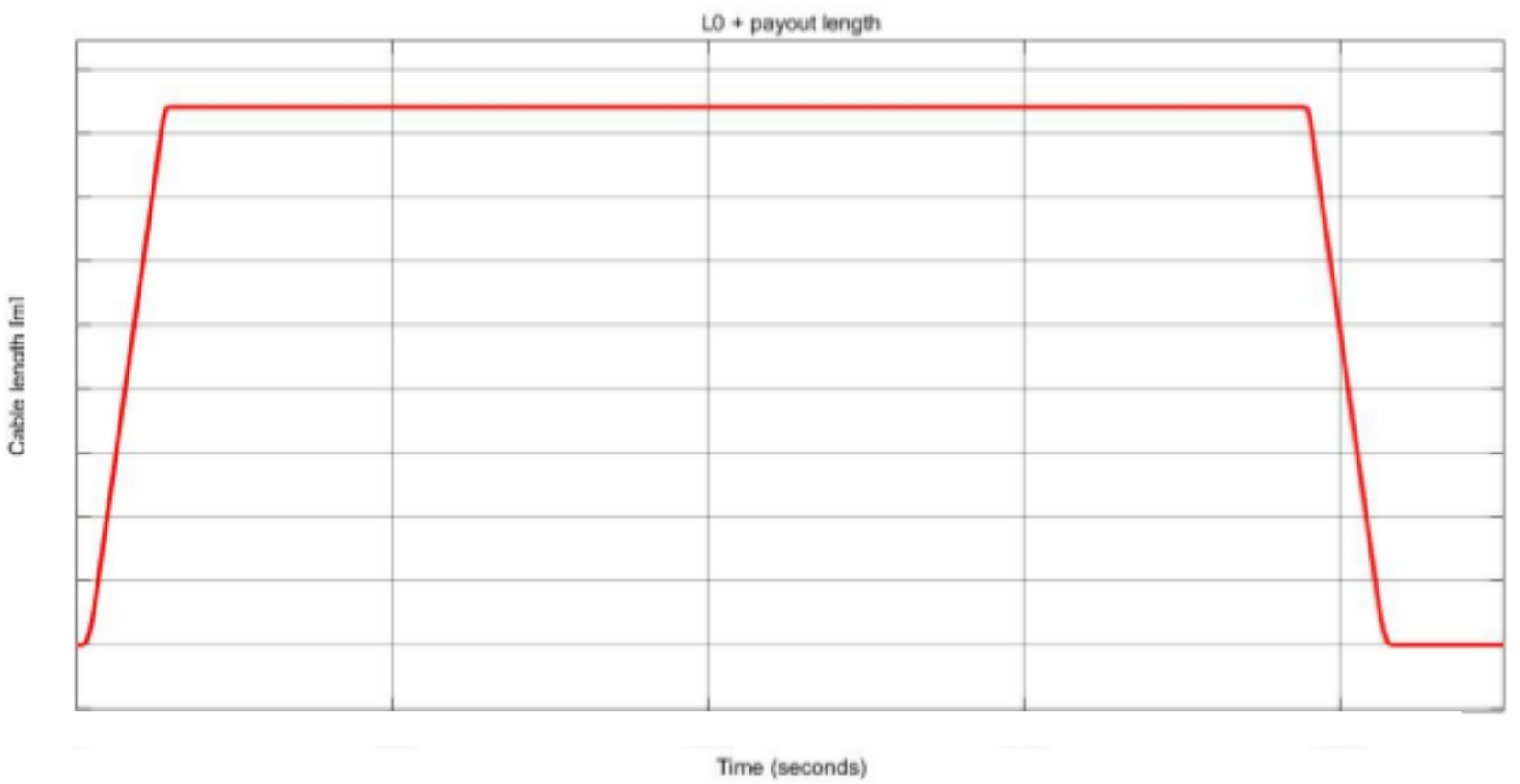

Figure A.2: The payout length of the cable plus the initial cable length, results in the total cable length (for experiment). Payout velocity is m/s.

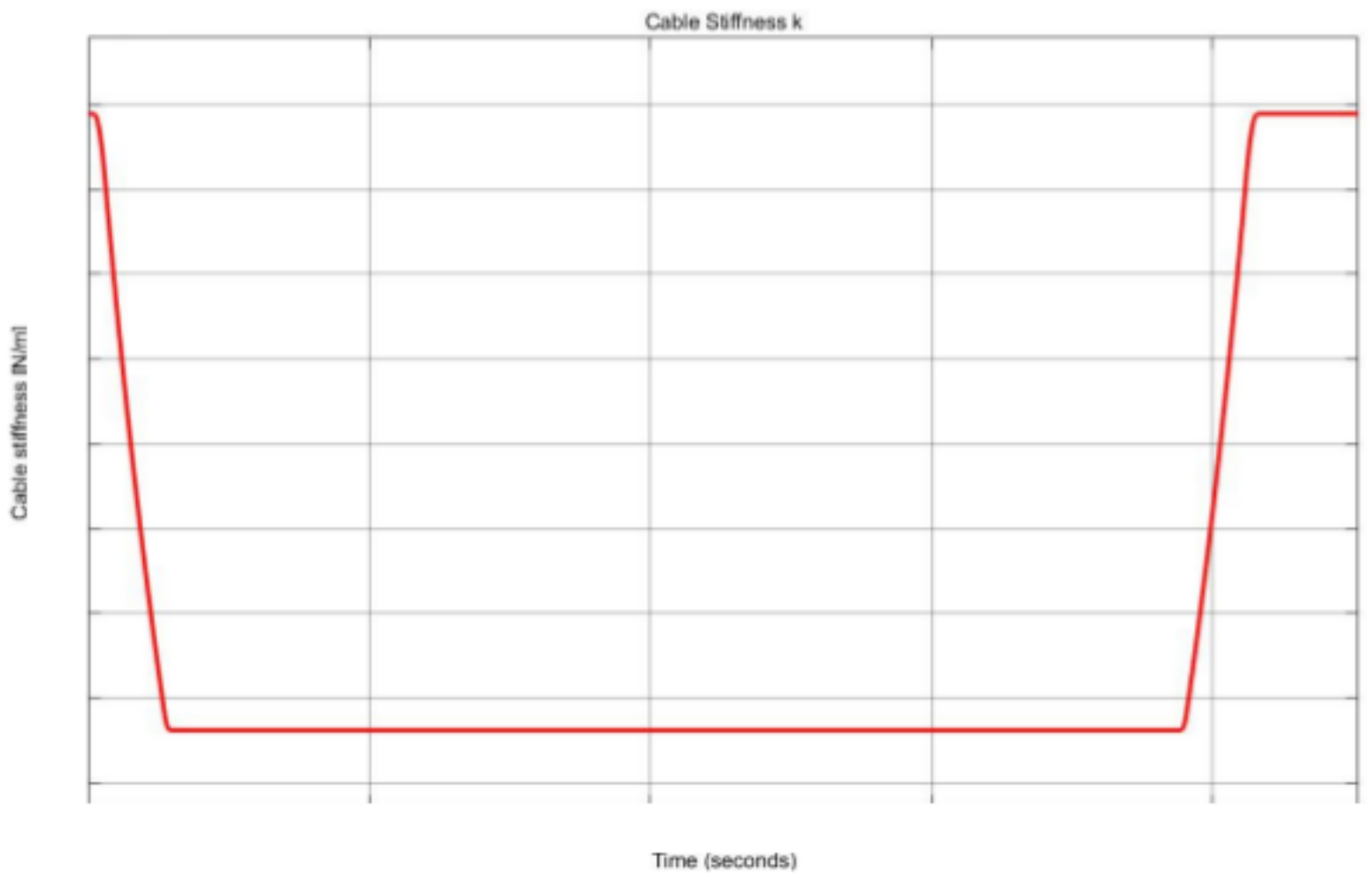

Figure A.3: Cable stiffness, decreases when cable length increases and visa versa.

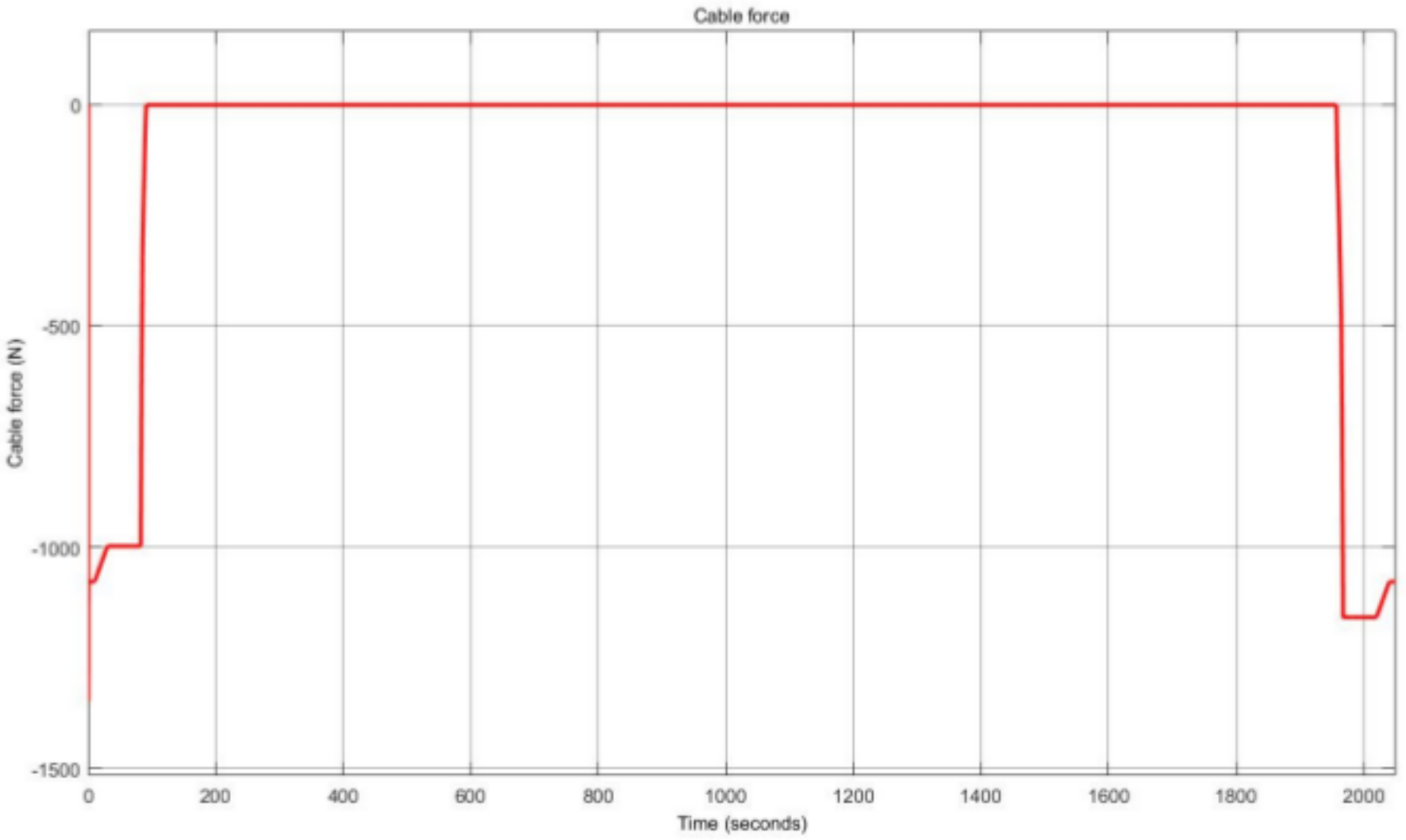

Figure A.4: Cable force becomes zero when object rests on soil. At the start and end of the lifting operation, the cable force is equal to the submerged weight (in this case with extra weights added on the frame).

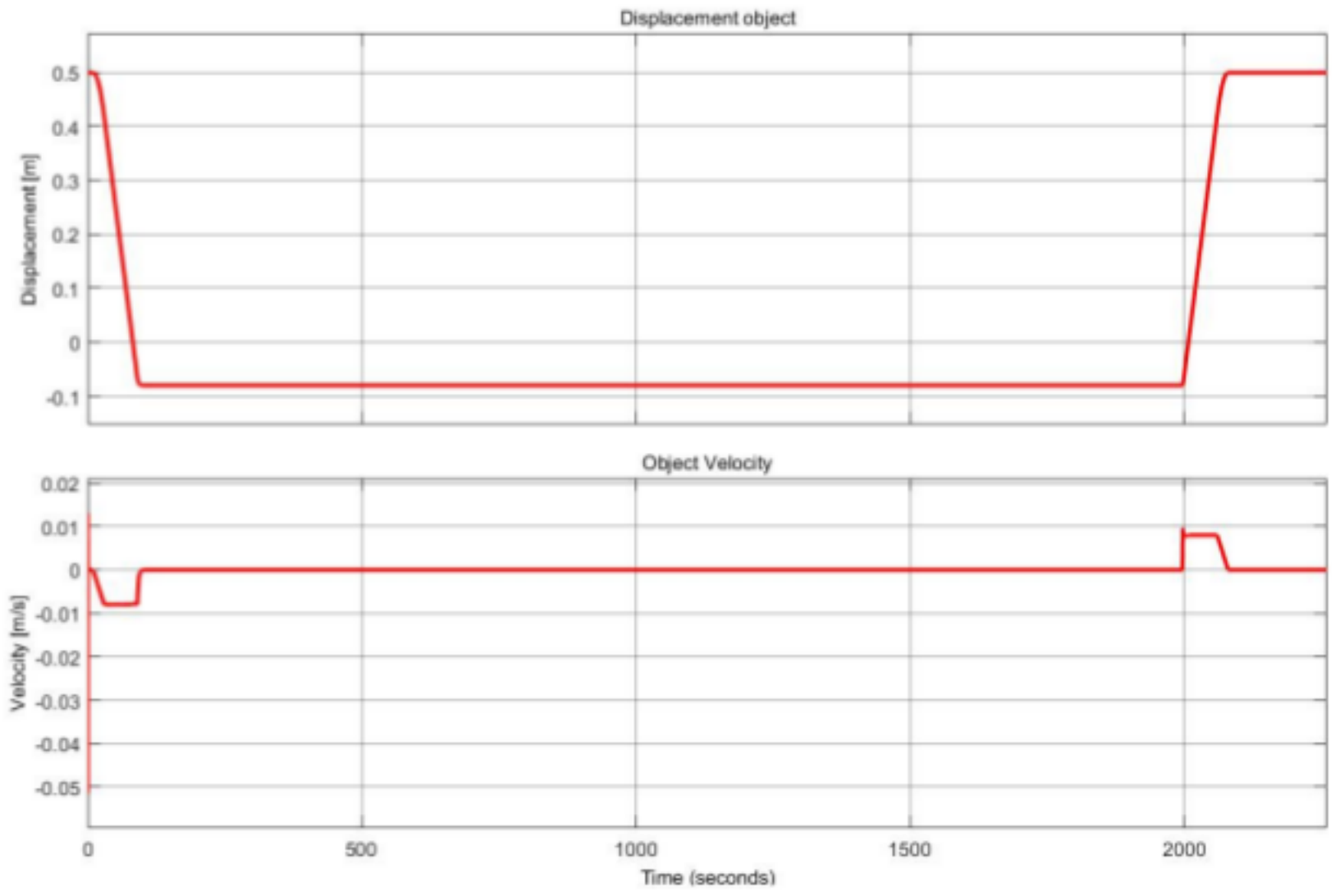

Figure A.5: Displacement and velocity of sample, based on cable behaviour. Settlement depth is 0.08 m and the velocity is 0.008 m/s

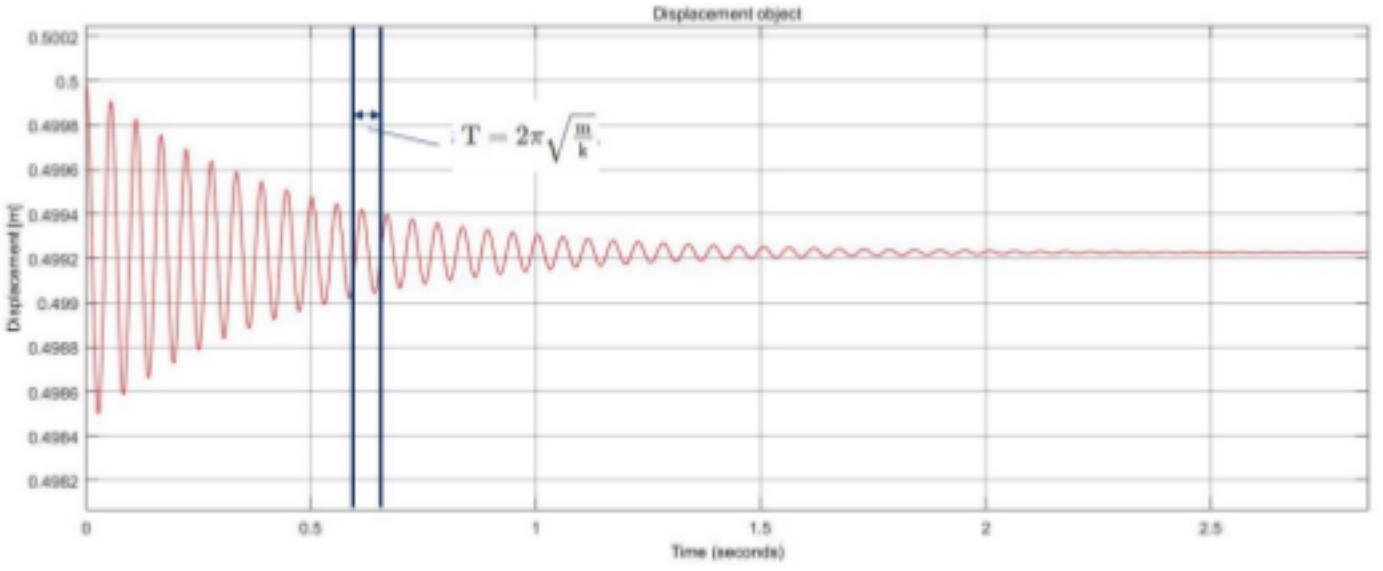

Figure A.6: Vibration of cable, damping out over time. Natural period of 0.056 seconds.

A.2. Non linear soil model

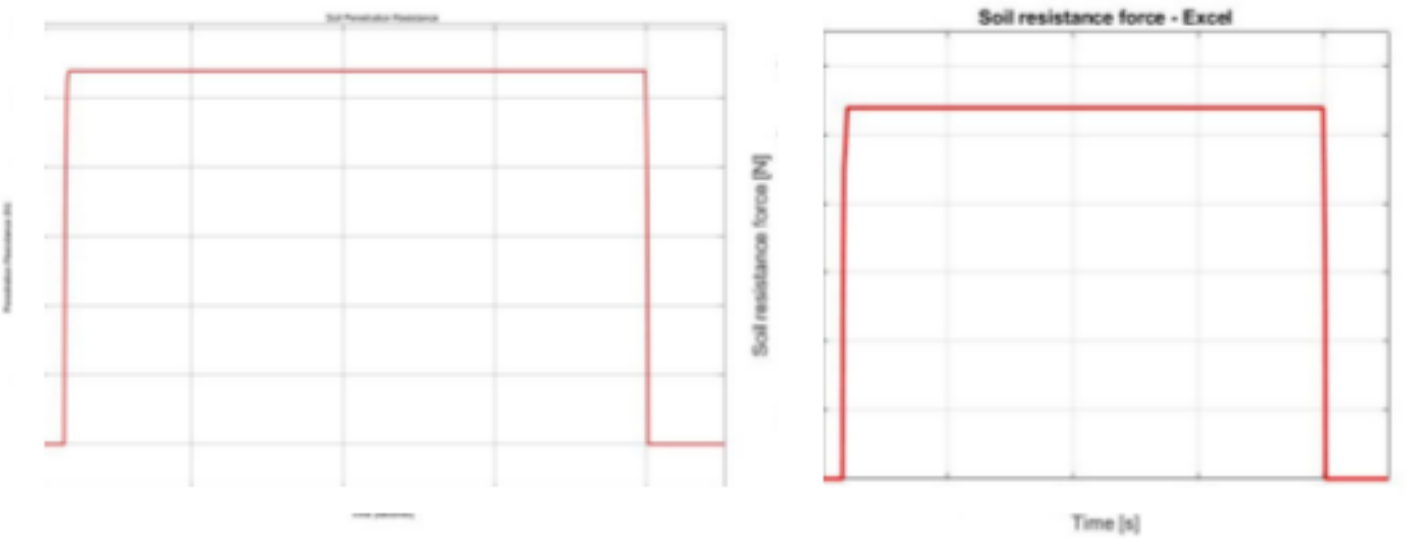

Figure A.7: Comparing the penetration resistance results of the Simulink model and the Excel file. Results for experiment sample 1.

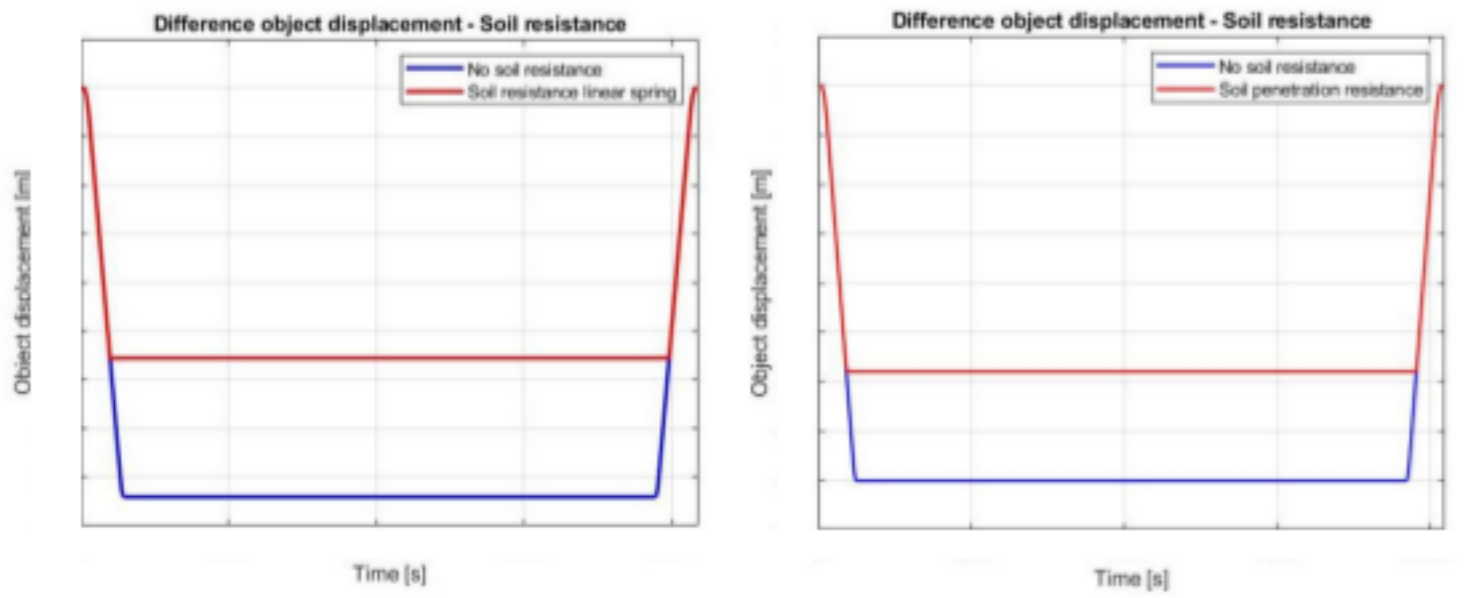

Figure A.8: Check if non linear soil model reacts the same as simple linear spring model. The parameters are different, so the figure is for visual confirmation. Left: linear spring soil model. Right: non-linear soil model (Quiggin and Randolph). Both figures show that the object experiences soil resistance.

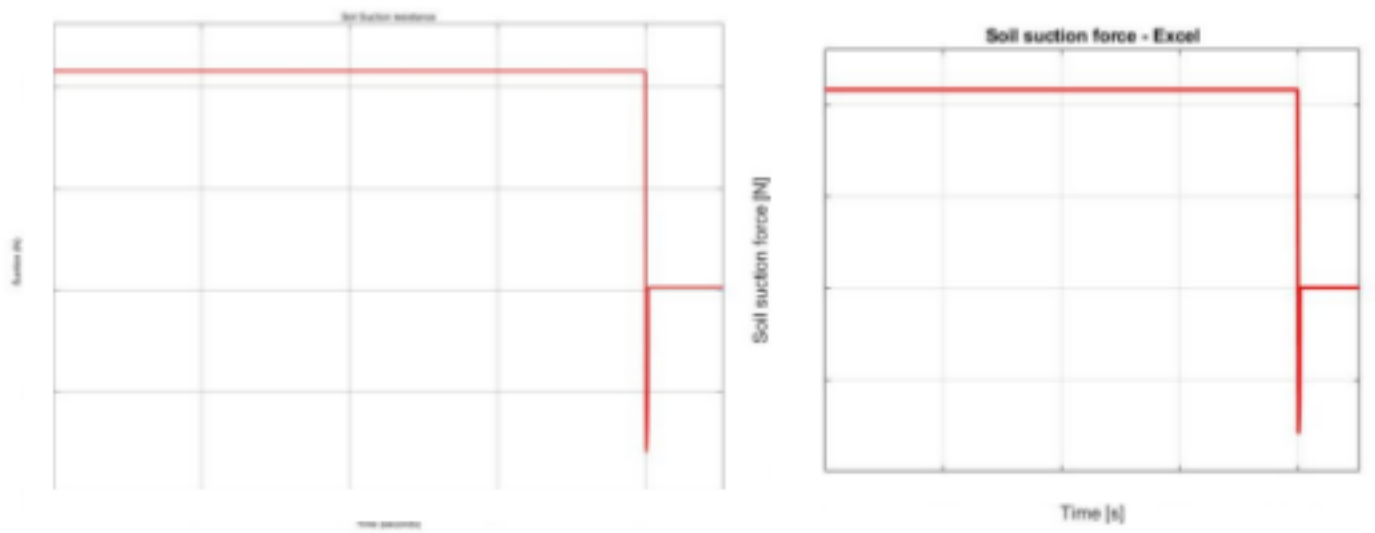

Figure A.9: Comparing the suction resistance results of the Simulink model and the Excel file. Results for experiment sample 1.

A.3. Collector

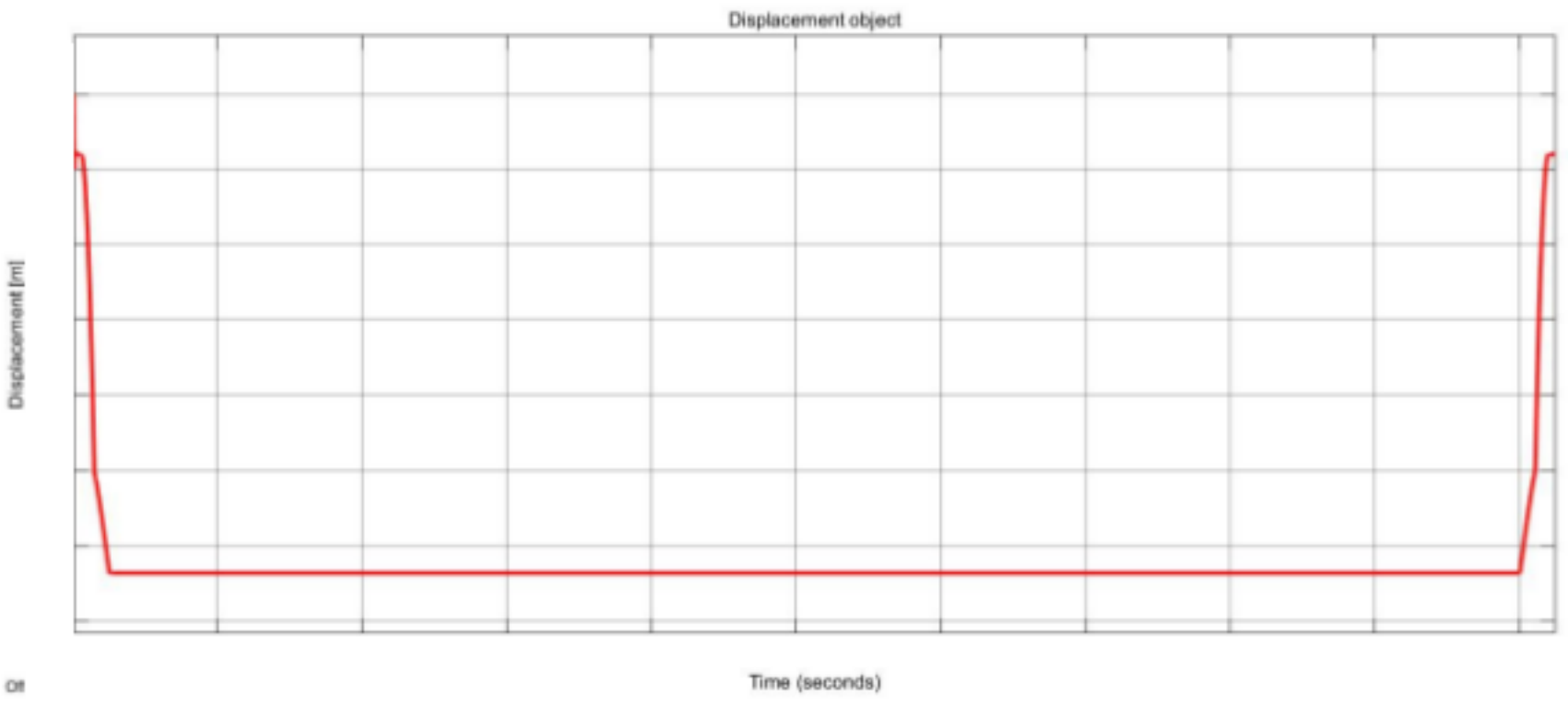

Figure A.10: Displacement and settlement of the collector, starting 0.42 meter above the seabed. A maximum settlement depth of m is established.

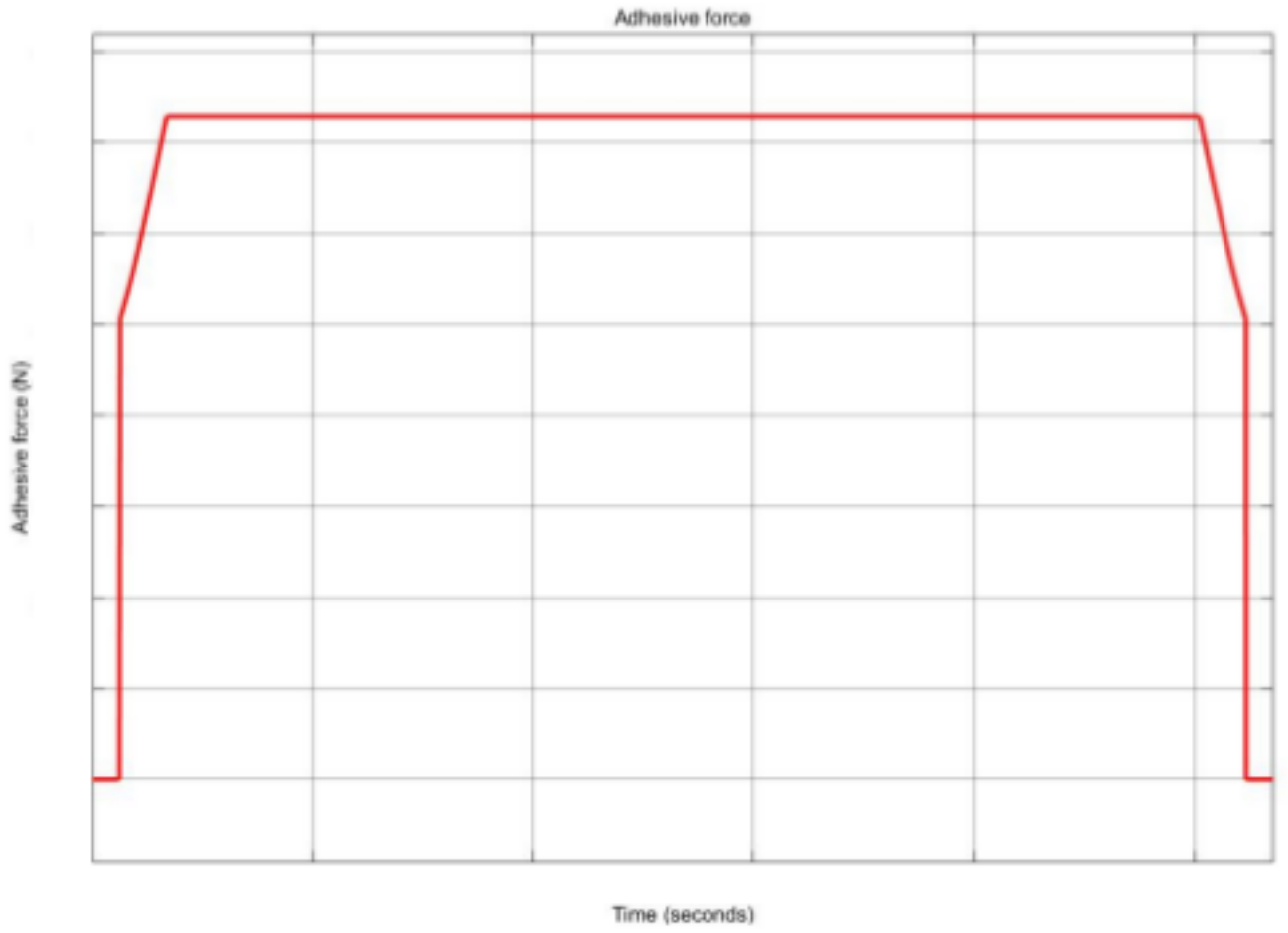

Figure A.11: Adhesive force acting on the tracks. Maximum adhesive force is N.

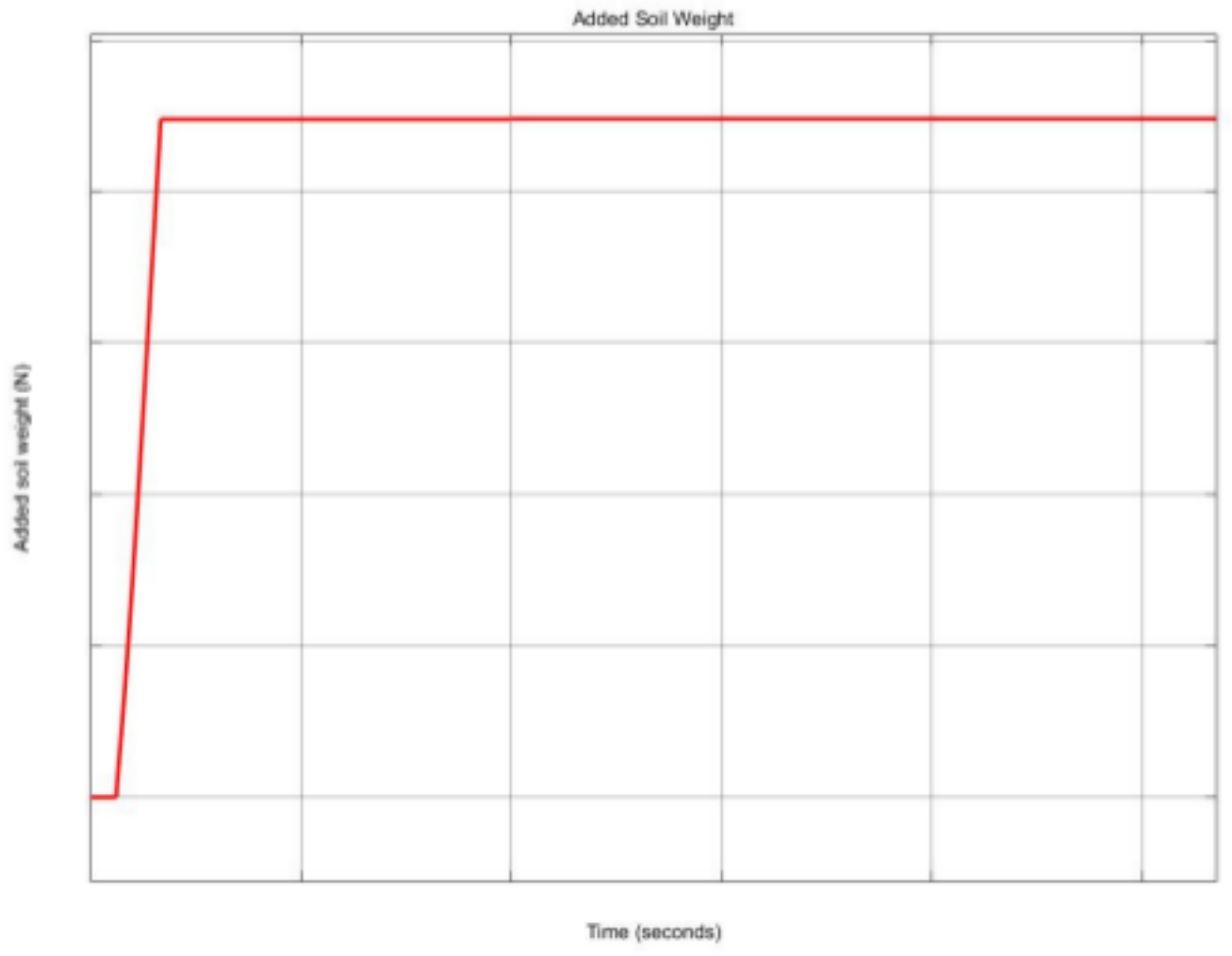

Figure A.12: Added soil weight acting on the tracks. Maximum added soil weight (with reduction factor) is N.

Figure A.13: Rough estimation for collector based on experimental results of sample 3.

B

Appendix B - Experiments

B.1. Calibration of sensors

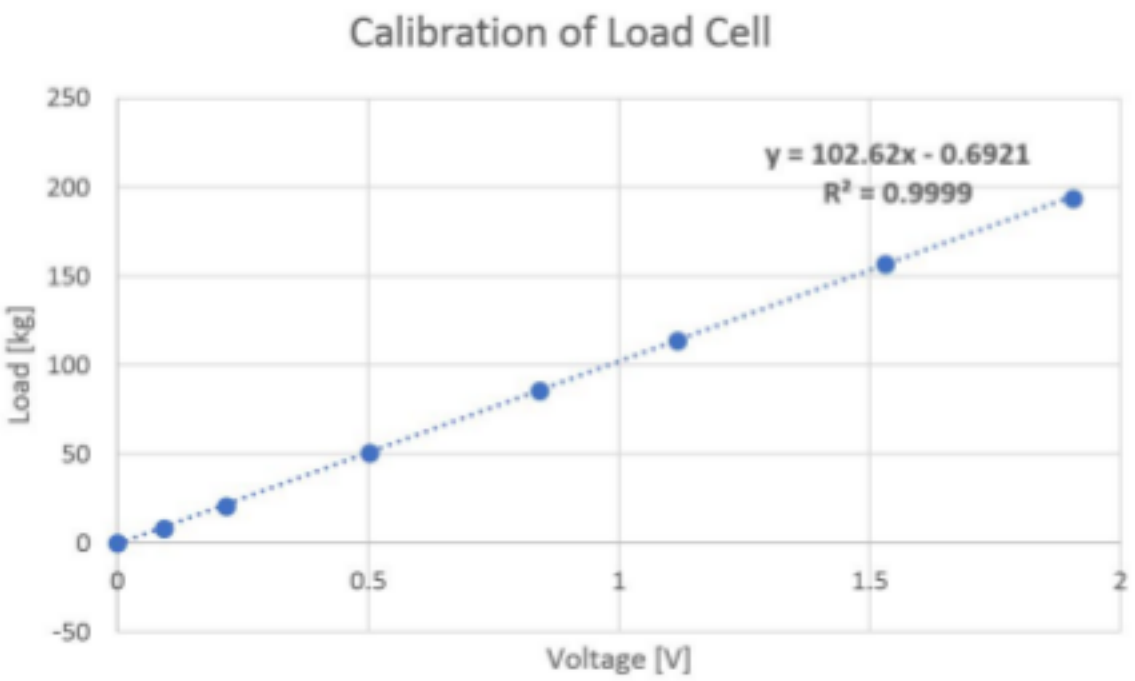

Figure B.1: Calibration of the load cell.

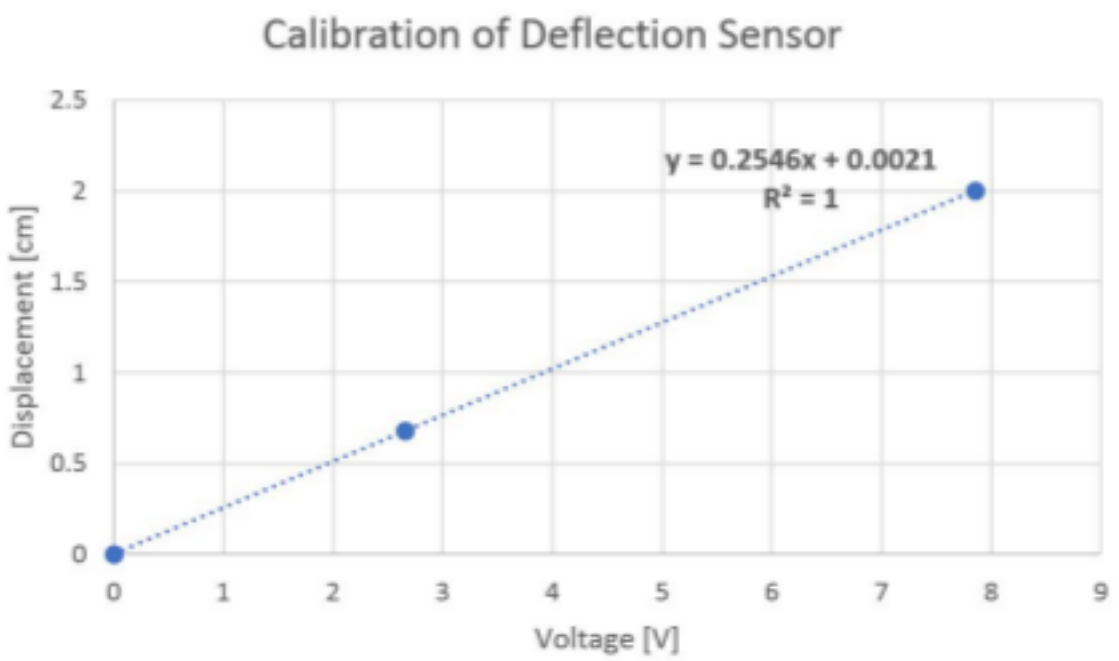

Figure B.2: Calibration of the deflection sensor.

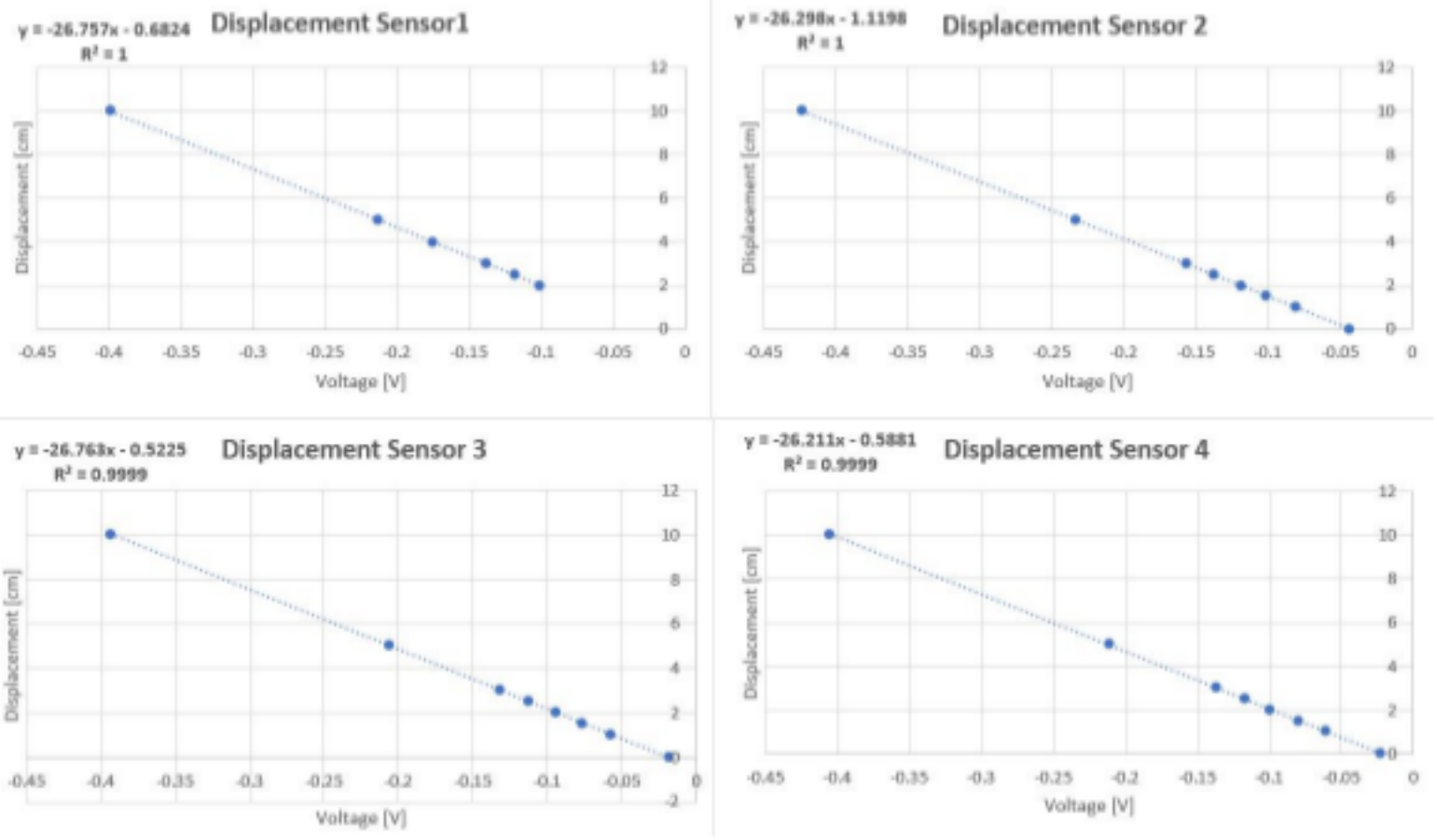

Figure B.3: Calibration of the four displacement sensors.

B.2. Artificial CCZ soil characteristics

Figure B.4: Artificial CCZ soil characteristics part 1.

Figure B.5: Artificial CCZ soil characteristics part 2.

B.3. Behaviour of frame and sample

B.3.1. Pitch

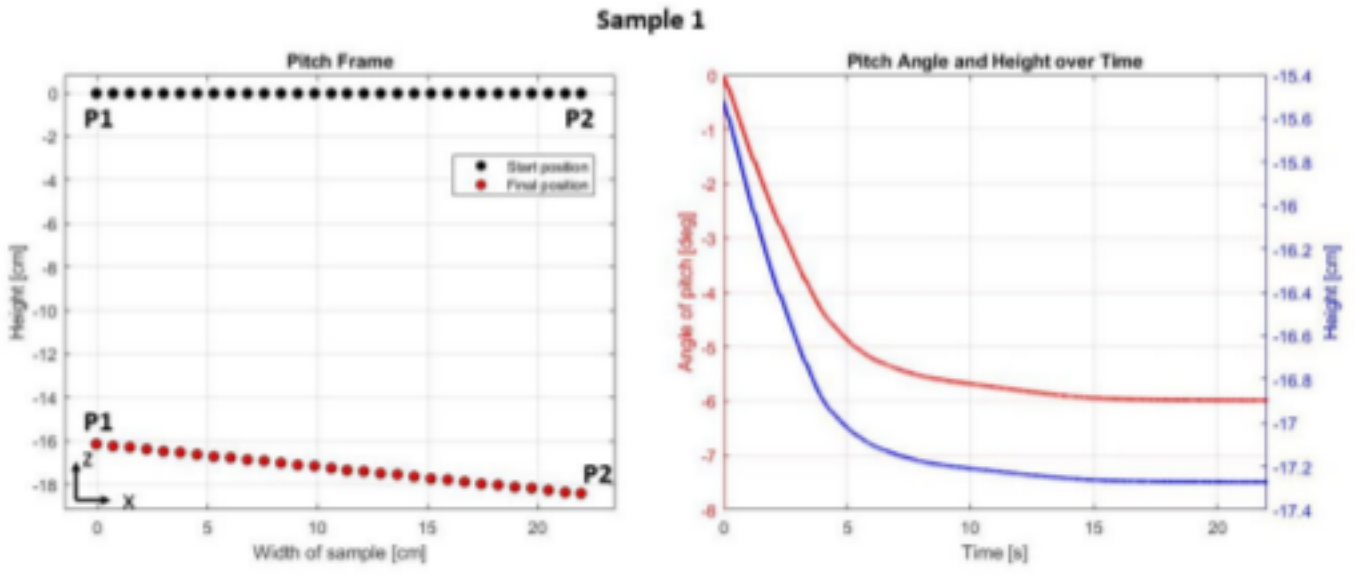

Figure B.6: Sample 1. Left: Pitch position of the frame (side view) at start and final position. Right: Pitch angle and height over time.

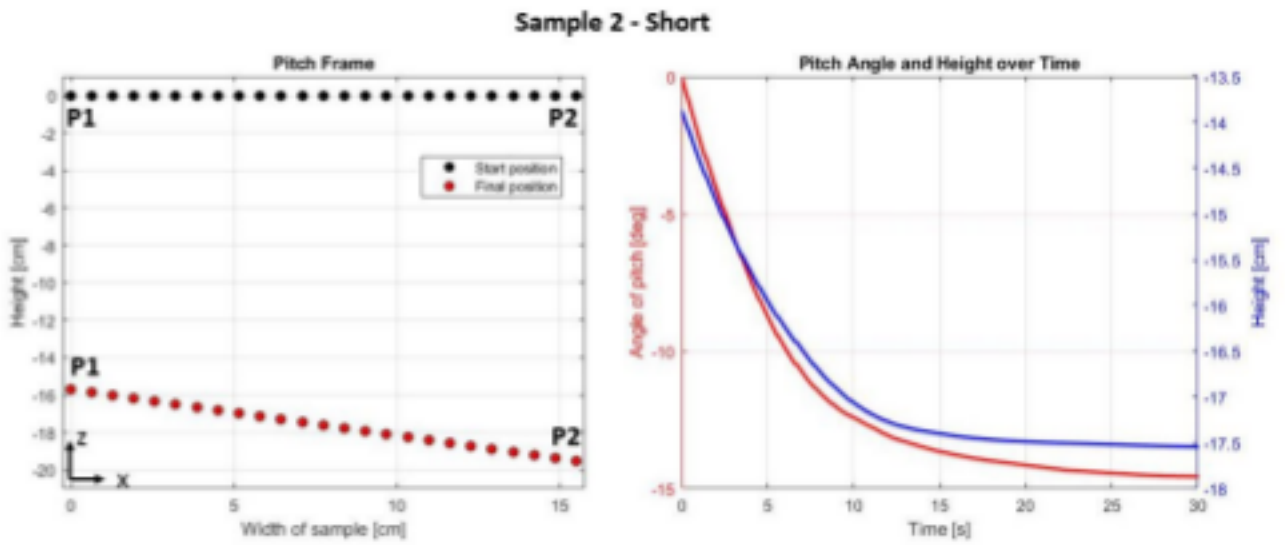

Figure B.7: Sample 2 short. Left: Pitch position of the frame (side view) at start and final position. Right: Pitch angle and height over time.

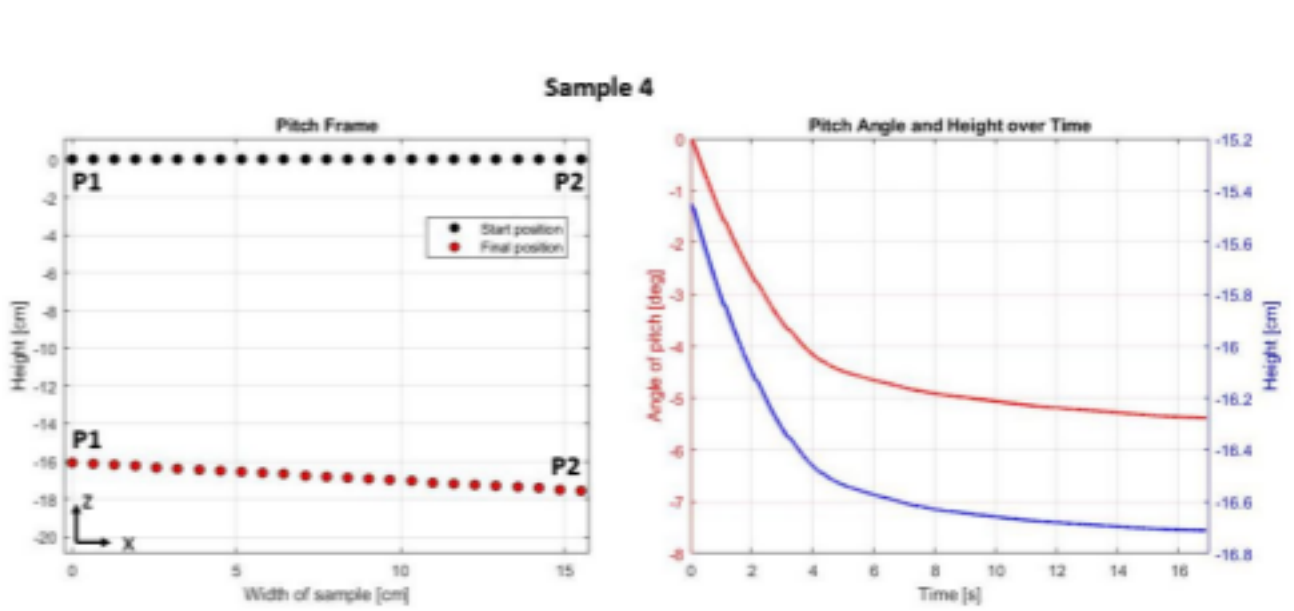

Figure B.8: Sample 4. Left: Pitch position of the frame (side view) at start and final position. Right: Pitch angle and height over time.

B.3.2. Roll

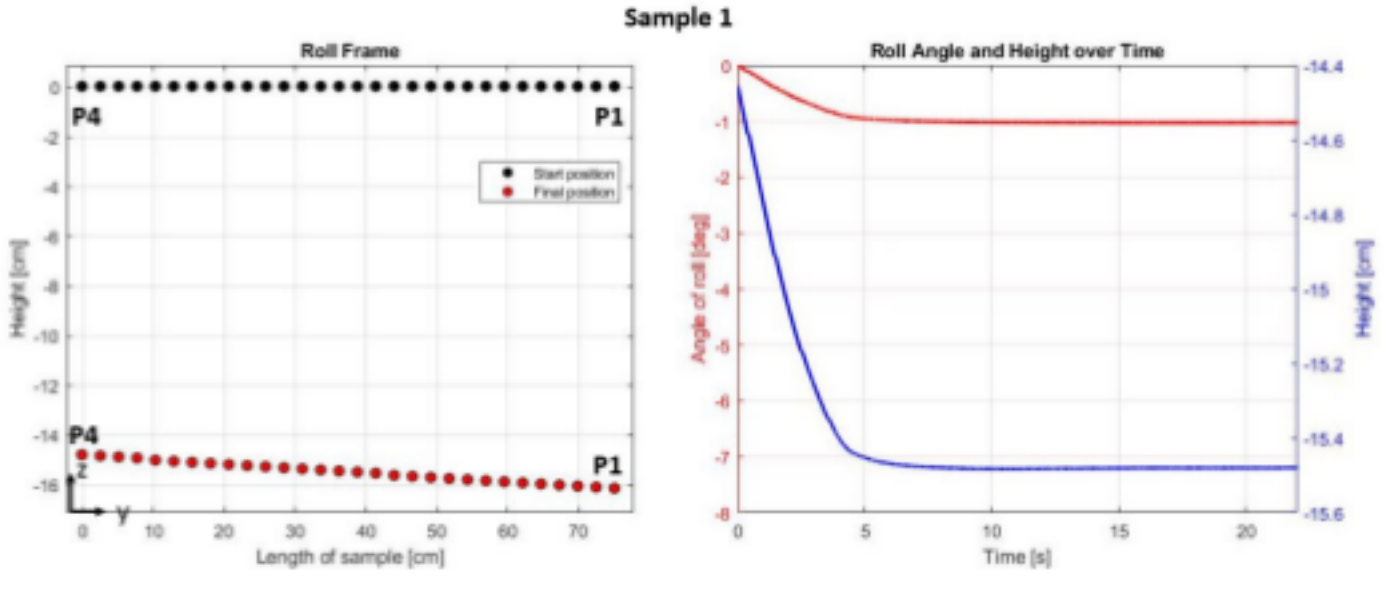

Figure B.9: Sample 1. Left: Roll position of the frame (side view) at start and final position. Right: Roll angle and height over time.

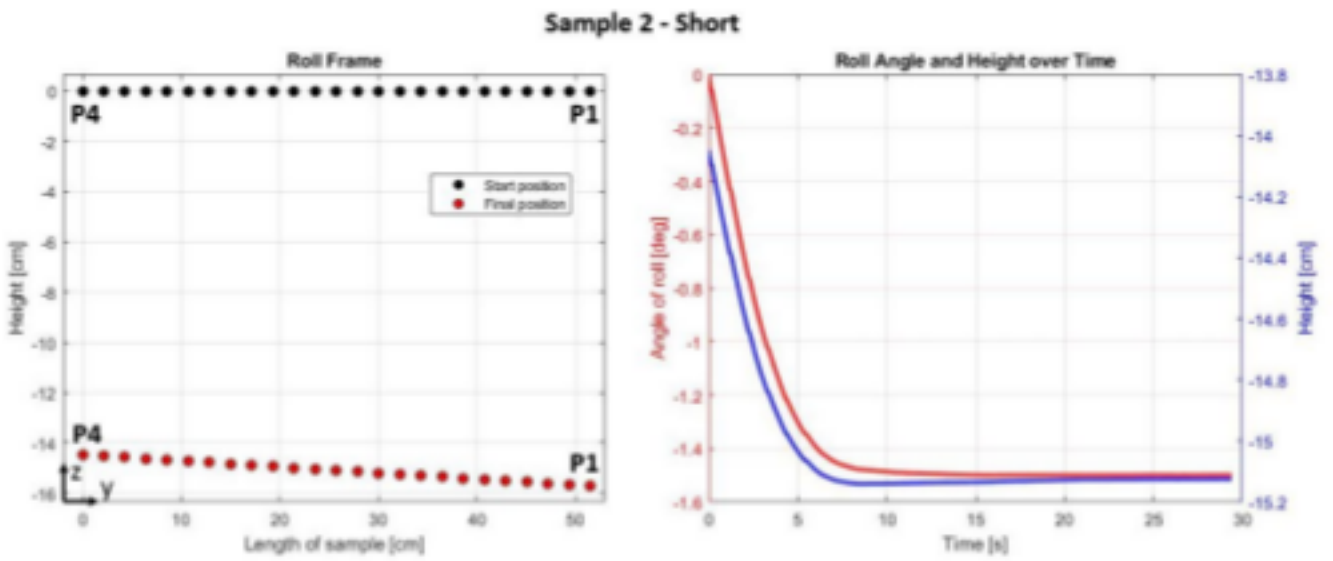

Figure B.10: Sample 2 short. Left: Roll position of the frame (side view) at start and final position. Right: Roll angle and height over time.

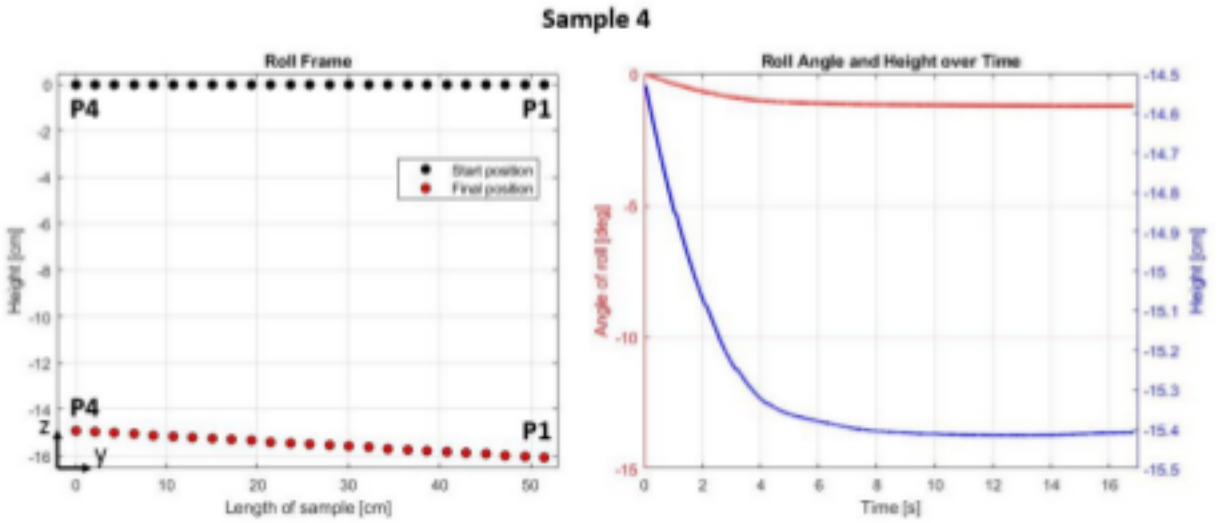

Figure B.11: Sample 4. Left: Roll position of the frame (side view) at start and final position. Right: Roll angle and height over time.

B.3.3. Deflection of samples

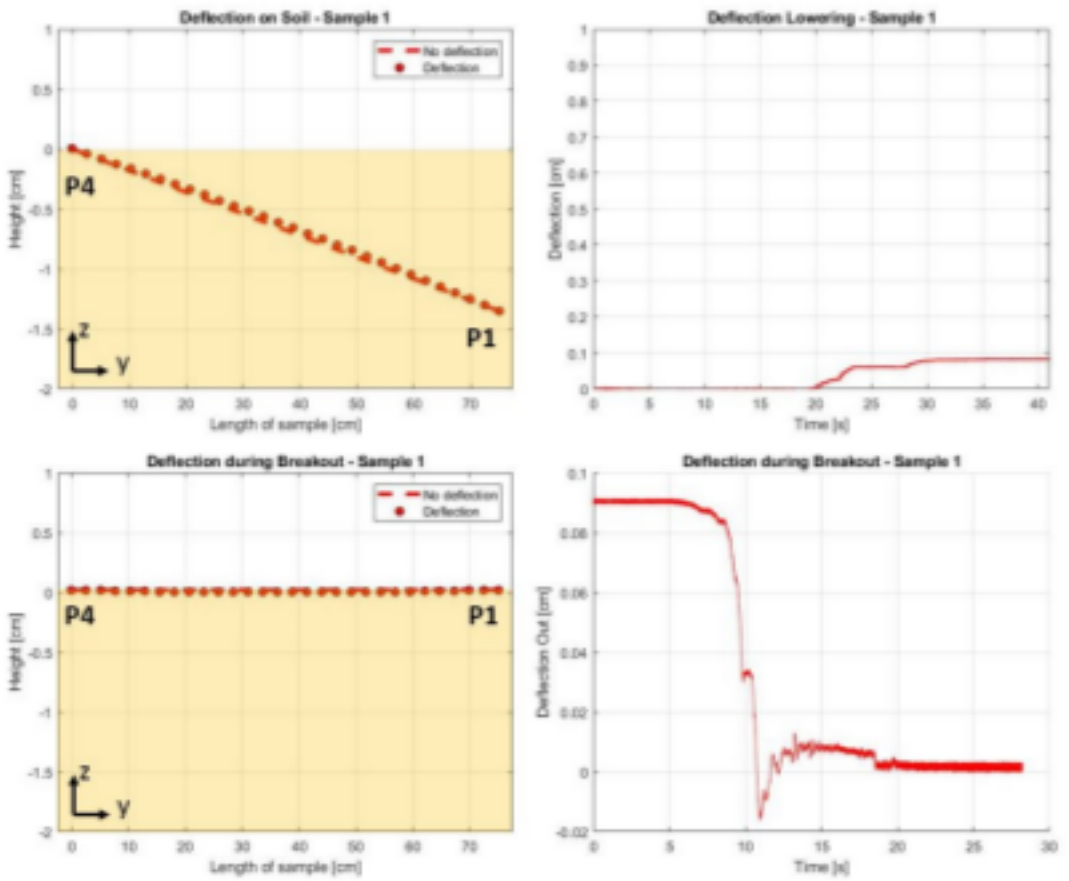

Figure B.12: Top left: Deflection of sample 1 on soil (side view). Top right: Deflection of sample 1 over time, when lowering the frame onto the soil. Bottom left: Deflection of sample 1 just before breakout (side view). Bottom right: Deflection of sample 1 over time, during breakout.

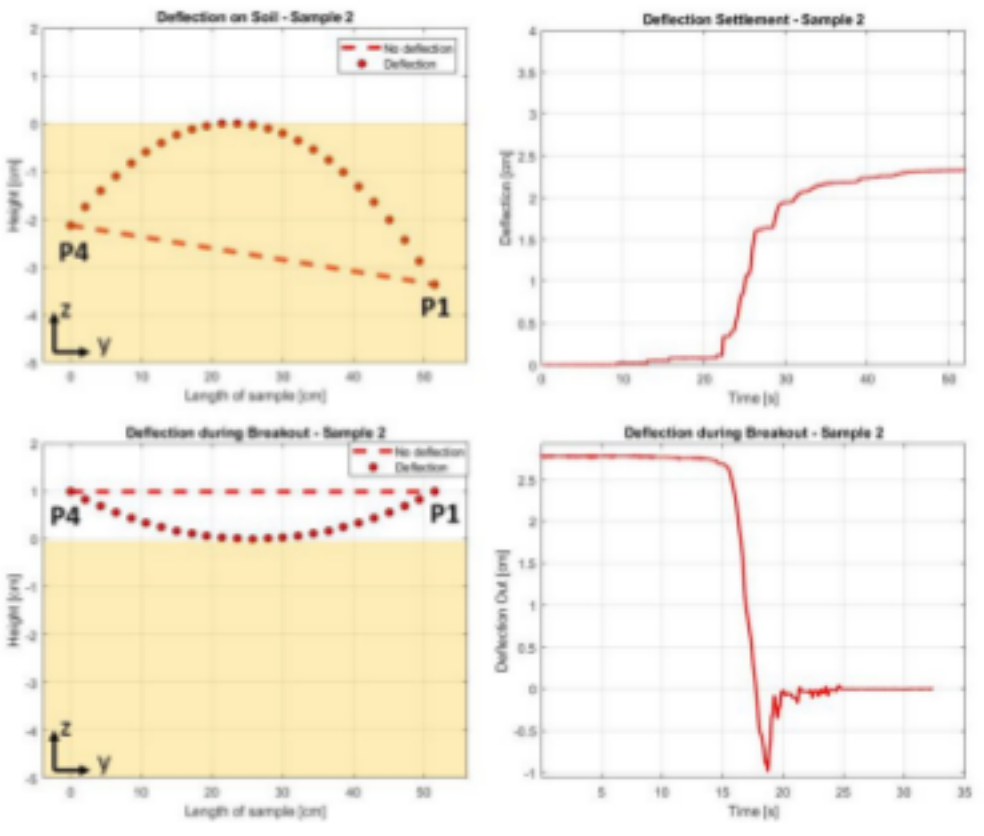

Figure B.13: Top left: Deflection of sample 2 (short) on soil (side view). Top right: Deflection of sample 2 (short) over time, when lowering the frame onto the soil. Bottom left: Deflection of sample 2 (short) just before breakout (side view). Bottom right: Deflection of sample 2 (short) over time, during breakout.

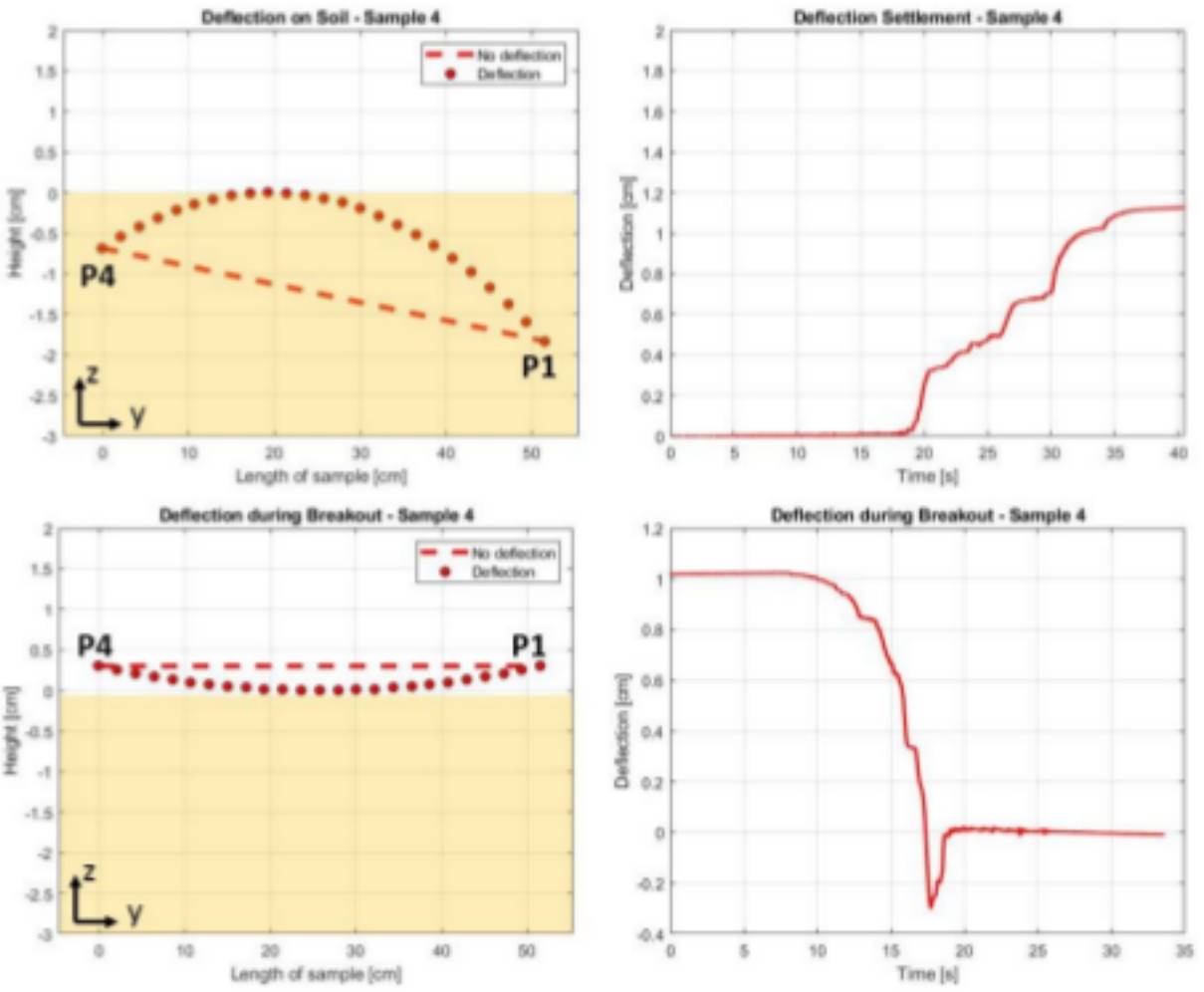

Figure B.14: Top left: Deflection of sample 4 on soil (side view). Top right: Deflection of sample 4 over time, when lowering the frame onto the soil. Bottom left: Deflection of sample 4 just before breakout (side view). Bottom right: Deflection of sample 4 over time, during breakout.

B.3.4. Winch and bucket breakout mechanism

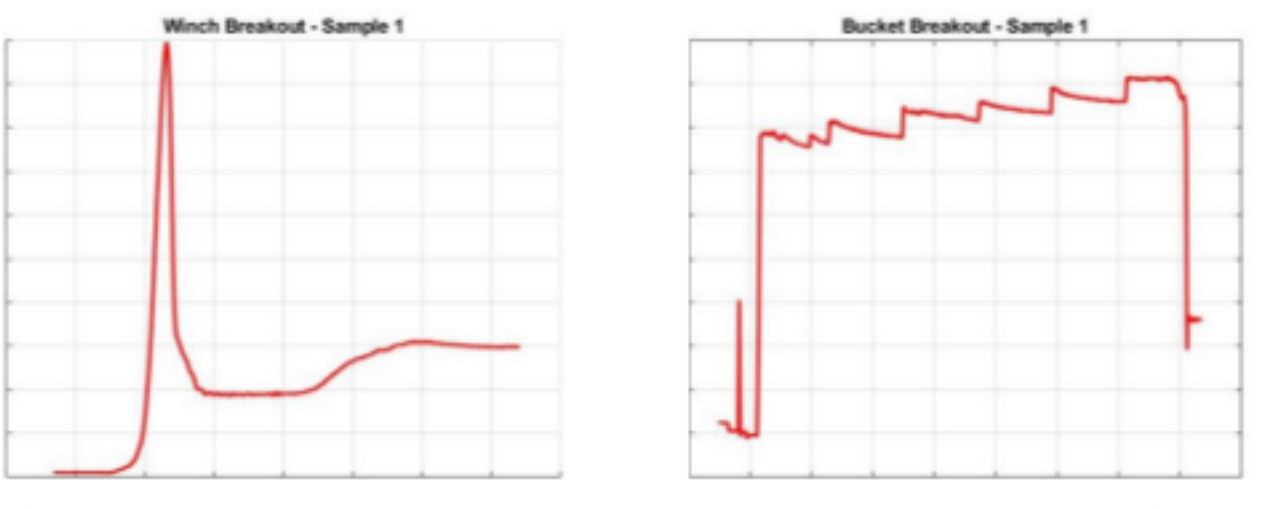

Figure B.15: Left: Winch breakout mechanism, short term breakout. Right: Bucket breakout mechanism, long term breakout. Peak at start of bucket breakout is due to manually pulling the cable.

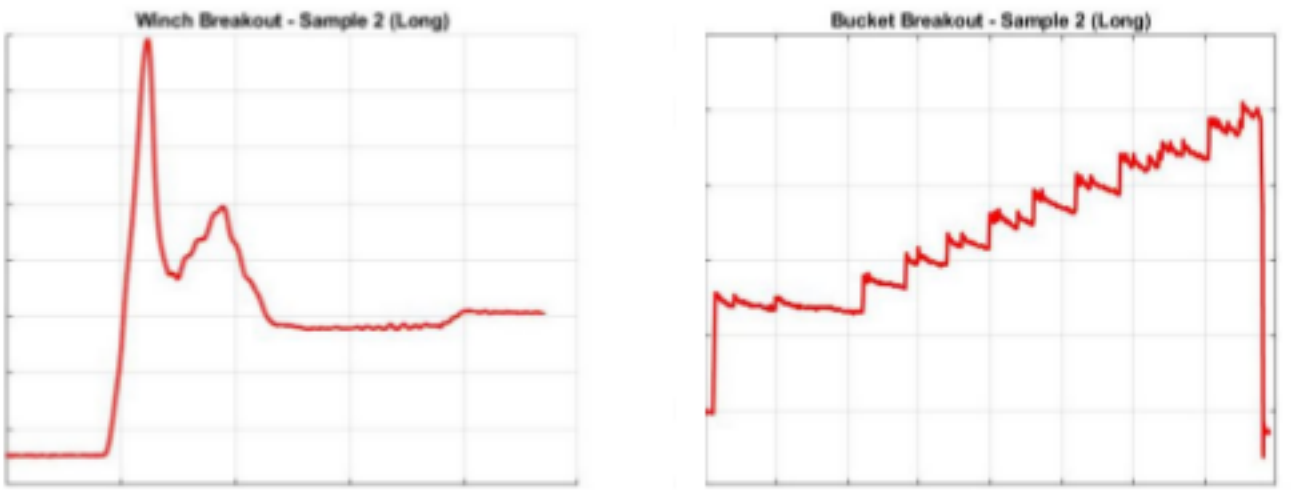

Figure B.16: Left: Winch breakout mechanism, short term breakout. Right: Bucket breakout mechanism, long term breakout.

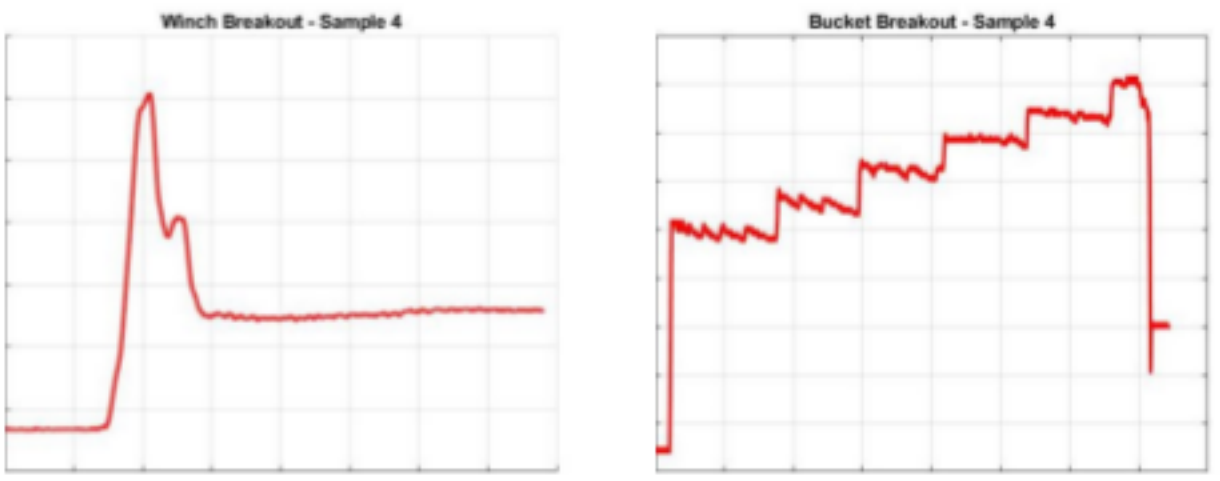

Figure B.17: Left: Winch breakout mechanism, short term breakout. Right: Bucket breakout mechanism, long term breakout.

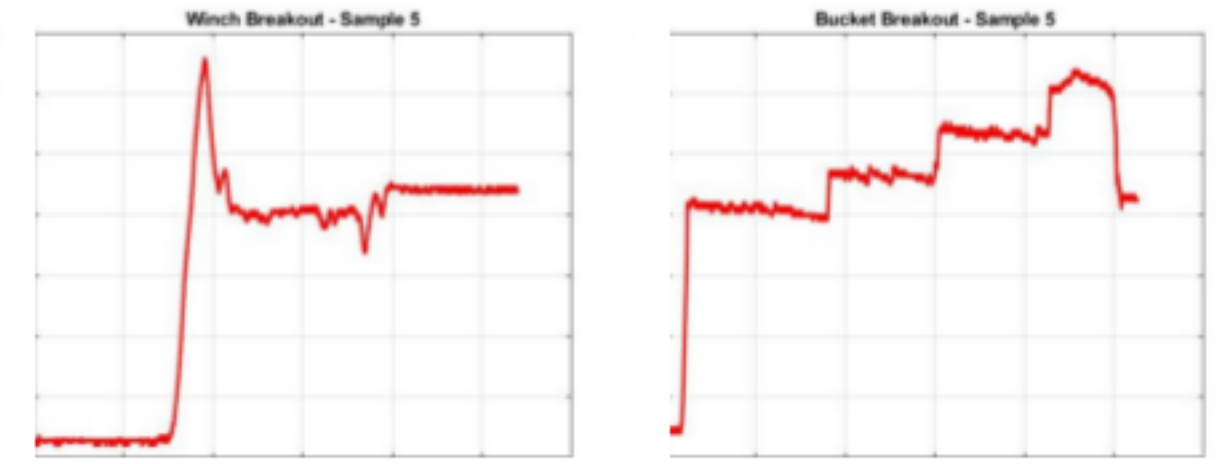

Figure B.18: Left: Winch breakout mechanism, short term breakout. Right: Bucket breakout mechanism, long term breakout.

B.4. Breakout force - flexibility

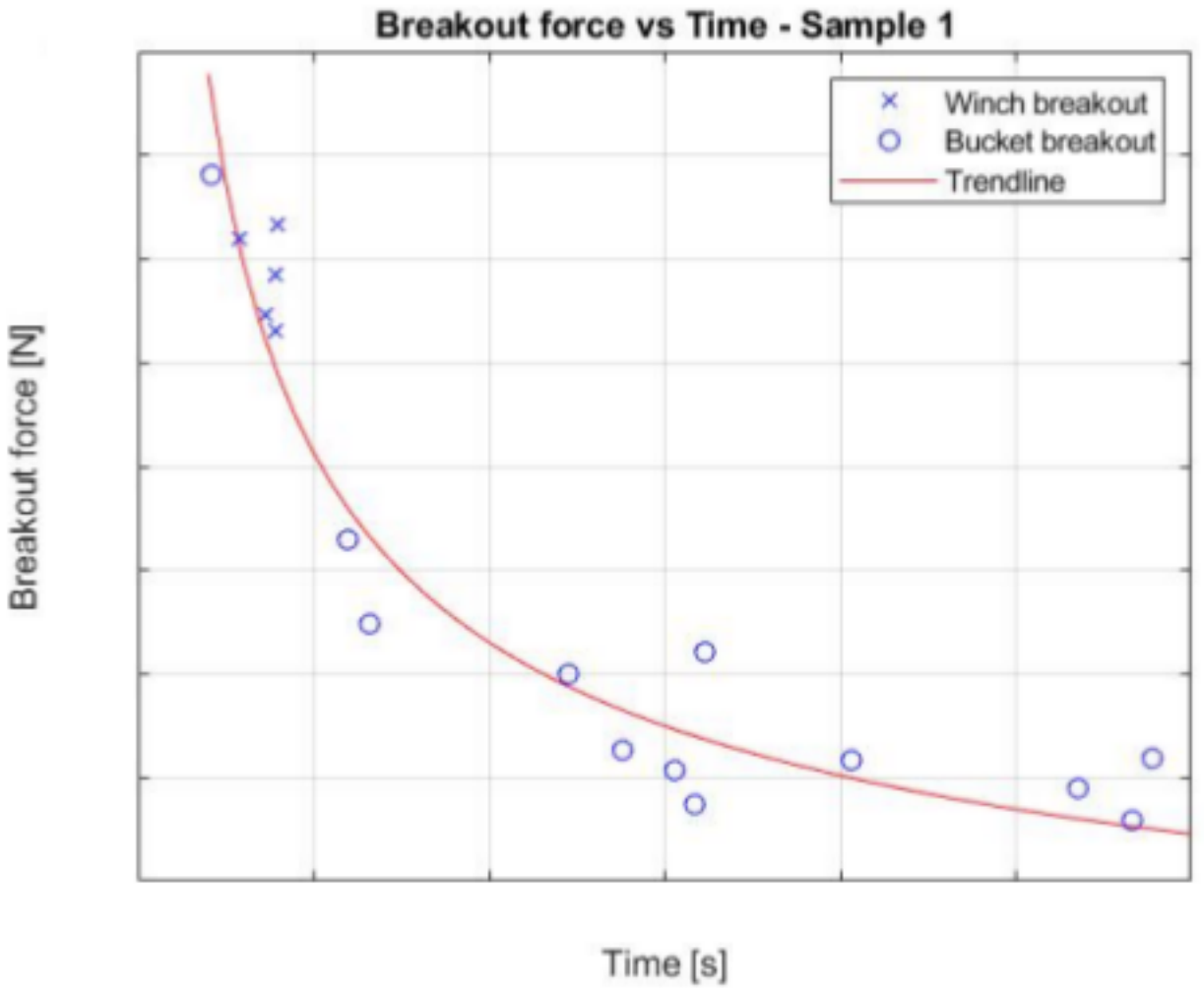

Figure B.19: Breakout force of sample 1 over time. Trend line: F = Reliability, R^2=0.91.

B.5. Breakout force - flexibility

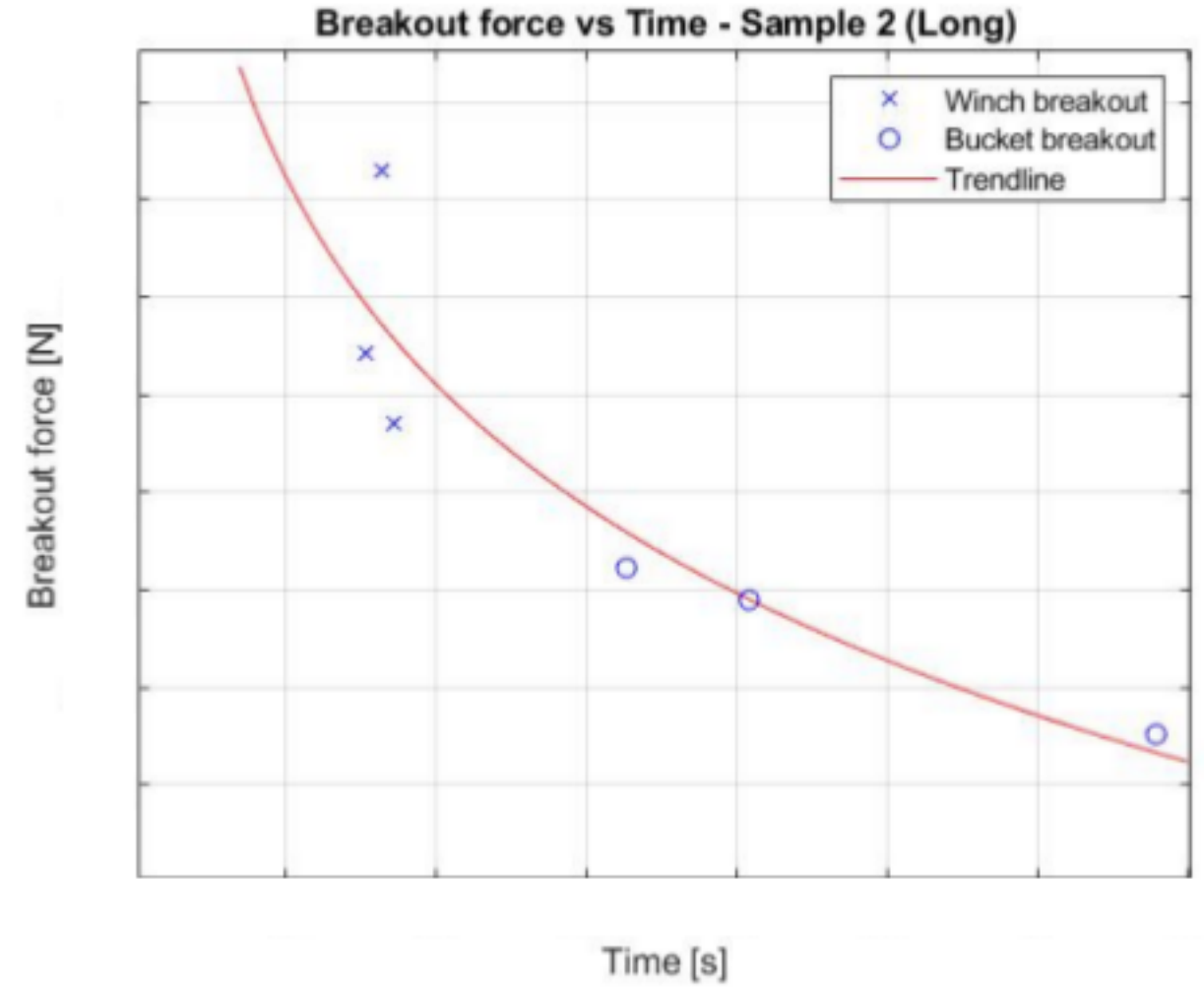

Figure B.20: Breakout force of sample 2 (long) over time. Trend line: F = Reliability, R^2=0.83.

B.5.1. Breakout force with and without tension applied

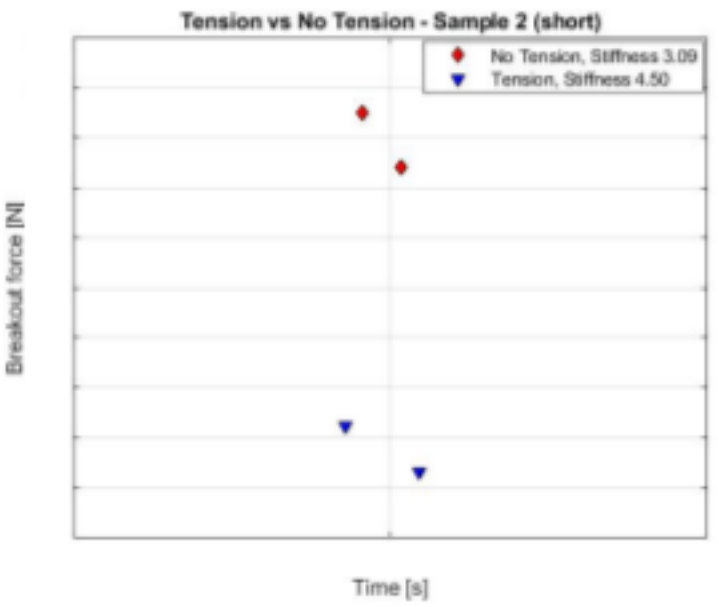

Figure B.21: Breakout force of sample 2 (short), with and without tension applied.

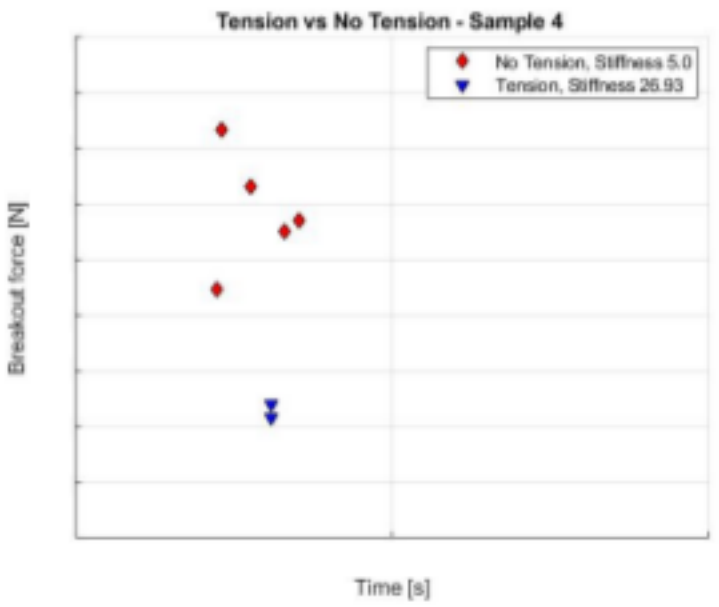

Figure B.22: Breakout force of sample 4, with and without tension applied.

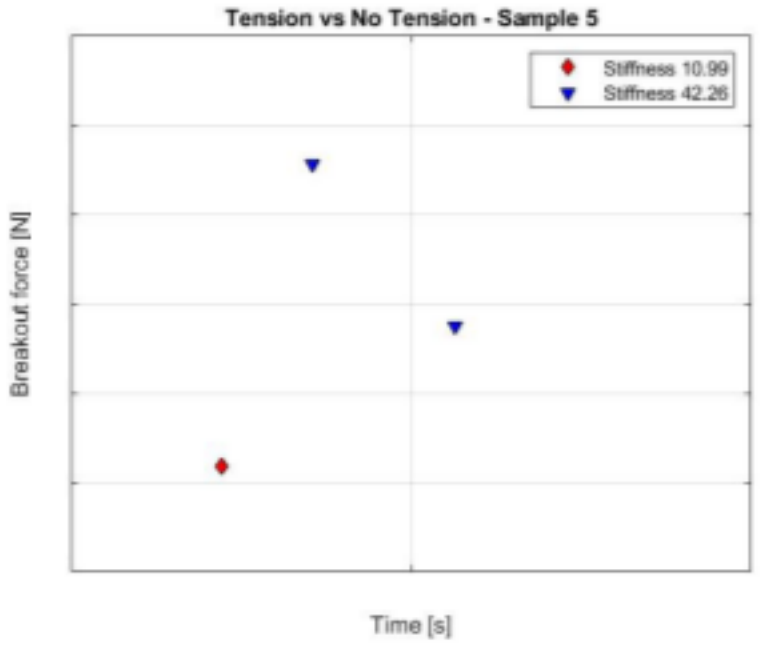

Figure B.23: Breakout force of sample 5, with and without tension applied.

B.6. Eccentric lift

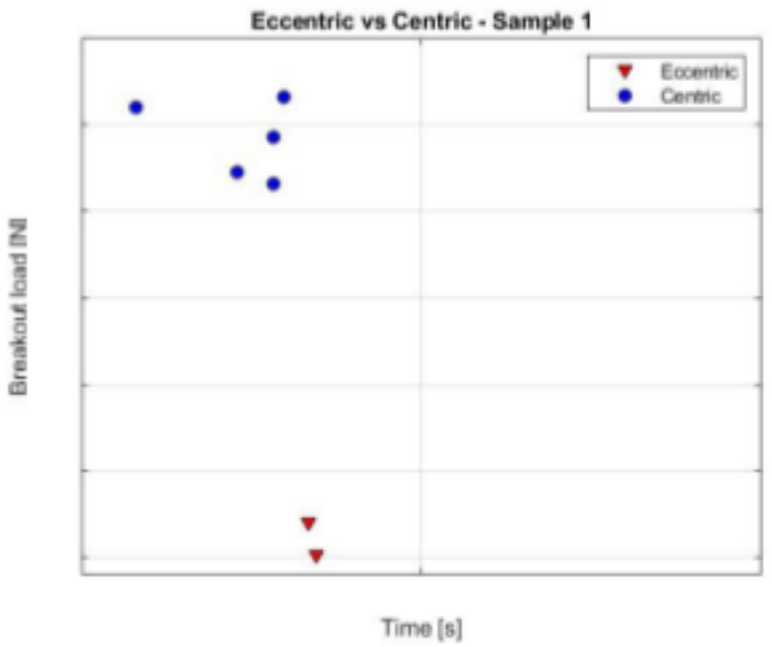

Figure B.24: Breakout force of sample 1 during a centric and eccentric lift.

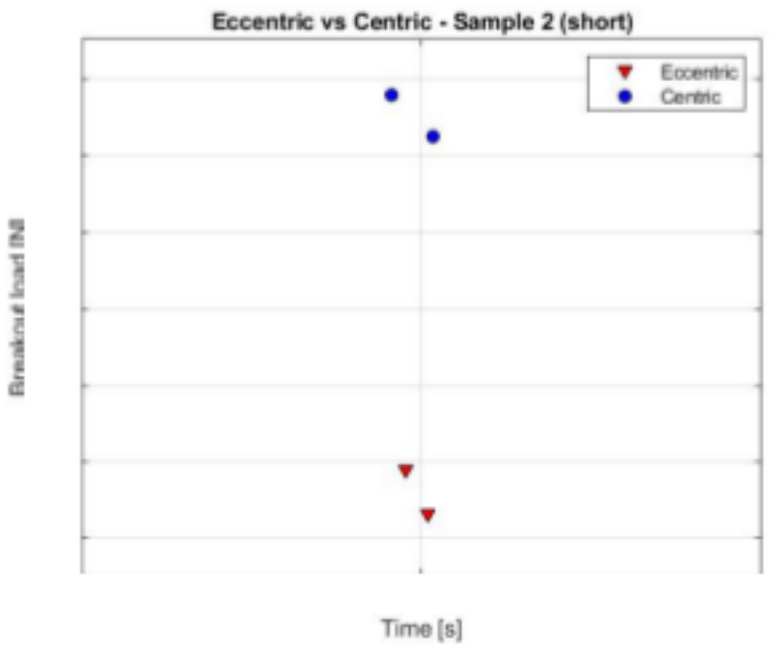

Figure B.25: Breakout force of sample 2 (short) during a centric and eccentric lift.

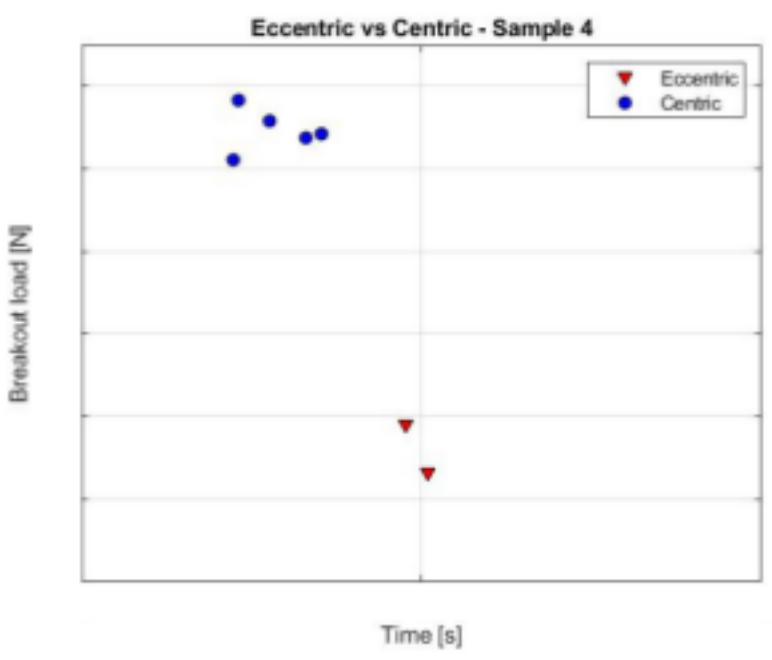

Figure B.26: Breakout force of sample 4 during a centric and eccentric lift.

B.6.1. Difference centric and eccentric when tension applied

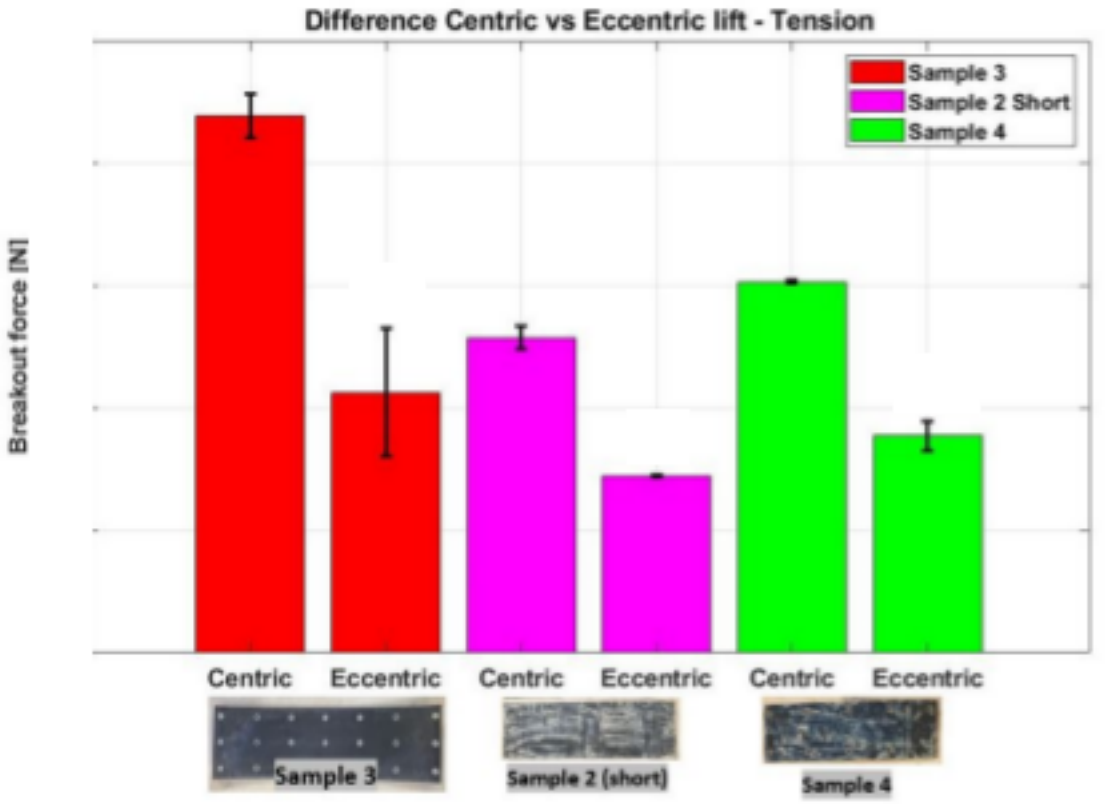

Figure B.27: Difference in breakout force for centric and eccentric lift per sample, with tension applied.